ABSTRACT

CHEMISTRY

BROWN, TRACY B.A. NORTH CAROLINA STATE UNIVERSITY, 2001

INVESTIGATION OF THE RHEOLOGY, CURE KINETICS, AND THERMO-MECHANICAL PROPERTIES OF GRC-A LOADED WITH ZEOLITES

Committee Chair: Eric A. Mintz, Ph.D.

Dissertation dated December 2010

Phenylethynyl terminated imides (PETI) are high temperature, high performance matrix resins that can be processed into composites by various methods including resin transfer molding (RTM) and vacuum assisted resin transfer molding (VARTM). PETI resins have experienced extremely rapid development in recent years, with major emphasis placed on engineering applications that take advantage of their high cured T_gs, high thermooxidative stability, high strength to weight ratio, outstanding mechanical properties, and compatibility with RTM and VARTM processing. In recent years the addition of nanoparticles to resin systems has been shown to further enhance the mechanical properties and thermooxidative stability. In this study, we incorporated nanoporous aluminosilicate materials, otherwise known as zeolites, into PETI resin GRC-A, and investigated the effect the zeolites have on the viscosity, cure kinetics, thermooxidative stability and other thermomechanical properties of GRC-A.

Rheological and differential scanning calorimetry studies conducted on the GRC-A/zeolite mixtures showed that zeolite L acts like a filler and retards the curing of the phenylethynyl end-groups, while zeolite Y catalyzes the curing process. Additionally, cure kinetic studies via melt rheology and DSC confirmed that the activation energies for GRC-A/zeolite Y mixtures was lower than for neat GRC-A and GRC-A/zeolite L mixtures, further supporting zeolite L acts as a filler while zeolite Y serves as a catalyst during the cure process. While the cured T_gs, from the DMA and TMA studies showed that in spite of the catalytic properties of zeolite Y; it did not afford additional properties over GRC-A and zeolite L mixtures. However, the catalytic properties of zeolite Y allows PETI resins to be cured at a lower temperatures, which could lead to lower energy costs in the production of composite parts from PETI resins.

INVESTIGATION OF THE RHEOLOGY, CURE KINETICS AND THERMOMECHANICAL PROPERTIES OF GRC-A LOADED WITH ZEOLITES

A DISSERTATION

SUBMITTED TO THE FACULTY OF CLARK-ATLANTA UNIVERSITY IN PARTIAL FULFILLMENT OF THE REQUIREMENTS FOR THE DEGREE OF DOCTOR OF PHILOSOPHY

BY

TRACY BROWN

DEPARTMENT OF CHEMISTRY

ATLANTA, GEORGIA

DECEMBER 2010

ACKNOWLEDGEMENTS

I will like to acknowledge my late father, Seward C. Brown, Jr., my late grandfather, Seward C. Brown, Sr., and my late stepmother Sherial R. Brown. Their presence was felt throughout the process. I definitely would like to thank my mother, Caleather C. Brown, for all of her encouraging and uplifting words that kept me from not giving up. I will also like to extend my greatest appreciation to my wonderful, caring sister, Racquel Brown-Dobbs, husband, Lawrence Dobbs, and my nephews Larry and Luke Dobbs. I will like to recognize my brother, Seward C. Brown, III for his presence, as well as other family, friends, and associates, including Anastesia Lyons and Yemaya Bordain. Most importantly I will like to extend my greatest thanks, throughout this process, to my dear friend Carlynn Murrrell. I will like to thank the members of the Mintz group, especially Candace James, Marcus Johnson, Aujanae Whigham, Calvin Foster. I will definitely like to thank my research advisor, Dr. Eric A. Mintz for all of his guidance and the opportunities that have been afforded to me under his mentorship. Additionally, I will like to show appreciation to my committee members Dr. Kofi B. Bota, Dr. Cass D. Parker, Dr. Conrad Ingram, Dr. Jim Criss and Mr. Hylton. I will also like to thank Ms. Williams and Ms. Ware for their support. Finally, I will like to acknowledge my adoring husband, Thomas Fox, for all of his love and support.

TABLE OF CONTENTS

TABLE OF CONTENTS

TABLE OF CONTENTS

TABLE OF CONTENTS

TABLE OF CONTENTS

LIST OF FIGURES

LIST OF FIGURES

LIST OF FIGURES

LIST OF FIGURES

LIST OF FIGURES

LIST OF FIGURES

LIST OF TABLES

LIST OF TABLES

LIST OF TABLES

LIST OF TABLES

ABBREVIATIONS

Phenylethynylterminated Imide	PETI
Complex Viscosity	η^*
Minimum Viscosity	η^*_{min}
Complex Modulus	G*
Elastic or Storage Modulus	G'
Viscous or Loss Modulus	G''
Crossover point of Gel point	G_c
Glass Transition Temperature	T_g
Heat of Reaction	ΔH_R
Activation Energy	E_A
Heating Rate, °C/min	β
Volume Fraction	φ
Gas constant, 8.3145 J/mol K^{-1}	R
Extent of Cure	x

CHAPTER 1

INTRODUCTION

1.0 Overview

Thermally stable, high performance resins are desirable for use in composite structures such as supersonic aircraft and reusable launch vehicles. Aromatic polyimides, prepared from dianhydrides and diamines have been accepted as high performance resins based on their excellent thermal, mechanical, and chemical properties, which makes them very good candidates for aerospace applications.[1-3] However, these materials are difficult to process into composites via compression molding, resin transfer molding (RTM), or vacuum-assisted resin transfer molding (VARTM), due to their high melt viscosities.[4,5] The introduction of the phenylethynyl group, as an end-capping agent in low molecular imide oligomers has been used to prepare resins with low melt viscosity which can be melt processed and then cured into high temperature polyimides.[6-10]

Aromatic polyimides prepared from the phenylethynyl terminated imide (PETI) resins exhibit many advantages; including processability and good material properties upon curing.[11-15] Phenylethynyl end groups are thermally unreactive up to 300 °C, giving a wide processing window. They also support product formation without volatile evolution that yield high molecular weight polyimides which exhibit good fracture toughness, high glass transition temperatures (T_gs), modulus, and excellent thermooxidative stability.[16-19]

Zeolites are microporous, crystalline aluminosilicates with intriguing properties,

including: catalytic activity, ion-exchange capability, adsorption capacity, and shape selectivity.[20] Many zeolites occur naturally as minerals and are extensively mined in many parts of the world. Others are synthetic, and are manufactured for specific uses. The specific pore size of zeolites can act as molecular sieves and adsorb molecules which can fit snugly inside the pores of the zeolites, while excluding molecules that are too large. These molecular sieves, with three-dimensional framework structures, are well entrenched in areas as diverse as water purification, laundry detergents, adsorbents, gas separations, agriculture, horticulture, pigments, and as catalysts in oil refining and petrochemistry.[21-29]

The framework structures of these microporous materials have uniformly sized pores that are of the molecular dimensions > 1 nm, with metal cations (e.g. Li^+, Na^+, K^+, Ca^{2+}, Sr^{2+}) or hydroxyl protons (H^+), sitting in the channels or cavities to preserve eletronuetrality.[30-32] The incorporation of these cations within the framework is dependent on the primary building units, SiO_4 and AlO_4^- tetrahedrons, being connected by sharing one oxygen atom between two tetrahedra. The SiO_4 tetrahedron is neutral, however, if the silicon atom (Si^{4+}) in the framework is substituted by a cation with a 3^+ charge, typically an aluminum atom (Al^{3+}), the formal charge of the tetrahedron changes from neutral to negative one.[20] The more aluminum substitutions the greater the negative charge; thus, the greater the number of cations or hydroxyl protons required for charge balance, resulting in the formation of weak Lewis acid sites or strong Brønsted acid sites. However, there is evidence of the formation of strong Lewis acid sites within zeolite structures due to extra-framework aluminum species and framework defects.[33-36] As a result, both strong Lewis and Brønsted acid sites are found in the framework of zeolites.

It also has been reported that metal-based Lewis acids can catalyze the cyclo-trimerization or polymerization of substituted acetylenes to benzene derivatives or polyenes, respectively.[37-40] In particular, Ziegler-Natta catalysts, which are titanium based, used in combination with organoaluminum compounds, such as triethylaluminum, $Al(C_2H_5)_3$ can promote the polymerization of acetylenes.[41-44] Additionally, metal-based Lewis acids can catalyze Diels-Alders reactions, by lowering the energy of the lowest unoccupied molecular orbital, LUMO, of the dienophile, decreasing the highest occupied molecular orbital, HOMO, LUMO energy gap. A decrease in the HOMO/LUMO energy gap translates into faster reaction times, requiring less energy.[45-51]

It has been shown that acetylenes can interact with Brønsted acid sites to yield vinyl carboncations, by protonation of an acetylene π bond.[52-54] Shchuckin and Vasilyev demonstrated that the vinyl carboncations formed from acetylenes in the presence of Brønsted acids and superacids react with arenes to give alkenylation products.[54] Brønsted acid-catalysts have been reported to react with acetylenes to afford bi- or tri-cycle compounds, through the formation of a vinyl carboncations.[55,56] It has been shown that the addition of a small amount of a Brønsted acid to a Lewis acid assists in accelerating Diels-Alder cycloadditions, resulting in higher product selectivity, relative to the Lewis acid alone.[57]

Recently there has been considerable interest in incorporating nanoscale fillers into polymer matrix composites (PMCs) to enhance thermal and mechanical properties.[58-61] Nanoscale fillers can yield dramatic changes in the properties of polymeric matrix systems, due to their large surface area for a given volume.[62] Zeolites in their pure crystalline structures microporous (less than 2 nm) form have large surface areas that can

enhance their catalytic properties and subsequently effect the cure chemistry of PETI resins.[20] Figure 1 gives an outline of our overall approach to this project: combining GRC-A resin with zeolites L and Y, resin processing, structure–property characterization of the resulting cured composites, and study of the fundamental chemistry and cure kinetics of the phenylethynyl end-groups upon cure in the presence of zeolites.

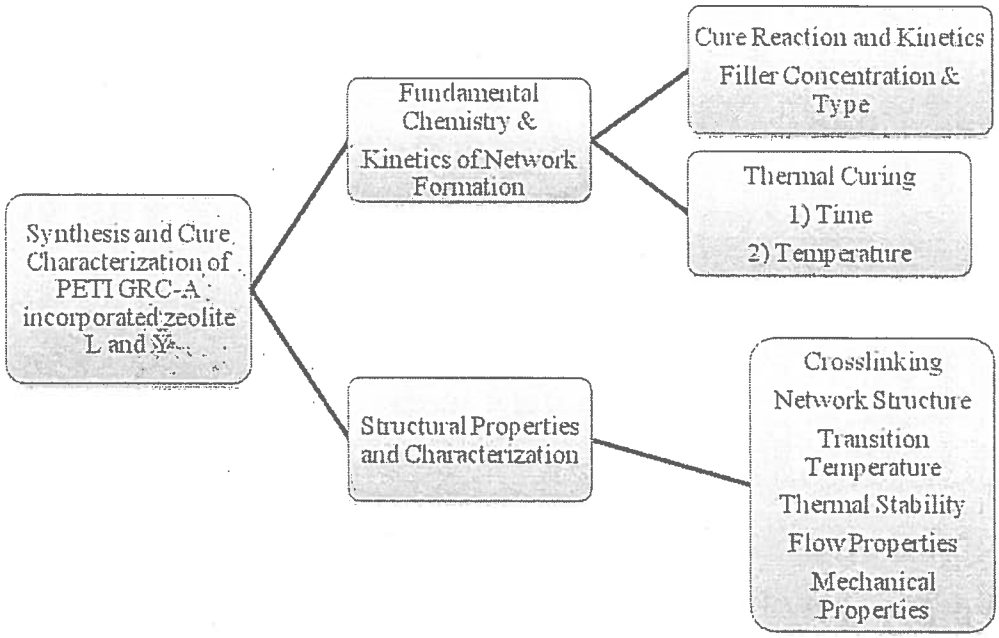

CHAPTER 2

LITERATURE REVIEW

2.0 General Considerations of High – Temperature Composites

Aromatic polyimides (APIs) are versatile materials, which can be utilized for a wide range of applications, including as matrices for high-performance fiber-reinforced composites, thin films in electronic applications, structural adhesives, sealants, and in composite laminate structures. These materials are leading candidates for high temperature, high performance applications in the aerospace industry, because of their excellent thermal, mechanical, and chemical resistance properties. APIs have the capability of performing at temperatures greater than 300 °C, along with the ability to be fabricated without the evolution of volatiles, Figure 2.

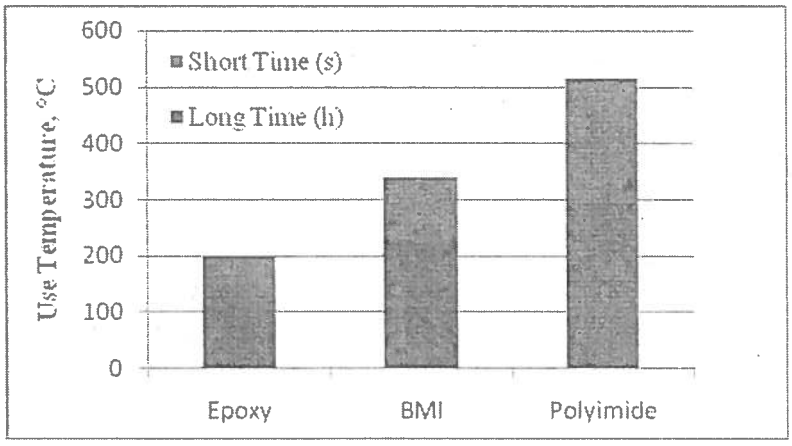

Figure 2. Temperatures used for resin epoxy, bismaleimide (BMI) and polyimide matrix composites.[63]

APIs are a class of thermally stable polymers that are often prepared from aromatic dianhydride and diamine monomers via an amide-acid precursor solution. Their usage in aerospace applications includes fabrication into high-strength-to-weight materials that exhibit excellent thermooxidative stability, high glass transition temperatures, and good fracture toughness. However, their structural units, which accounts for their thermal stability for high temperature applications are also responsible for their inherent insolubility and infusibility during processability. Delvigs et al. and Serafini showed that altering the chemistry of the pre-polymers of the API's structure can improve their processability.[64,65] While other researchers prepared low molecular weight end-capped polyimides pre-polymers.[66,67]

2.1 History and Classification of Aromatic Polyimides

In the 1950's and 1960's DuPont developed the first commercial polyimides, Pyralin™ and Kapton-H™ (Figure 3), to be used as wire coatings and films, respectively.[68] Through modification of nylon chemistry, polyimides were produced using a two–step process involving an aromatic diamine and dianhydride to form a polyamic acid, then losing water to form the polyimide. Other condensation polyimides like DuPont's Avimid N have been used for thin films for electronic packaging, wire insulation, and gas separator membranes, and most importantly, as a good matrix for making polyimide-carbon fiber reinforced composites.[69]

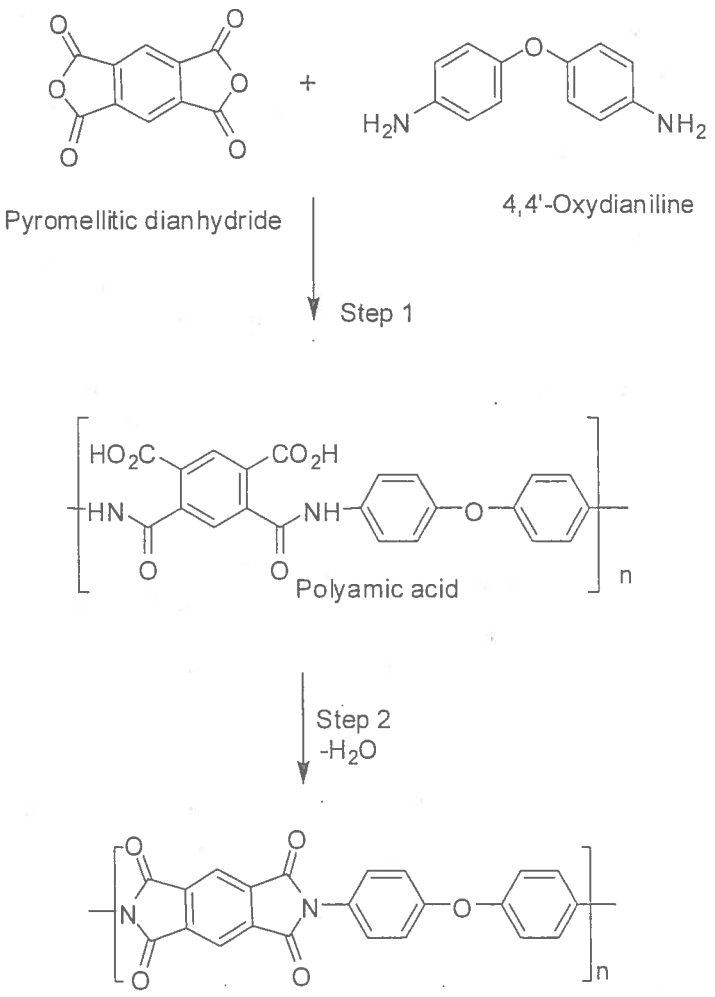

Figure 3. Two step condensation synthesis of Kapton™.

Avimid N (Figure 4) has a T_g close to 360 °C, low weight loss, and good retention of mechanical properties after 100 h aging in air at 371 °C.[70] These properties make this condensation polyimide, upon curing, suitable for structural application at high temperatures. However, the solvent used to prepare the impregnating solution for the carbon-reinforced fibers is a mixture of N-methyl pyrollidone (NMP) and ethanol. NMP has a very low vapor pressure; and intricate, time-consuming curing schedules must be used to remove the solvent in order to produce low-void composites. Additionally, the

evolution of volatile reaction byproducts such as water and alcohol lead to void formation during composite processing.[71,72]

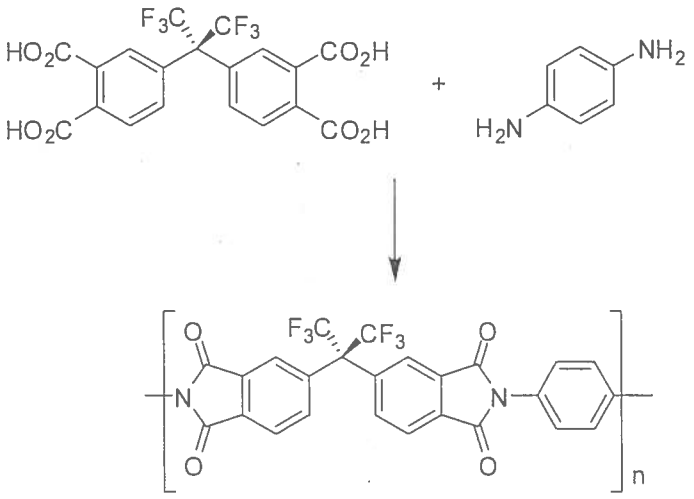

Figure 4. The preparation of Avimid N.

Polymerization of monomer reactants (PMR) was an approach developed at NASA Lewis (renamed Glenn) Research Center (GRC) to eliminate volatile byproducts while improving processability, without adversely affecting their stability and high-temperature performance.[73] This approach involved a two-step process in which the volatiles are removed in a lower temperature step (200 °C) that produces low-molecular-oligomers. PMR-15 is prepared from 3,3′,4,4′-benzophenone tetracarboxylic acid (BTDE), methylene dianiline (MDA) and the monoalkyl ester of 5-norbornene-2,3-dicarboxylic acid (NE), in a low boiling solvent (typically methanol or ethanol) to yield short chain imide oligomers with norbornyl end-groups (MW theoretical = 1500 g/mol), Figure 5. The process yielded composites with a post cure T_g of 365 °C, good retention of structural properties, and low weight losses in air for long exposure times (>10,000 h)

up to 230 °C, and for shorter times at temperatures as high as 316 °C. However, the PMR regime has some draw backs: (i) concern over the mutagenicity of MDA, and (ii) the high cost of fabrication.

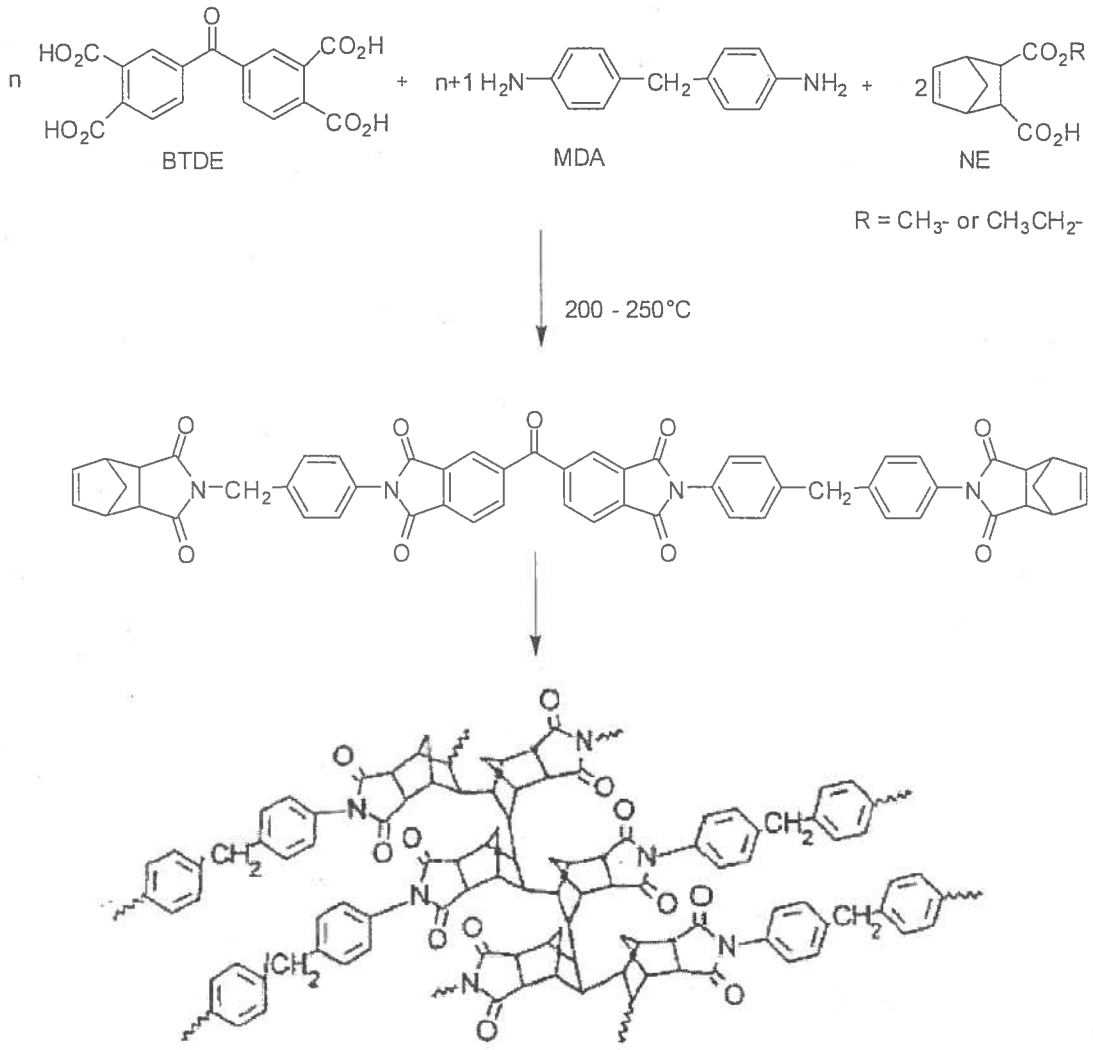

Figure 5. The chemistry of PMR-15, and the polymerization of the nadic-end cap.[63]

Other norbornyl end–capped resins, such as LaRC-160 (Figure 6) and AFR-700B (Figure 7) have been developed to provide materials with improved processing and/or

better high-temperature performance than PMR-15. However, the thermal-oxidative stability of the norborene ring is poor due to the large number of saturated carbons present in the structure, subsequently limiting its use.

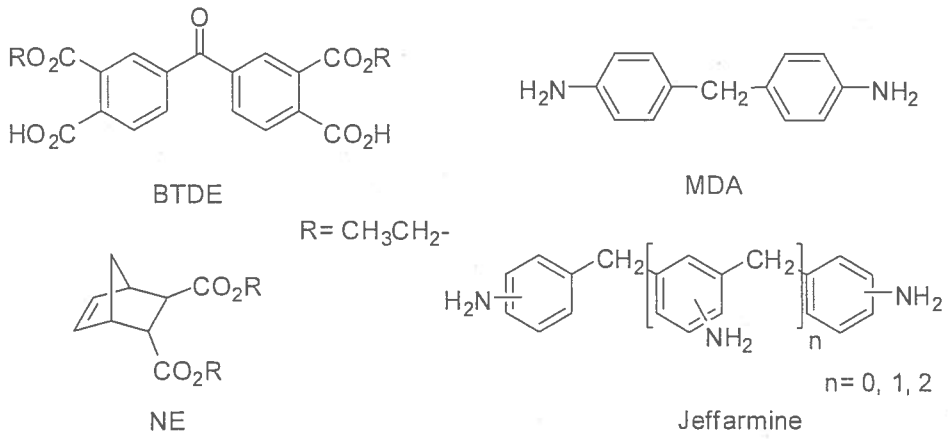

Figure 6. LaRC-160 monomers: BTDE; NE; MDA, and Jeffamine.

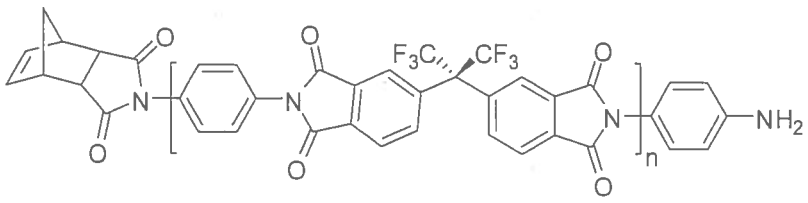

Figure 7. Structure of AFR-700B

Acetylene terminated imide resins, such as Thermid 600 (Figure 8), have high T_gs and good thermooxidative stability at temperatures as high as 316 °C. However, the acetylene group in these systems polymerizes at 195 °C, which is too close to the imidization temperature to allow for complete removal of condensation by-products. Thus, the introduction of the phenylethynyl (PE) end-group by incorporating a second

phenyl ring on the acetylene end-groups resulted in an increase of the polymerization temperature to almost 300 °C.

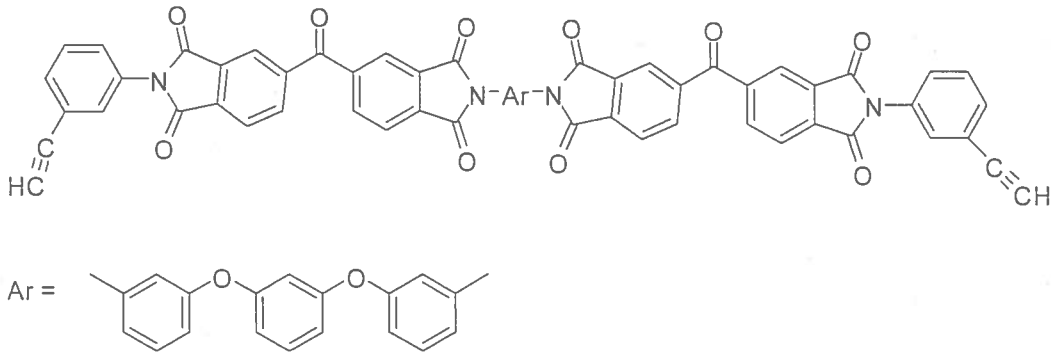

Figure 8. Structure of Thermid 600 polyimide, T_g = 370°C.

Researchers at NASA Langley Research Center (LaRC) demonstrated that PETI-5 (MW = 5000 g/mol), a phenylethynyl (PE) terminated imide (PETI) resin (Figure 9), exhibited low minimum melt viscosity. The PETI-5 resin, which is comprised of symmetrical 3,3′,4,4′-biphenylene dianhydride (s-BPDA), 3,4′-bis[4-phenylethnylphthalimido]diphenyl ether (3,4′-ODA), 1,3-bis(3-aminophenoxy)benzene (APB), and 4-phenylethynylphthalic anhydride (PEPA) was investigated as a composite matrix and adhesive for the high speed civil transport (HSCT) program. This PETI resin also exhibited excellent mechanical properties, excellent solvent resistance under stress, and long term durability at 177 °C, with a T_g of 270 °C. It cross-links between 320 °C to 371 °C at a pressure of 1 MPA; and can be easily processed by resin transfer molding.

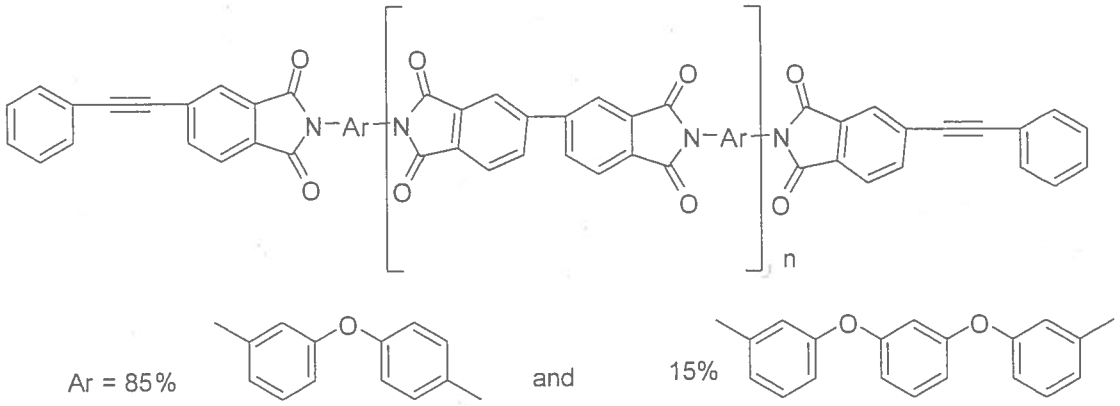

Figure 9. Structure of PETI 5, cured T_g = 270 °C

The chemistry and performance of PETI resins can be modified by either changing the diamine or the dianhydride.[74-78] In one study, Scola et al. substituted the linear rigid s-BPDA with two bulky fluorinated dianhydrides, 4,4′-(2,2,-triflouro-1-phenyl(ethylidene)diphthalic (3FDA) and 4,4′-(hexafluoroisopropylidene)diphthalic anhydride (6FDA) dianhydride (Figure 10), and compared the reactivity and melt viscosities of the resulting resins.[75] They found the order of phenylethynyl reactivity, based on the dianhydrides, as follows: s-BPDA>3FDA>6FDA.

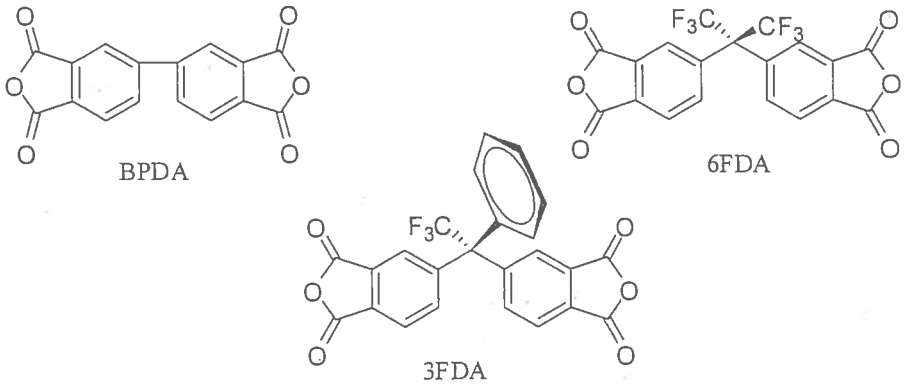

Figure 10. Dianhydrides BPDA, 6FDA, and 3FDA

The Molecular Orbital Package (MOPAC) was used to explain the melt viscosities by calculating the solvent accessible surface area, molecular surface area, and solvent excluded volume. The calculated values for s-BPDA were less than for 3FDA and 6FDA. This suggested that there may be less distance between the adjacent molecules in s-BPDA oligomers than 3FDA and 6FDA. This was supported by the complex viscosity data.

In other well-established PETI resin systems, such as PETI 298 and PETI 330 (Figure 11), the diamine or the diamine ratio, or the dianhydride have been varied.[18,19,79-86] The T_g for PETI-5 was 270°C, which was too low for supporting the structure of reusable launch vehicle. PETI 298 and PETI 330 resins, which were developed at NASA LaRC, emerged as leading candidates for composites requiring high temperature performance (≥ 288 °C for 1000 h); combined with the ability to be readily processed into composites by RTM and VARTM.

PETI 298 exhibits a cured T_g at 298 °C while retaining a low melt viscosity. It is formulated from s-BPDA, 1,3,-bis(3-aminophenoxy)benzene (1,3,3-APB), 3,4′-oxydianliline (3,4′-ODA) and end-capped with PEPA, with a molecular weight of 750g/mol.[4,5] The melt viscosity of PETI 298 is about 0.1–10 Pa·s, at 280 °C, and the oligomer is stable for at least 1 h at this temperature.[83] PETI 330, which is formulated with asymmetrical 2,3,3′,4′-biphenyltetracarboxylic dianhydride (a-BPDA) and PEPA end-cap along with mixtures of 1,3-bis(4-aminophenoxy)benzene (1,3,4-APB) and *m*-phenylendiamine (*m* –PDA), has a lower melt viscosity and higher T_g than PETI 298. It was proposed that the highly irregular structure of this imide oligomer causes it to exhibit lower melt viscosity than PETI 298; 0.06-0.10 Pa·s at 280 °C. PETI 330 has a glass

transition temperature of 330 °C, after curing for 1-2 h at 371 °C. PETI 330 was designed specifically for RTM processing, and has been processed to give composites, which exhibit excellent thermal and mechanical properties. PETI 298 and 330 are polydispersed, as shown in the GPC, Figure 12. The synthesis of polydispersed PETIs were by design to lower the melt viscosity in order to support processability and fabrication.[18,19]

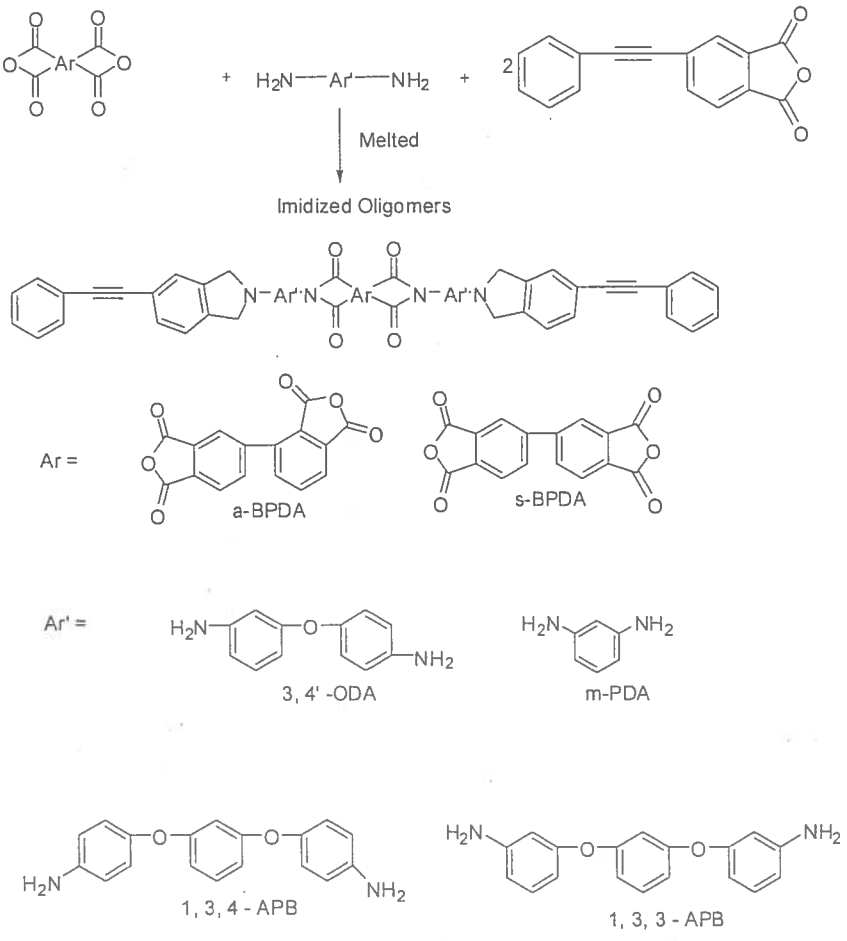

Figure 11. Synthesis of PETI 298 and PETI 330 imide oligomers.[84-86]

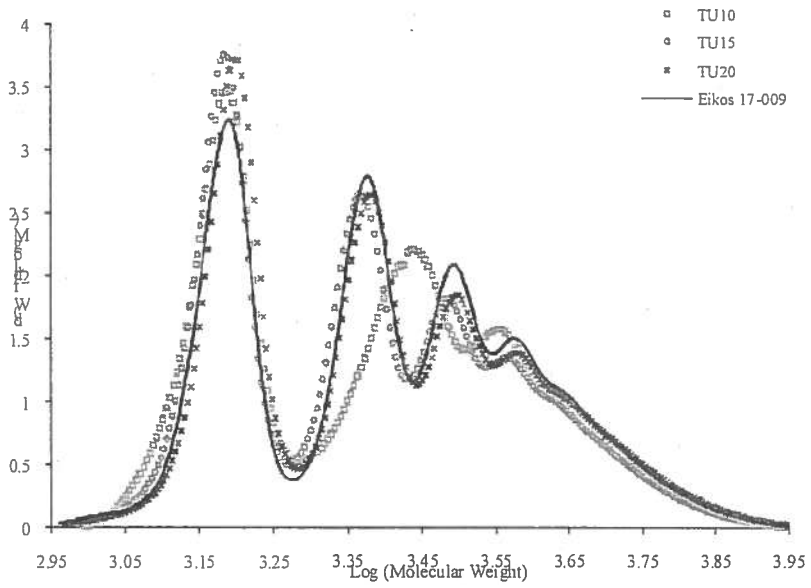

Figure 12. GPC of four samplesPETI-298 prepared by microwave based synthetic route (Calc. 750 g/mole)[87]

2.2 Processability of Polyimides

The incorporation of phenylethynyl groups made processing polyimides amenable for RTM and VARTM.[4,5] RTM and VARTM are solvent–free processes for fabricating composite parts, making them very attractive processing methods. Typically these processes involve the placement of a woven fiber preform or mat (i.e. carbon fiber fabric, glass, etc.) into a mold cavity. Then molten PETI resin is subsequently injected or infused at an elevated temperature into the mold cavity, whereby it permeates through the woven preform. In these processes, resin flow and fiber wet-out are critical, because the resin flows in the plane of the preform, as well as the transverse directions of the preform. It is imperative to have good fiber wet-out, and this often depends on the architecture of the fiber and permeability of the preform. Therefore these processes can utilize

rheological tests (temperature and time sweeps) to support fiber wet-out, and yield composites less of voids with reliable mechanical properties.

2.3 Cure Chemistry and Products of PETI Resins

The chemistry of the phenylethynyl end-cap has been studied extensively; however, the mechanism of cure has not been fully elucidated due to the intractability of the cross-linked resin.[87-91] The chemistry of PETI resins has been proposed to include the following: chain extension, chain branching, and cross-linking brought on by the initial formation of polyenes, followed by Cope rearrangements and Diels-Alder intra- and intermolecular reactions of polyenes (Figures 13 and 14).[86] Studies by Amdur et al. on the free radical polymerization of phenylaceteylenes, and by Preston et al. on the thermal and radiation curing of the phenylethynyl-terminated oligomers suggest that the cure reaction occurs by thermally induced free radical initiation.[89,90] Once initiated, the phenylethynyl end groups are expected to react by: ethynyl to ethynyl addition chain reaction; or by an ethynyl to ethynyl chain extension reaction; and more complex ethynyl to ethynyl trimerization or tetramerization reactions. Ethynyl to vinyl, and vinyl to vinyl cross-linking and branching reactions are also very viable possibilities. Figure 13 shows polyene formation via the ethynyl-ethynyl addition chain reaction, and the formation of cyclotriemers and cyclotetramers.

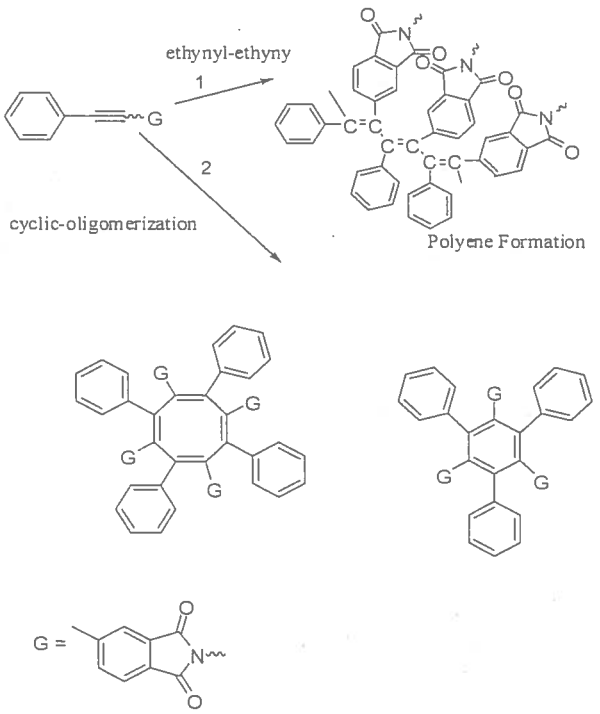

Figure 13. Formation of polyenes and cyclic trimers and tetramers.[88]

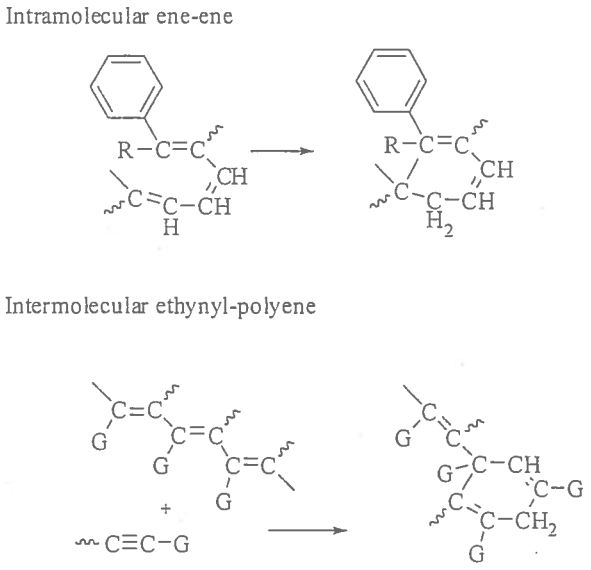

Figure 14. Intra- and intermolecular interactions of the polyene structure via Cope rearrangement (top) and Diels-Alder reactions (bottom), respectively.[88]

One of the first study of the cure chemistry of a phenylethynyl model compound was carried out by Harrington et al. using high-pressure liquid chromatography (HPLC).[92] The model compound 4-phenoxy-4′-phenylethynylbenzophenone was cured at 375 °C, quenched, and a chromatogram of the sample revealed numerous distinguishable peaks; however, attempts to characterize the fractionated peaks by mass spectroscopy (MS) were unsuccessful. Solution ^{13}C NMR for 4-phenoxy-4′-phenylethynylbenzophenone in the uncured state and the fully cured state were obtained, and the spectra revealed several peaks in the aromatic region but no assignments were made (Figure 15). A follow up study by Wood et al., on this model compound used reverse-phase liquid chromatography (LC) in combination with mass spectrometry to identify soluble components from the cured sample.[93] The combined LC/MS analysis revealed that dimers, trimers, and possibly tetramers were formed during the initial cure. Both Meyer and Takekoshi et al. used HPLC/MS, and reported the observation of dimers, trimers, tetramers, and pentamers of model compounds N-[3 (phenylethynyl)phenyl]phthalimide (3PEA/PA) and N-phenyl-[4-(phenylethynyl)phthalimide] (PEPA/An), Figure 16.[94,95]

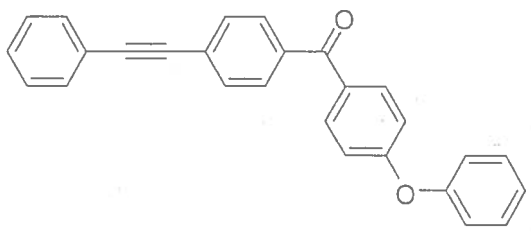

Figure 15. 4-phenoxy-4′-phenylethynylbenzophenone

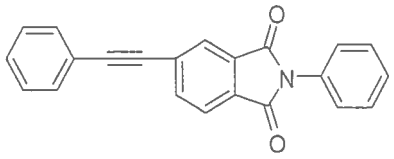

3PEA/PA and

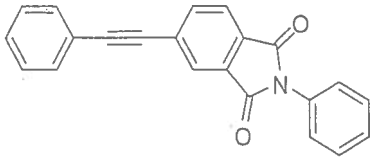

PEPA/An

Figure 16. 3PEA/PA and PEPA/An.

Swanson et al. used solid-state ^{13}C NMR to study the cure mechanism of an ethynyl end-capped polyimides systems. They proposed that trisubstituted benzenes were derived by cyclotrimerization, by thermal cyclization via Diels-Alder reaction, or from biradical polyene products and condensed polycyclic aromatic structures and alkenylaromatics.[91] Meyer et al. synthesized 3PEA/PA and PEPA/An, and attempted to follow the curing of these model compounds using ^{13}C NMR by following the depletion of the ethynyl peaks, and the increasing intensity of resonances in the range of 120-125 and 136-144 ppm, suggesting that both aromatic and polyene products were formed, but no definite assignment was made due to overlapping peaks.[96] Using ^{13}C NMR, Scola et al. determined that the main reaction products for ^{13}C enriched 3, 4′ bis[4-phenylethynylphthalimido]diphenyl ether (PEPA 3, 4′ - ODA) was the ethynyl to ethynyl reaction, resulting in polyenes, Figure 17.[86] The ethynyl to ethynyl reaction was also found for the corresponding ^{13}C enriched PETI-5 imide oligomer. Additionally, the study revealed the formation of ^{13}C enriched single-bonded structures, suggesting further chemistry on the polyene system upon heating.

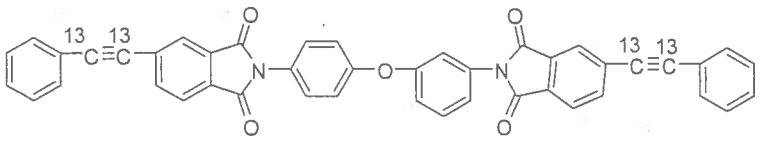

Figure 17. PEPA 3,4′-ODA

This additional chemistry of the polyenes led to new compounds exhibiting cyclic resonances which were attributed to cyclotrimerization or cyclotetramerization to form hexasubstituted benzenes or octasubstituted cylcooctatetrenes, respectively; which make comprised of the major products of the final cross-link material. Roberts et al. were also able to identify the cured products of two ^{13}C enriched PETI oligomers, PETI-A 2000 (MW = 2000 g/mol) and PETI-A 9000 (MW = 9000 g/mol), synthesized from 4-(Phenylethynyl-α,β-^{13}C phthalic anhydride (PEPA), see Figure 18.[97] Using solid state ^{13}C NMR they observed resonances that they assigned to three different classes of cure products: cyclic compounds, products from backbone addition (substituted stillbenes and tetraphenyl ethanes), and polyenes. Additionally, the study revealed that the molecular weight of the oligomers had a profound effect on the structure of the cured products. For example, polyene formation was more permanent with PETI-A 2000 than with PETI-A 9000 because of the high proportion of phenylethynyl (PE) end-groups that could participate in ethynyl-ethynyl chain extension reaction in PETI-A 2000. Whereas, PETI-A 9000 had lower amount of PE end-groups relative PETI-A 2000, to which extension was severely limited as a result of a rapid increase in viscosity upon curing. Consequently, the major products of the high molecular weight imide oligomer were found to be cyclic aromatics.

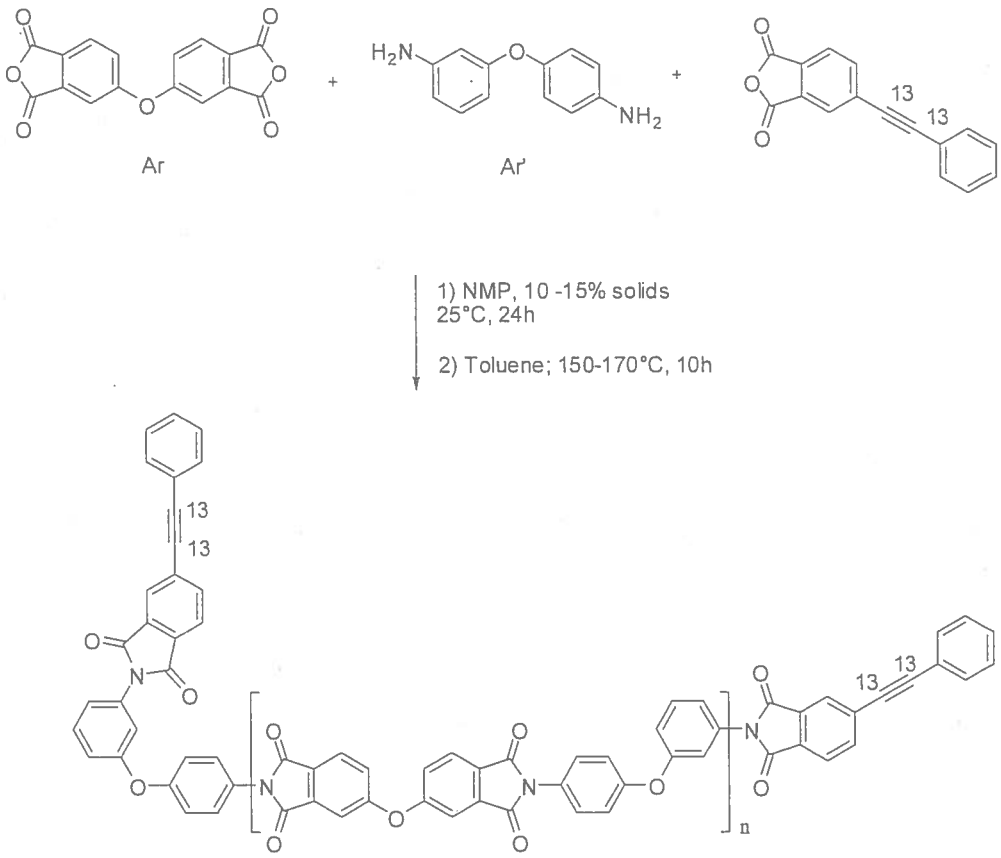

Figure 18. PETI-A 2000 g/mol and 9000 g/mol

2.4 Cure Kinetics of Phenylethynyl Compounds

A variety of analytical tools, including Fourier transform infrared spectroscopy (FTIR), differential scanning calorimetry (DSC), HPLC, ^{1}H and ^{13}C NMR, and melt rheology have been used to monitor the cure kinetics of PETI resins.[95,97-99] Takekoshi et al. determine the kinetics of the thermal conversion of 3PEA/PA and PEPA/An by monitoring the disappearance of the reactants via HPLC (see Figure 16).[95] When the high speed civil transport (HSCT) program was examining the NASA developed the PETI-5 imide oligomer as resin matrix, infrared spectroscopy was used to study the cure

kinetics for a simple model compound, analogous to the PETI-5 imide. Model compound, PEPA-3,4′ODA, Figure 17, exhibited first-order kinetics upon cure for the entire reaction time when monitored by the disappearance of the ethynyl groups at various temperatures.[98] Pickard et al. investigated the kinetics and mechanism of bulk thermal polymerization of 3-phenoxyphenyl acetylene (Figure 19), and determined a first order reaction with 20 – 60% conversion over the temperature range 127- 327 °C, via temperature ramp DSC.[97] However, reaction orders were found by isothermal DSC experiments to be 2.3 to 2.9 for first 50% of the reaction, over the temperature range of 220-267 °C.

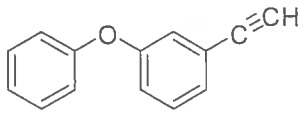

Figure 19. 3-phenoxyphenyl acetylene

In another study, Wright and Schorzman studied key model compounds: N-phenyl-4-(1-naphthylethynyl)phthalimide and N-phenyl-4-phenylethynylphthalimide, and observed that the thermal cure kinetics best fit a first-order rate law, based on DSC studies (Figure 20).[99] The study also determine that the reaction rate of reaction for N-phenyl-4-(1-naphthylethynyl)phthalimide was faster than N-phenyl-4-phenylethynylphthalimide.

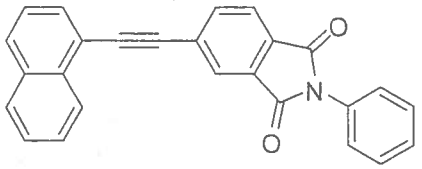

N-phenyl-4-(1-naphthylethynyl)-phthalimide

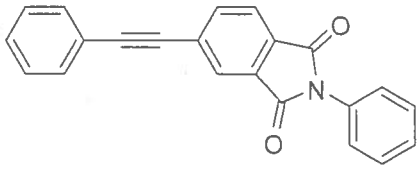

N-phenyl-4-phenylethynylphthalimide

Figure 20. N-phenyl-4-(1-naphthylethynyl)-phthalimide and N-phenyl-4-phenylethynylphthalimide.

Using melt rheology, Bullions developed a two-stage, dual-Arrhenius rheology model to calculate the activation energy for the cure phenylethynyl-terminated Ultem™ type poly(etherimide) (PETU), Figure 21.[100] The cure reaction on the ethynyl groups followed first-order reaction kinetics, which agreed well with DSC measurements of the same system.[101]

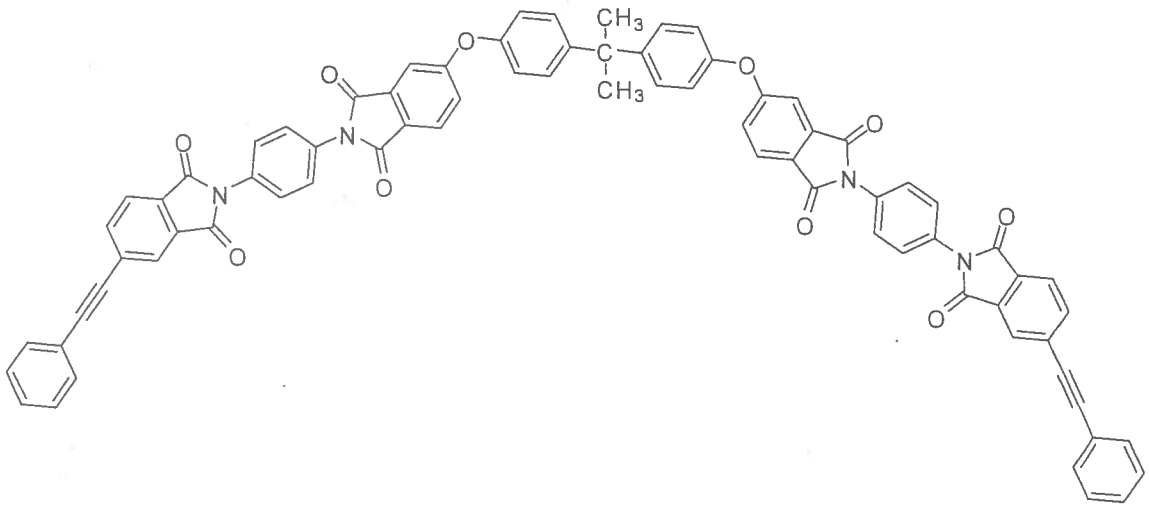

Figure 21. PETU Ultem™

2.5 Properties of Zeolites

Zeolites are crystalline aluminosilicates materials that have a three-dimensional framework structure that forms uniformly sized pores of molecular dimensions with

interconnecting channels or cavities.[20] Well know zeolites in their pure form, have perfect crystalline structures and possess only micropores; less than > 2 nm.[102] However, the range of their pores can be expanded to sizes greater than 50 nm via soft and hard template synthesis.[103-106] When the pore diameters are between 2 nm and 50 nm, the materials are categorized as mesoporous, and materials with pore diameters larger than 50 nm are macroporous. Zeolites can also have a combination of pores sizes, such as micro-mesoporous materials.

The primary building units for the zeolites framework are the SiO_4 and AlO_4^- tetrahedra connected by sharing one oxygen atom that is positioned between two tetrahedra. These building units are responsible for producing a three-dimensional framework containing channels and cavities of molecular dimensions. The framework is neutral, but if a silicon atom (Si^{4+}) is substituted by an aluminum atom (Al^{3+}), the framework then becomes negative. Therefore, metal cations (e.g. Li^+, Na^+, K^+, Ca^{2+}, Sr^{2+}) sit in the channel or cavity to preserve eletronuetrality while also forming a weak Lewis acid site.[30-32]

2.6 Catalytic Behavior of Zeolites

Sometimes, in place of cations, hydroxyl protons acting as Brønsted acid sites, i.e., proton donors can balance the negative charge. The hydroxyl proton is located on oxygen bridges, connecting a tetrahedrally coordinated silicon and aluminum atom within the framework. As a result of the negative charge being balanced by metal cations or hydroxyl protons, the zeolitic framework now has weak Lewis acid sites and strong Brønsted acid sites. Furthermore, there is evidence of strong Lewis acid sites due to framework defects and extra-framework aluminum (Al) or EFAL species as a result

tricoordinated or partially dislodged aluminum centers within the pores or on the surfaces of the zeolites.[33,35] Thereby zeolites may contain both strong Brønsted and Lewis sites.[107]

There have been reports of EFAL Lewis sites interacting with Brønsted sites to enhance Brønsted acidity, subsequently forming superacids.[108-111] Lago et al. demonstrated improvement in catalytic activity of *n*-hexane cracking using zeolite H-ZSM-5, upon mild steaming.[109] A possible explanation of this behavior is the partial hydrolysis of framework aluminum tetrahedra in the vicinity of bridging OH groups due to mild steaming. These partially hydrolyzed framework aluminum tetrahedra are viewed as strong electron-withdrawing sites for the neighboring bridging OH groups, thereby decreasing the amount of energy of deprotonation and increasing the strength of the Brønsted acid sites, i.e., exerting an indirect effect on the catalytic activity of Brønsted acid sites.[109]

The accessibility of these Brønsted and Lewis sites are governed by the surface area of these microporous materials, in which the surface area is related to the zeolites catalytic activity properties.[20] When the Bronsted and Lewis acid sites are available the zeolites are able to participate in many different chemical reactions, including the following: Freidel-Crafts acylations and alkylations, oxidations, and catalysis of 'ene' and Diels-Alder reactions.[112-120]

CHAPTER 3

EXPERIMENTAL SECTION

3.0 Materials.

PETI GRC- resin and 2,3,3′,4′-tetramethylbenzophenone were provided by NASA Glenn Research Center (Cleveland, OH). GRC-A resin was prepared from 4,4'-bisphenol A dianhydride, 2,2′-bis[4-(4-aminophenoxy)phenyl]propane, and 4-phenylethynylphthalic anhydride in a 1: 2: 2 mole ratio, and by heating above 210 °C for 1 h and subsequently grounded into powders. Zeolite L in the K^+ form and zeolite Y in the Na^+ were purchased form CU Chemie Uetikon AG. Carbon tetrachloride (CCl_4) (99%), dichloromethane (CH_2Cl_2) (99.5%), chloroform ($CHCl_3$) (99.8%), N,N-Dimethylformamide (DMF) (99.8%), were used as received from Acros. Sodium nitrate and ammonium nitrate were purchased from and used as received Fisher Scientific.

3.1 Ball Milling as Received GRC-A.

As-received GRC-A (10.0 g) was placed into a Roalox alumina-fortified mill jar containing twenty 13 x 13 mm ceramic cylinders. The mill jar was securely sealed with the fitted top and gasket and placed on a US Stoneware ball mill at 100 RPM for 4 h. After ball-milling 4 h approximately 5-7 g of the GRC-A was collected using a plastic spatula. Additional samples of GRC-A were ball milled for 8 and 24 h.

3.2 Ball Milling GRC-A with Zeolite L for 4 h.

Approximately a 10.0 g mixture of 0.5 wt% zeolite L in GRC-A was prepared by combining 9.950 g of as-received GRC-A and 0.050 g of zeolite L in the K^+ form. The mixture was then transferred into a mill jar with twenty 13 x 13 mm ceramic cylinders the jar then was placed on ball mill for 4 h at 100 RMP. This procedure was then repeated in a similar manner for 1, 2, and 4 wt% GRC-A with zeolite L.

3.3 Mixing of GRC-A and GRC-A with Zeolite L in $CHCl_3$.

As received GRC-A (5.0 g) and chloroform (250 mL) were added to 500 mL round bottom flask fitted with a reflux condenser, and heated under reflux with stirring for 4 h. After 4 h, the mixture was cooled to room temperature and the solvent removed under reduced pressure using a rotary evaporator. The flask was then placed in a vacuum oven overnight at 75 °C to remove any residual solvent. Samples of GRC-A with 0.5, 1.0, 2.0 and 4 wt% of zeolite L were prepared in a similar manner.

3.4 Dry Mixing GRC-A with Zeolites L and Y.

As-received GRC-A (4.975 g) and zeolite L in K^+ form (0.025 g) were added to a 50 mL centrifuge tube was then secured on a Wrist Action Shaker model #75, and then shaken at75 - 100 shakes/min for 4 h. Samples of GRC-A with 0.5, 1.0, 2.0 and 4 wt% of zeolites L and Y were prepared in a similar manner.

3.5 Dry Mixing Ground Zeolite L and Cured GRC-A with GRC-A.

Approximately 500 mg of zeolite L and 500 mg of cured GRC-A were ground, separately, in a Crescent WIG-L-BUG for 5-7 min. Dry mixed samples were prepared with ground zeolite L and ground cured GRC-A to yield 0.5 wt% and 4.0 wt% mixtures.

3.6 Cationic Exchanging Na^+ and H^+ ions with K^+ ions in Zeolite L.[121]

Zeolite L in K^+ form (500 mg) and 50 mL of 0.500 M sodium nitrate $NaNO_3$ were added to 100 mL round bottom flask with a reflux condenser and refluxed with stirring for 4 h. The mixture was cooled to room temperature and filtered. The zeolite L was air dried for 24 h, and the ion exchange process repeated. After the second exchange, the recovered zeolite was placed in a porcelain crucible and calcined at 550 °C for 1 h. In a similar manner, zeolite L in the K^+ form was also ion exchanged to the H^+ form, using 0.500 M ammonium nitrate NH_4NO_3 in place of the $NaNO_3$ solution.

3.7 Fabrication of Cured Plaques GRC-A and GRC-A/Zeolite.

Approximately 25 g of powdered dry mixed as received GRC-A was transferred to a steel mold with dimensions of 8 x 8 x 0.3 cm, that had previously been treated with Freecoat™, and placed on hot plate pre-heated to 300 °C. As the resin melted it was stirred carefully to remove bubbles. The top was placed on the mold and it was transferred to an autoclave that had been pre-heated to 288 °C. The autoclave was pressurized to 100 psi and heated to 371 °C at 5 °C/min, and held for one hour. The autoclave was cooled slowly to room temperature and de-pressurized. The neat resin plaque was then removed from the tool and characterized as described below. Cured plaques of GRC-A with 0.5, 1.0, 2.0 and 4 wt% of zeolites L were prepared in a similar manner.

3.8 Determining the Percent (%) Strain for Rheological Measurements.

Rheological measurements were conducted on a TA Instruments AR G2 rheometer. Dynamic rheological data was collected using circular parallel aluminum plates (diameter = 25 mm). Samples were prepared by pressing 1.0 g of GRC-A powder into 25 x 1.0 mm disks under a pressure of 13,000 psi for 1-3 min in a steal die.

Temperature ramp experiments were carried out at 5° C/min from 50 to 400 °C. A series of experiments were carried out with varying strain rates from 0.025% to 25%. Based upon analysis of these experiments, a shear strain rate of 20% and an oscillation frequency of 6.283 rad/sec, were selected for the rest of rheological measurements.

3.9 Isothermal Rheology Measurements and Kinetics Studies on Neat GRC-A and GRC-A with Zeolites.

Based on the results from the rheology temperature sweep measurements, isothermal rheology measurements were carried out to study the effect of temperature on the curing of the neat GRC-A resin at 300, 315, and 330 °C. GRC-A with 0.5, 1, 2, and 4 wt% for zeolite L and Y were studied in a similar manner.

3.10 Differential Scanning Calorimetry (DSC).

The DSC of neat GRC-A was recorded using a TA Instruments DSC Q 2000 series analysis system. DSC data was collected by weighing 5 to 7 mg of sample into aluminum pans which were then hermetically sealed. The cure cycle consisted of four individually temperature ramp experiments carried out at 3, 5, 7, and 9 °C/min from 50 to 450 °C under nitrogen with a flow rate of 50 mL/min. The glass transition temperatures were then obtained by following each cure cycle with a heating ramp at 20 °C/min, a cooling ramp and another heating step at 20 °C/min. The glass transition temperature was determined by finding the temperature at half height between the onset and end of the transition using the TA Universal Analysis software. The activation energy for cure was obtained from the four temperature ramp experiments using ASTM E 698-05 method.[122] The same procedure was then carried out in a similar manner with 0.5, 1, 2, and 4 wt% GRC-A for both zeolite L and Y.

3.11 Isothermal DSC Measurements and Kinetics Studies on Neat GRC-A and GRC-A with Zeolites.

DSC samples were prepared as described above. The DSC furnace was preheated to 285 °C prior to sample insertion. The DSC instrument started to record data when the furnace reached the set temperate. Data was then recovered for 4 h. This test was repeated with new samples at 300 °C and 315 °C. Samples of GRC-A with 0.5, 1.0, 2.0, and 4.0 wt% zeolite L were measured in similar manner.

3.12 Thermogravimetric Analysis (TGA).

TGA experiments were carried out on cured specimens GRC-A on a TA Instruments TGA Q 50 series analysis at heating rates of 3, 5, 7, and 9 °C/min under nitrogen and oxygen atmospheres at flow rates of 60 mL/min from 25 to 450 °C. The cured samples, 10 to 15 mg, were placed in a platinum sample holder prior to thermo-oxidative studies. Samples of GRC-A with 0.5, 1.0, 2.0, and 4.0 wt% zeolite L and Y were measured in similar manner.

3.13 Dynamic Mechanical Thermal Analysis (DMTA).

DMTA studies were carried out on a TA Instruments AR G2 rheometer on cured rectangular samples of neat GRC-A, with dimensions of 30 x 6.5 x 3.5 mm machined from the cured plaques described above. The neat GRC-A sample were securely placed between rectangular fixtures. The temperature ramp was 5° C/min from 50 to 400 °C. All experiments were carried out at 6.283 rad/sec and 0.05 percent strain. Samples of GRC-A with 0.5, 1.0, 2.0, and 4.0 wt% zeolite L and Y were measured in similar manner.

3.14 Thermomechanical Analysis TMA.

TMA expansion and penetration studies were carried out on a TA Instruments TMA Q 400 series on cured GRC-A square samples with approximate dimensions of 4 x 4 x 3 mm machined from the cured plaques described above. The samples were securely place on the sample holder and a 0.020 N force was applied to the sample, followed by a temperature ramp of 3 °C/min to 400 °C. Samples of GRC-A with 0.5, 1.0, 2.0, and 4.0 wt% zeolite L and Y were measured in similar manner.

CHAPTER 4

RESULTS AND DISCUSSION

4.0 Overview

Zeolites L and Y were incorporated in PETI resin GRC-A via ball-milling, solution, and dry-mixing in order to determine the optimum method for incorporation and the effect of these porous materials have on the melt rheology, cure kinetics, and cured composite properties.

4.1 PETI GRC-A Resin

PETI GRC-A resin as received from NASA Glenn was formulated from 4,4'-bisphenol A dianhydride, 2,2'-bis[4-(4-aminophenoxy)phenyl]propane, and 4-phenylethynylphthalic anhydride in a 1:2:2 mole ratio, see Figure 22. GRC-A imide oligomers were prepared by melting and heating these components to 210 °C for 1 h, cooling to room temperature, and then subsequently ground into powders GRC-A is polydispersed, i.e., having a range of molecular weights, and GPC data indicated a number average molecular weight of $1.9x10^3$ g/mole. PETI resins like GRC-A were designed to be a mixture of various molecular weight oligomers that provide for low melt viscosity. The gel permeation chromatography (GPC) results for representative batches of GRC-A are presented in Figure 23 and clearly show that the samples contain at least five different oligomers. GRC-A can be melt processed and then cured into a high performance polyimde.[123]

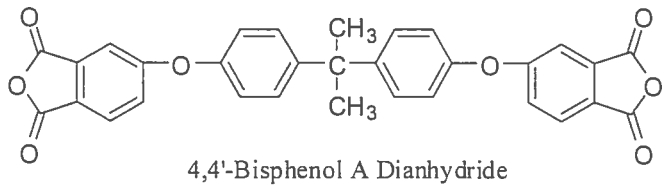

4,4'-Bisphenol A Dianhydride

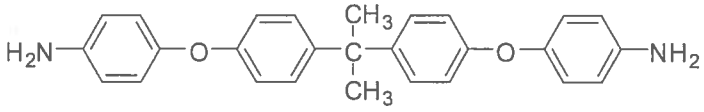

2,2'Bis[4-(4-aminophenoxy)phenyl]propane

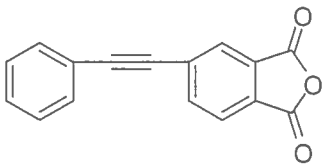

4-Phenylethynylphthalic anhydride

↓ 210 °C for 1 h

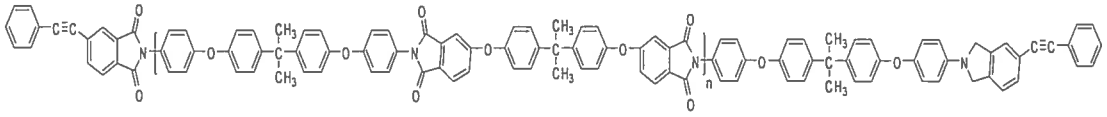

Figure 22. Formulation of GRC-A.

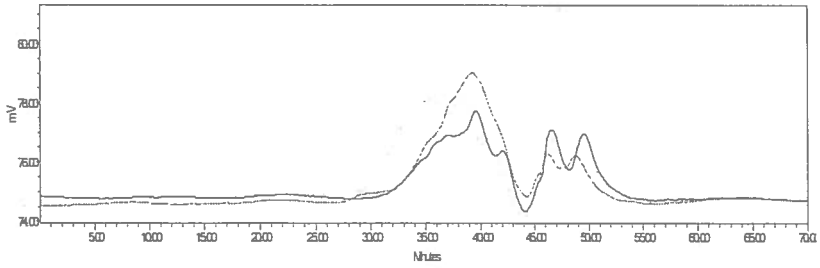

Figure 23. The GPC data for the various lots of GRC-A, showing the polydispersity. Light Blue is lot 1; Black is lot 2, and Pink is lot 3.

4.2 Zeolites L and Y

The properties of zeolite L and Y are summarized in Table 1 and Figure 24 shows the scanning electron micrographs (SEMs) of zeolites L and Y used in this study. In the SEMs, zeolite L is shown to be composed of uniformly cylindrical particles while zeolite Y is composed of clusters spherically particles. Figure 25 gives a schematic diagram of the cross section of the channels in zeolites L and Y. Zeolite L has one-dimensional channels that lead to cavities while zeolite Y has three-dimensional, also leading to cavities.[20,112]

Table 1. Zeolite L and Y Properties and Characteristics

Zeolite	L	Y
SAR Value[a]	3	2.32
Aspect Ratio	2.0	1.5
Cation	K^+	Na^+
Tetrahedra[b]	12	12
Pore Size	Large	Large
Pore Dimensions (Å)	7.1	7.4
Channel Dimensionality[c]	1 R	3R
Surface Area ($Å^2/g$)	1205.	3556.
Volume ($Å^3$)	2153.	14428.
Topological density (g/cm^3)	0.619048	0.476190

[a] Typical SAR values for zeolite L and Y. SAR (Silicon to Aluminum Ratio)
[b] Tetrahedra correlated to the building units, SiO_4 and AlO_4 that leads to the channel system.
[c] R means dimensionality.

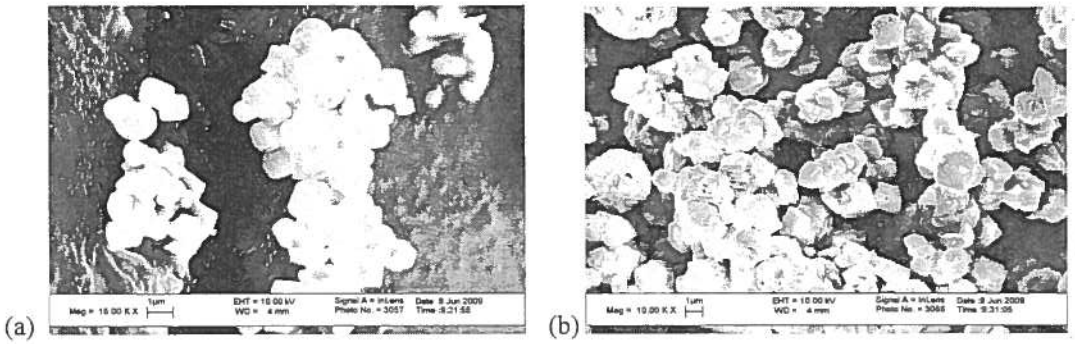

Figure 24. SEMs of zeolites: (a) L and (b) Y

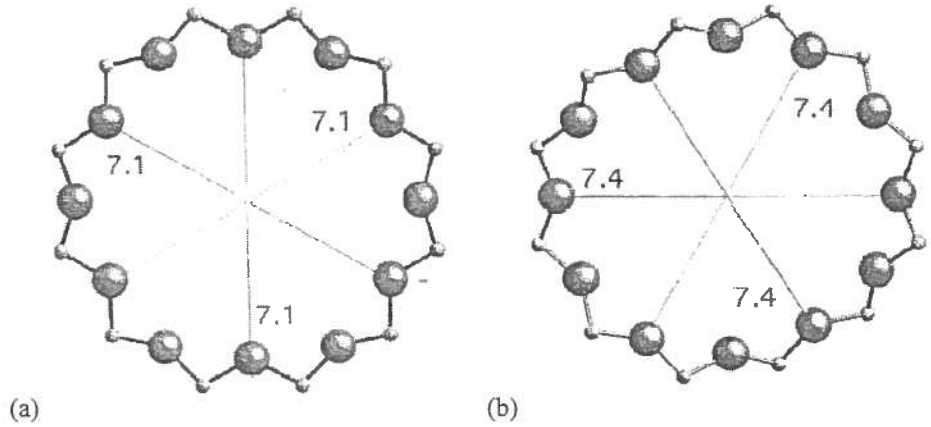

Figure 25. The dimensions of the channels of zeolites in nanometers (a) L and (b) Y.[124]

4.3 Determining the Rheological Properties of Viscoelastic Materials

We have used rheology to study the viscoelastic behavior of PETI GRC-A as a function of time, temperature, and zeolite loading. Rheology is the study of the way a material responds (i.e., deformation and flow) when forces are applied to them. Isaac

Newton was the first to express the viscosity of an ideal linear (Newtonian) fluid with equation 1.[125]

$$\tau = \eta \gamma \qquad \text{Eq 1}$$

Rearranging equation 1, viscosity is then defined as:

$$\eta = \tau/\gamma \qquad \text{Eq 2}$$

where τ is the shear stress (force) applied tangentially to sample, causing deformation; η is viscosity (measure of the resistance to continuous deformation) and γ is shear rate (rate of change in the shear strain per unit time, as a result of the force being applied). Equation 1 shows a linear relationship of shear stress versus shear rate, with the viscosity being the proportionality constant between the two. For a Newtonian fluid, the viscosity of the material remains constant, and does not depend on the shear rate. However, for viscoelastic materials, such as GRC-A, the relationship between shear stress and the shear rate was found to be nonlinear. These materials are call non-Newtonian, because the viscosity of these materials varies in a non-linear manner as function of shear rate. Equation 3 gives the viscosity as a function of shear rate:[125]

$$\eta(\gamma) = \tau/\gamma \qquad \text{Eq 3}$$

4.4 Flow and Elastic Behavior of PETI GRC-A as Function of Percent (%) Strain

The relationship between the viscosity, η, and shear modulus, G, is used to characterize viscoelastic materials. Oscillatory rheology has been widely used to determine this relationship in terms of complex viscosity, η^*, and complex modulus, G*, as described in Equation 4.[125]

$$\eta^* = G^*/\omega \qquad \text{Eq 4}$$

Where $G^* = G'(\omega) + iG''(\omega)$. G' is elastic modulus (solid-like behavior) and G" is the viscous modulus (liquid-like behavior) of the material and ω is angular velocity.

In this study, the complex viscosity was determined at various applied strains, in order to determine the optimum strain for studying the melt rheology as a function of time and temperature. Figure 26, shows the complex viscosity, η*, for neat GRC-A, as a function of temperature at percent strains between 0.025-25% .

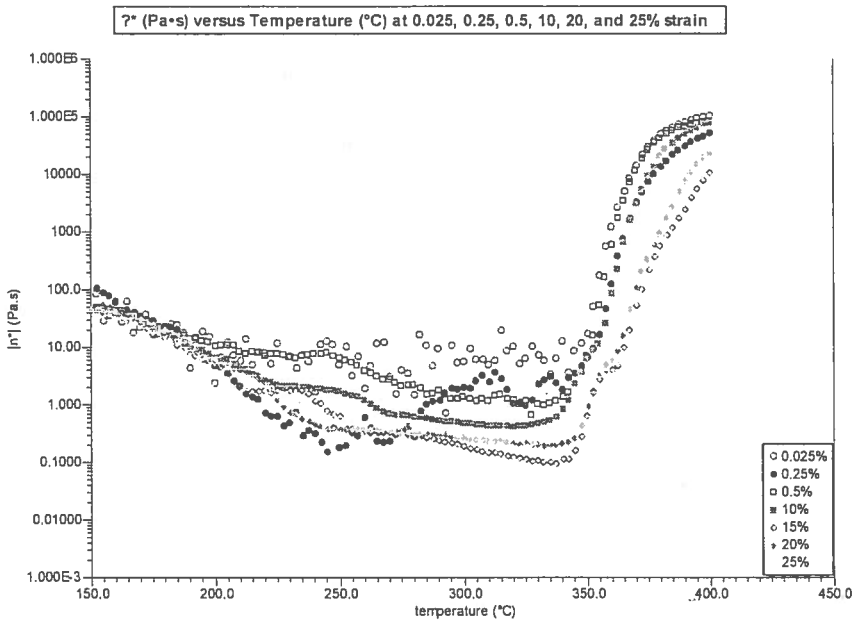

Figure 26. Complex viscosity, η*, as a function of temperature and percent strain for neat GRC-A.

Figures 27 and 28 give G' (elastic modulus) and G" (viscous modulus), respectively, as a function of temperature and percent strain. Based upon the data we determined that 20 percent strain yielded the best condition for carrying out our studies, because percent strains lowers than 20% demonstrated that the data will be noisy and non-reproducible.

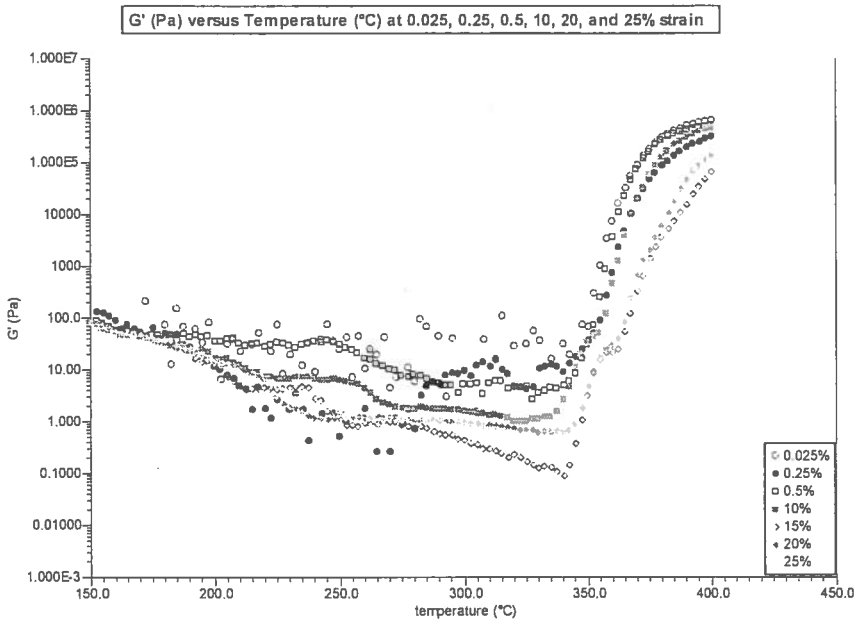

Figure 27. Elastic modulus, G', as a function of temperature and percent strain for neat GRC-A.

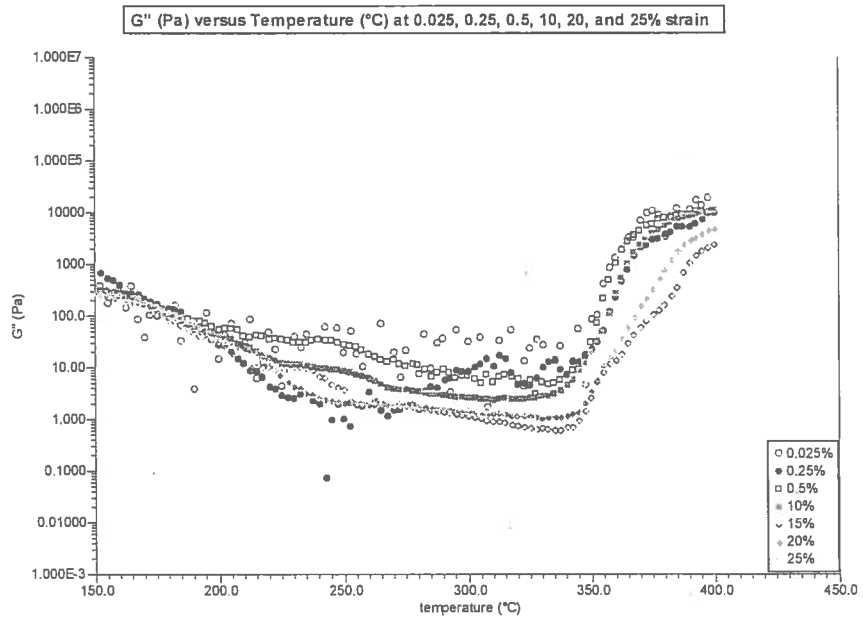

Figure 28. Viscous modulus, G", as a function of temperature and percent strain for neat GRC-A.

4.5 Chemorheology for Neat GRC-A

Chemorheology is the study of viscoelastic behavior of chemical reacting thermosetting systems such as GRC-A.[126] Figure 29 is a plot of complex viscosity, η*, vs. temperature for neat GRC-A when heated at 5 °C/min, and with a 20% strain. The viscosity curve of neat GRC-A illustrates: 1) melting at ~ 187 °C; 2) GRC-A completely melted at ~ 237 °C; and 3) the minimum viscosity η* of 0.57 Pa·s; at 315 °C; further heating leads to increase in viscosity, resulting from the curing of the resin and network formation.

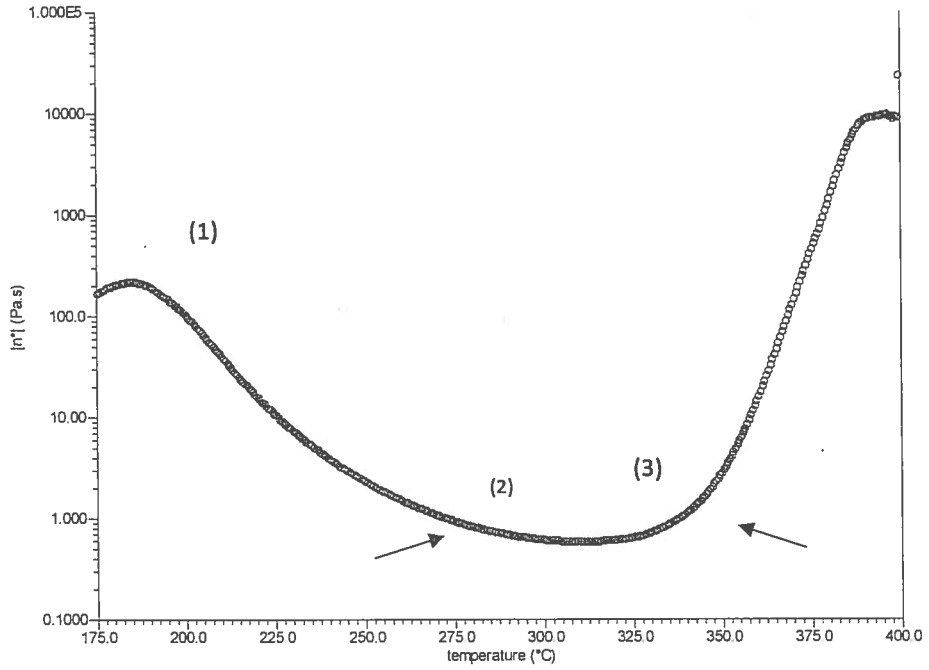

Figure 29. Complex viscosity, η*, versus temperature for GRC-A, at a heating rate of 5 °C/min, and with a 20% strain. (1) initial melting of the resin, (2) decrease in η* with increasing temperature until it reaches a minimum viscosity, and (3) increase in η* during the curing stage.

Figure 30 gives the plot of G′ and G″ vs. temperature for GRC-A, which allows the determination of the crossover gel point, G_c, as the resin continues to cure via chain

elongation and cross linking. During the cure, viscosity rapidly increases and the polymer undergoes an almost instantaneous change from a liquid to a gel. The crossover gel point is defined as the time or temperature at which G′ = G″, indicating sufficient cross linking has occurred that the resin system behaves as an infinite network.[127-129] The crossover gel point for GRC-A was determined to be at 350 °C under these testing conditions. Beyond the gel point the viscosity and molecular weight diverge to infinity.

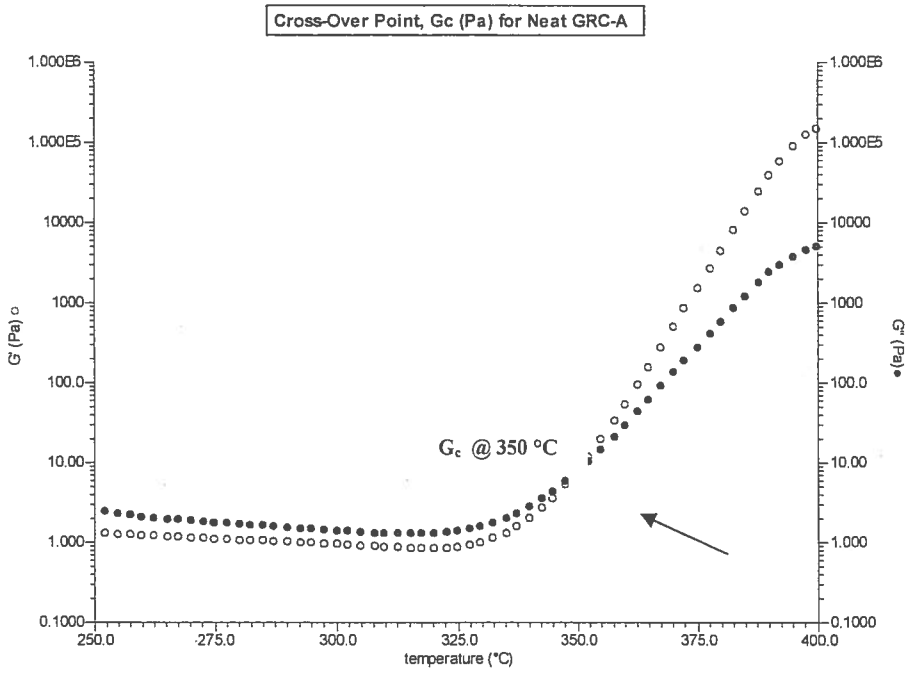

Figure 30. Plot of G' and G" vs. temperature for GRC-A at a heating rate of 5 °C/min, and with a 20% strain.

Below is a schematic description of the chemrheology behavior of a thermoset material, such as GRC-A, which undergoes chain elongation and cross linking, Figure 31. The initial chemical reaction begins with reactive pre-polymer monomers or oligomers, (a), which upon heating start to chain elongate and cross link, (b). Further heating leads

to more chain elongation and cross linking as shown in (c), with the eventual formation of an infinite irreversible network as shown in (d).[130]

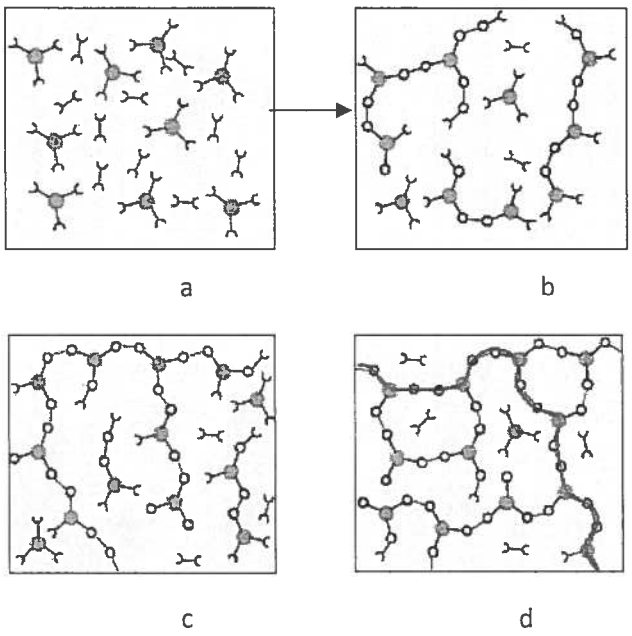

Figure 31. Schematic of representation of structural development during the cure of thermosetting resin.[130]

4.6 Chemorheology Studies for GRC-A Ball-Milled for 4, 8, and 24 h

Ghose et al. used ball milling to incorporate multi-walled carbon nanotubes (MWNTs) into PETI-330.[131] They reported that high resolution SEM images showed that this mechanical process did not appear to damage the nanotubes; however, transmission electron microscopy (TEM) did show that the length of MWNTs was reduced as result of the collision between the grinding media during the ball-milling process.[132] To develop a baseline for compression, we attempted to incorporate zeolites in to GRC-A via ball milling for various times.

GRC-A was ball milled for 4, 8, and 24 h, and then its melt rheology studied. Figure 32 shows plots of η^* vs, temperature for as received GRC-A and ball milled GRC-A, and Table 2 gives a summary of the initial melt rheology data. Interestingly, ball milling the GRC-A alone lead to a reduction in the minimum viscosity η^*_{min} from 0.25 Pa·s at 315 °C for the as received resin to ~0.10 Pa·s at 305 °C for the resin that had been ball-milled 4 h, and ~0.09 Pa·s at 295 °C for the resin ball milled for 8 and 24 h. This reduction in η^*_{min} may be due to reduction in particle size and better mixing of the various molecular weight fractions of GRC-A.

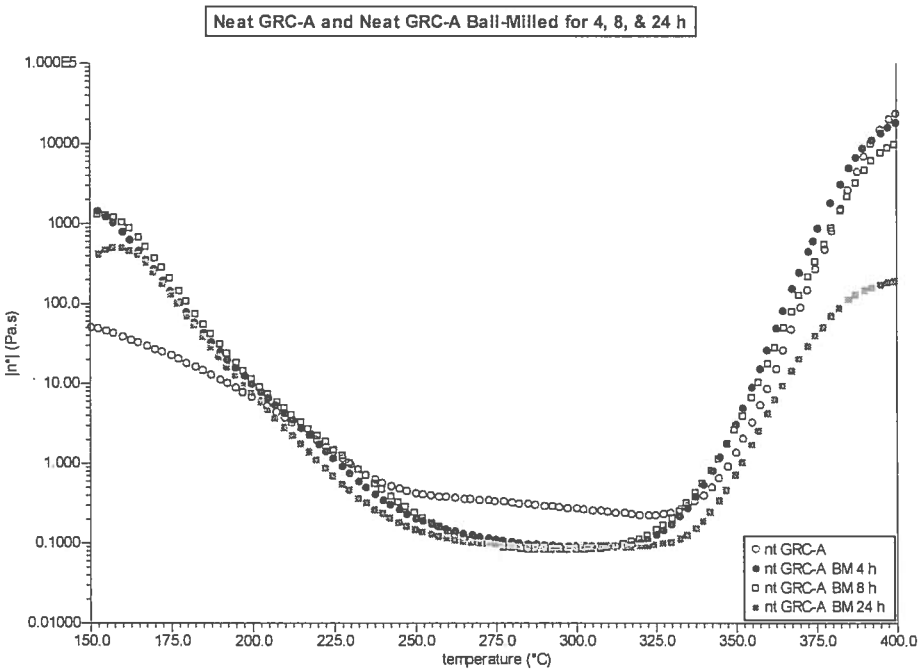

Figure 32. Complex viscosity, η^*,versus temperature of Neat GRC-A ball-milled for 4, 8, and 24 h at 5 °C/min and 20 % strain.

Table 2. Minimum viscosity, temperature at minimum viscosity, and the observed cross-over point of samples of neat GRC-A ball milled for 4, 8, and 24 h, 5 °C/min and 20% strain.

	minimum viscosity, (η^*_{min}) Pa·s	**T (°C) @ minimum viscosity (η^*)**	**G_c (°C)**
Neat As-Received	0.25	315	350
Neat GRC-A, BM 4	0.095	305	338
Neat GRC-A, BM 8	0.091	295	325
Neat GRC-A, BM 24	0.090	295	325

The GRC-A resin used in this study was prepared in three different lots. Initial melt rheology studies were conducted on Lot 1. Figure 23 on page 33, shows the GPC data for these three lots and Table 3 gives η^*, temperature at η^*, and G_c, for the three lots of GRC-A provided by NASA GRC. Based on the data, all future tests were carried out using Lots 2 and 3.

Table 3. Minimum viscosity, temperature at minimum viscosity, and the observed cross-over point of neat GRC-A as-received, for lots 1-3.

Neat GRC-A	**minimum viscosity, (η^*_{min}) Pa·s**	**T (°C) @ minimum viscosity (η^*)**	**G_c (°C)**
Lot 1	0.37 ± 0.024	315 ± 1.5	350 ± 1.3
Lot 2	0.73 ± 0.061	312 ± 1.8	349 ± 2.1
Lot 3	0.88 ± 0.046	314 ± 1.3	347 ± 2.7

4.7 Chemorheology Studies for GRC-A Ball-Milled with Zeolite L and Y

Based on the melt rheology data from the ball-milling results, it was decided to ball-mill GRC-A with zeolite L and Y for 4 h. As was the case with neat GRC-A, it was difficult to get high recovery of the mixed GRC-A/zeolite mixture from ball mill. Because of the high local forces generated by ball milling we examined the zeolite by

SEM to determine if the zeolite had been damaged during ball milling and if the samples recovered were representative of the materials that had been mixed. Figures 33 and 34 show the SEM images of the 2 % and 4 % GRC-A/zeolite L after ball milling for 4 h. Comparison these figures with Figure 24 of the as received zeolite L, show that the structure of some of the zeolites had been altered or collapsed during the ball-milling process. The integrity of the zeolite structure, which will be discussed later, is very important to the performance of the zeolite within GRC-A system.

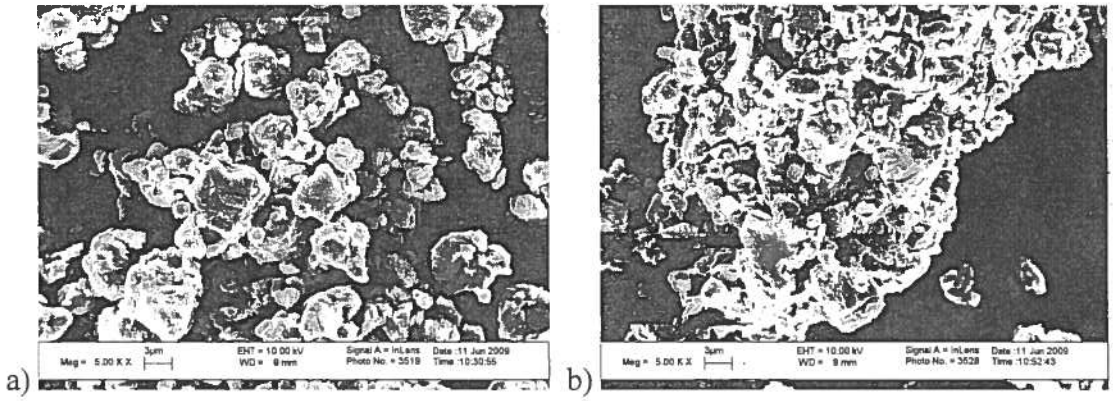

Figures 33. SEM of GRC-A BM with a) 2.0 and b)4.0 wt%; magnified 5.00K x 3μm

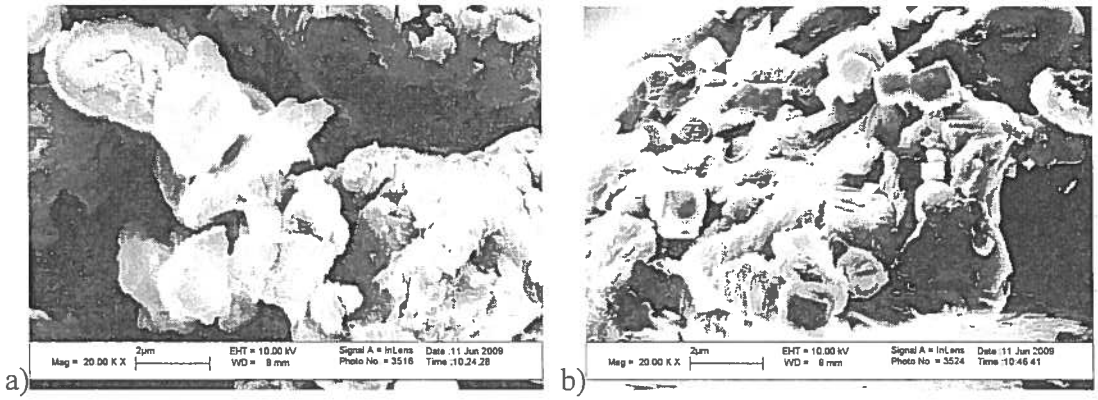

Figure 34. SEMs of GRC-A BM with a) 2.0 and b) 4.0 wt%; magnified 10.00K x 3μm

Samples of GRC-A/zeolite L mixtures recovered from ball milling were cured at 371 °C for 1 h and then subjected to thermogravimetric analysis to determine how closely the percentage of zeolite L in the recovered samples corresponded to the prepared mixtures. Figure 35 shows the weight loss of these samples upon heating at 10 °C/min to 900 °C and Table 4 summarizes this data.

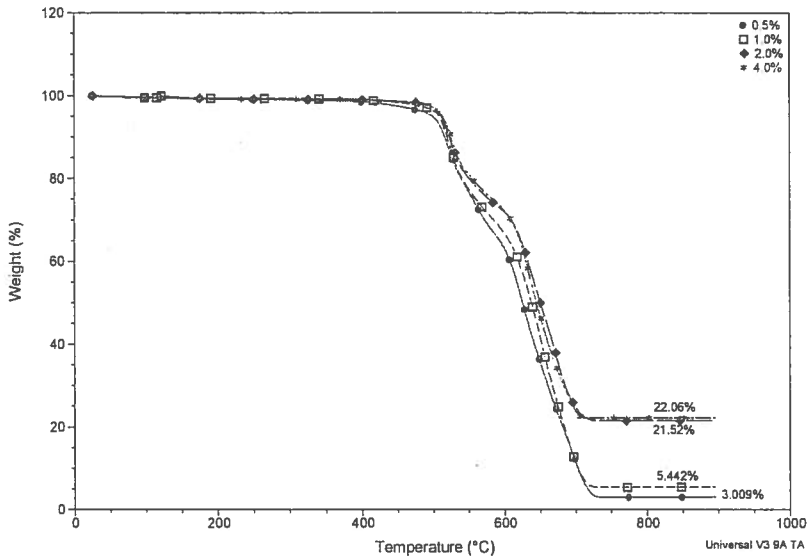

Figure 35. TGA curves with at ramp rate of 10°C/min in air for GRC-A loaded with zeolite L via ball-milling.

Table 4. Percent weight of zeolite L mixed with GRC-A, and percent weight determined by TGA in the recovered mixtures from GRC-A/zeolites mixtures prepared by via ball milling 0.5, 1.0, 2.0, and 4.0 wt% zeolite with GRC-A.

Wt % of zeolite L Ball-Milled with GRC-A	**Cured Material (%)**
0.0	0.0
0.5	3.01
1.0	5.44
2.0	21.52
4.0	22.06

Plots of η* versus temperature for neat GRC-A, and GRC-A/zeolite L mixtures prepared by ball milling are given in Figure36. Table 5 gives the minimum η*, temperature at minimum η*, and temperature at G_c. It was observed that the cross-over point, minimum viscosity, and temperature at minimum viscosity increased in the samples containing zeolite relative to the neat resin. The curing section of the η* vs. temperature curve for GRC-A, loaded with zeolite L, shifted to higher temperatures than the neat resin alone. Thus, zeolite L appeared to retard the cure reaction of the phenylethynyl groups. GRC-A loaded with 3 and 5.4 wt% zeolite L exhibited similar curing curves, in addition to shifting the onset of cure approximately 13 to17 degrees higher, when compared to the neat resin. Likewise, higher loadings of zeolite L, 21.5 wt% and 22.1 wt% shifted the curing an additional ~13 degrees higher than lower loading of zeolites. This shift to higher onset of curing to higher temperature widens the operating window for additional processing of the resin via RTM or VARTM, making the addition of zeolites to resins an attracting attribute for processing.

Table 5. Minimum viscosity, temperature at minimum viscosity, and observed gel points of samples of neat GRC-A and GRC-A with zeolite L, by ball milling for 4 h.

Wt % zeolite L in GRC-A ball milled	**Wt % zeolite in GRC-A as measured**	**minimum viscosity, (η*) Pa·s**	**T (°C) @ minimum viscosity (η*)**	**G_c (°C)**
Neat	neat	0.82	313	350
0.5	3.0 %	1.0	326	349
1.0	5.4 %	0.91	330	365
2.0	21.5 %	0.86	342	372
4.0	22.1%	0.68	343	375

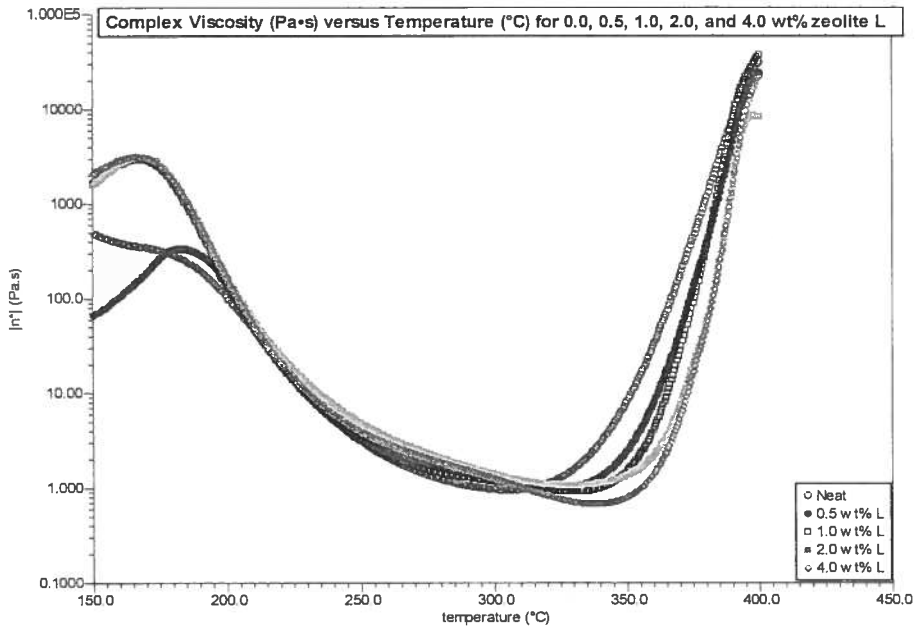

Figure 36. Complex viscosity η* vs. temperature for sample of GRC-A and GRC-A with 0.5, 1.0, 2.0, and 4.0 wt% zeolite L ball-milled for 4h.

4.8 Melt Rheology for Solution Mixing of GRC-A with Zeolite L

Since we found the ballmilling damaged the zeolites an yielded recovered material not representative of the initial mixture, we attempted to incorporate zeolites into GRC-A via solution mixing. Fillers and nanostructured fillers have previously been incorporated into polymers via solvent processing.[61] We examined several of solvents including N,N-dimethylformamide, carbon tetrachloride, dichloromethane and chloroform, for the dissolution of GRC-A and incorporation of zeolite L. Chloroform gave the best results for dissolution of GRC-A, and the solvent subsequently used for incorporating zeolite L into GRC-A. Five grams of GRC-A was dissolved in 250 mL of $CHCl_3$ and the desired amount of zeolite was L added to give 0.5, 1.0, 2.0, and 4.0 wt%

loading. The suspension was heated to reflux of for 4 h with rapid stirring. The mixtures were cooled to room temperature and the solvent removed on a rotary evaporator. Figure 37 below gives the SEM images of GRC-A loaded with 2 wt% and 4 wt% zeolite L, prepared by solvent mixing. The photomicrograph reveals that zeolite L is well dispersed in the GRC-A and has been coated the GRC-A.

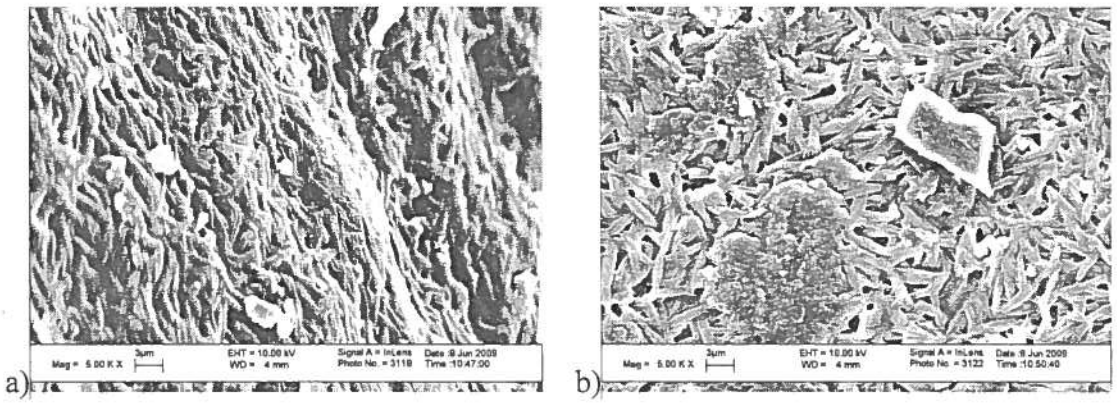

Figure 37. SEMs of GRC-A with 2.0 wt% (a) and 4.0 wt% (b) zeolite L that had been solvent mixed; magnified 5.00K x 3μm

In figure 38 shows η* vs. temperature for as received GRC-A and GRC-A that had been refluxed in $CHCl_3$ for 4 hours followed by rotary evaporation of the solvent. It was observed that the minimum viscosity for the processed sample is lower than the as received GRC-A, and that the rapid decrease in melt viscosity starts a higher temperature and the gelation occurs at a lower temperature than the as received GRC-A. This behavior may reflect that the solvent processing has changed the chemistry and intimacy of the mixture of the various molecular weight oligomers.

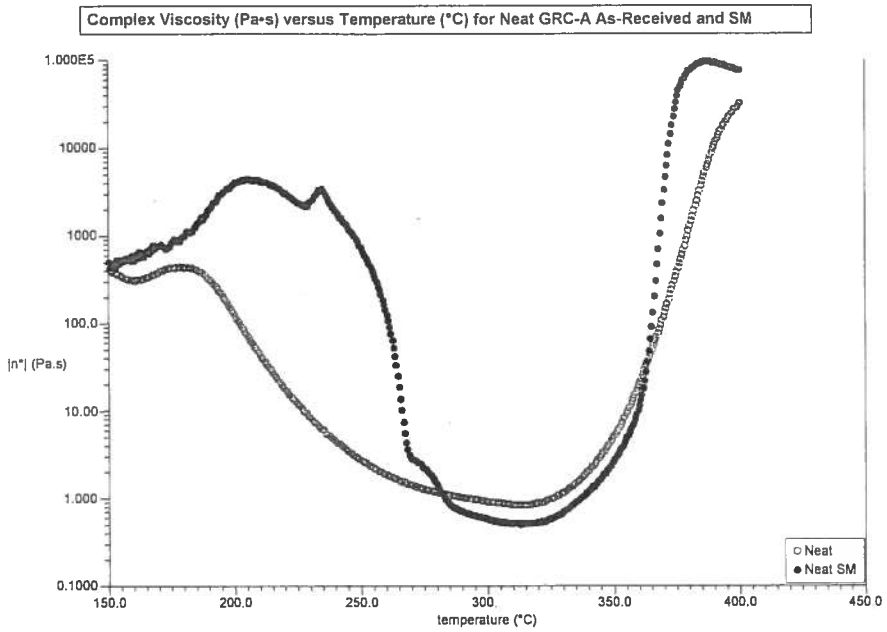

Figure 38. Complex viscosity η* vs. temperature for samples of neat GRC-A as received, and GRC-A refluxed in $CHCl_3$ for 4h and then recovered.

Table 6. Minimum viscosity, temperature at minimum viscosity, and observed gel points of samples of neat GRC-A and GRC-A with 0.5, 1.0, 2.0 and 4.0wt% zeolite L; using the solution method.

GRC-A/Zeolite L by mixing in $CHCl_3$	**minimum viscosity, (η*) Pa·s**	**T (°C) @ minimum viscosity (η*)**	**G_c (°C)**
Neat	0.59	312	367
0.5 wt%	1.51	319	355
1.0 wt%	1.36	315	356
2.0 wt%	1.30	317	353
4.0 wt%	1.44	326	360

4.9 Melt Rheology for Dry Mixing of GRC-A with Zeolites

As a result of the issues presented with ball-milling and solvent mixing, zeolite L was incorporated in GRC-A by simple dry mixing using a wrist shaker. Figure 39 shows the SEMs for GRC-A which were been dry-mixed with 2.0 and 4.0 wt% zeolite L. These

photomicrographs show that the zeolite is well distributed in the GRC-A, and that zeolite L remained intact.

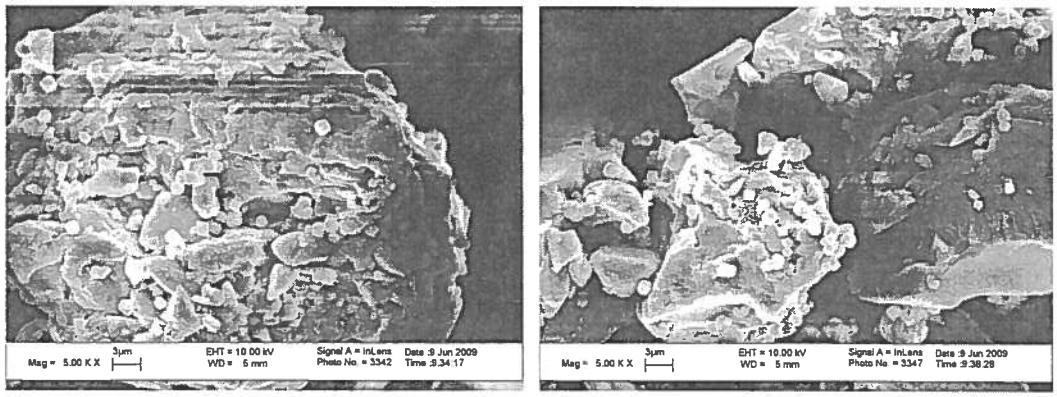

Figure 39. SEM images of GRC-A dry mixed with a) 2.0 wt% and b) 4 wt% zeolite L; magnified 5.00K x 3µm.

Samples of GRC-A/zeolite L prepared by dry mixing were cured at 371 °C for 1 h and then subjected to thermogravimetric analysis to determine how closely the percentage of zeolite L in the recovered samples corresponded to the prepared mixtures. Figure 40 shows the weight loss of these samples upon heating at a rate of 10 °C/min to 900 °C, and Table 7 summarizes this data. In contrast to ball milling, samples of GRC-A/zeolite L prepared by dry mixing were found by TGA to be in good agreement with what was initially mixed.

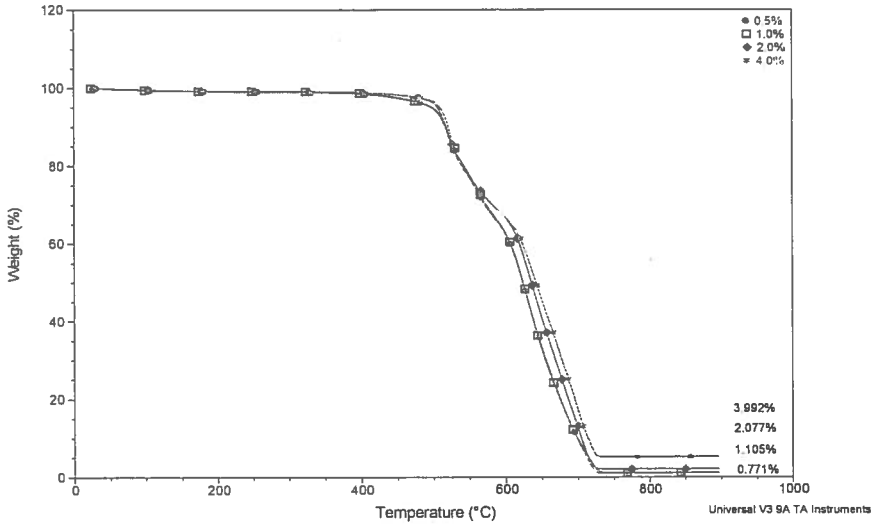

Figure 40. TGA curves for GRC-A loaded with zeolite L via dry-mixing at 10°C/min in air.

Table 7. TGA results of GRC-A loaded with zeolites 0.5, 1.0, 2.0, and 4.0 wt% zeolite L dry-mixed for 4 h

Wt% of zeolite L Dry Mixed with GRC-A	**Cured Material (%)**
0.5 wt%	0.78
1.0 wt%	1.10
2.0 wt%	2.08
4.0 wt%	3.99

Figure 41 show the rheology curves for neat GRC-A and GRC-A dry-mixed with zeolite L. Table 8 gives the minimum η^*, temperature at minimum η^*, and temperature at G_c GRC-A dry-mixed with zeolite L. It can be clearly observed from Figure 41 that the onset of cure is shifted to higher temperature when zeolite L is incorporated into GRC-A. This may result from zeolite L simply acting as a filler and slowing the reaction

chemistry between the phenylethynyl end groups, thereby preventing chain elongation and crosslinking.

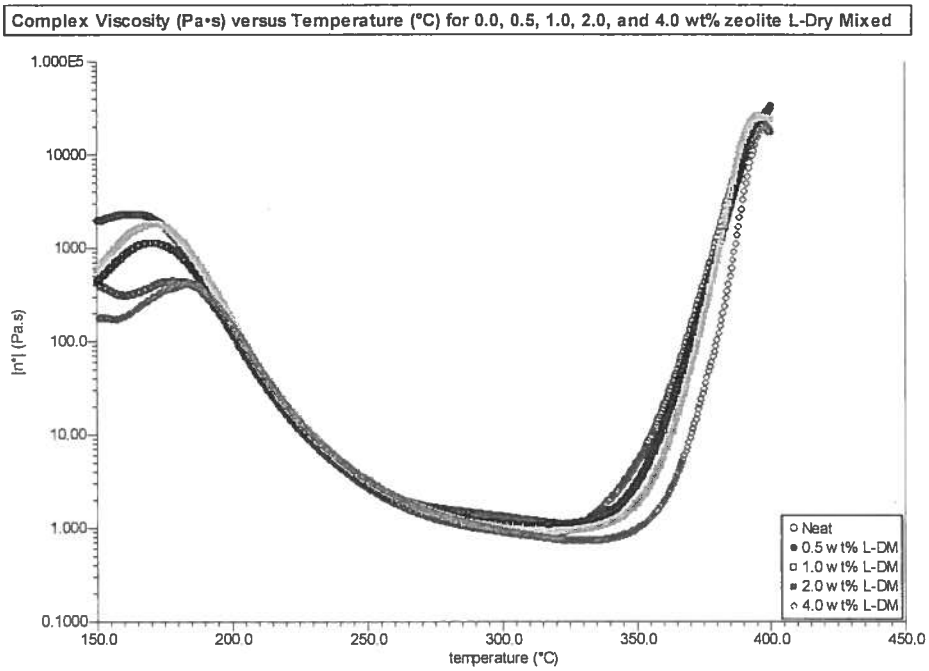

Figure 41. Complex viscosity η* vs. temperature for sample of GRC-A and GRC-A with 0.5, 1.0, 2.0, and 4.0 wt% zeolite L dry-mixed for 4h

Table 8. Minimum viscosity, temperature at minimum viscosity, and observed gel points of samples of neat GRC-A and GRC-A with 2.0 wt% zeolite L that had dry-mixed 4 h.

GRC-A mixed with Zeolite L by dry mixing	**Wt % zeolite in GRC-A as measured**	**minimum viscosity, (η*) Pa·s**	**T (°C) @ minimum viscosity (η*)**	**G_c (°C)**
Neat	neat	0.67	315	352
0.5 wt%	0.78 %	1.11	328	351
1.0 wt%	1.108%	1.28	332	358
2.0 wt%	2.08%	0.92	341	353
4.0 wt%	3.99%	0.90	347	360

In another study, zeolite Y was incorporated into GRC-A by dry mixing in a manner similar to that used for the incorporation of zeolite L. The rheology data showed

zeolite Y catalyzing the cure by shifting the onset of cure to lower temperatures, when compared to dry mixed samples with zeolite L, Figure 42. Table 9 also shows that the temperature at the minimum viscosity and at the cross-over point decrease significantly. Additionally, there appears to be some pre-melting of the GRC-A in the presence of zeolite Y between 150 °C and 200 °C, before consistent melting takes place after 200 °C. This was not observed in previously mixed samples with zeolite L. Figure 43 shows the comparison in the melt rheology curves between the as-received GRC-A, dry-mixed samples of GRC-A loaded with zeolite L and GRC-A loaded with Y at 0.5, 1.0, 2.0 and 4.0 wt% loadings. The diagrams show how the onset of cure of the mixed samples are affected and shifted relative to the each other and the neat resin.

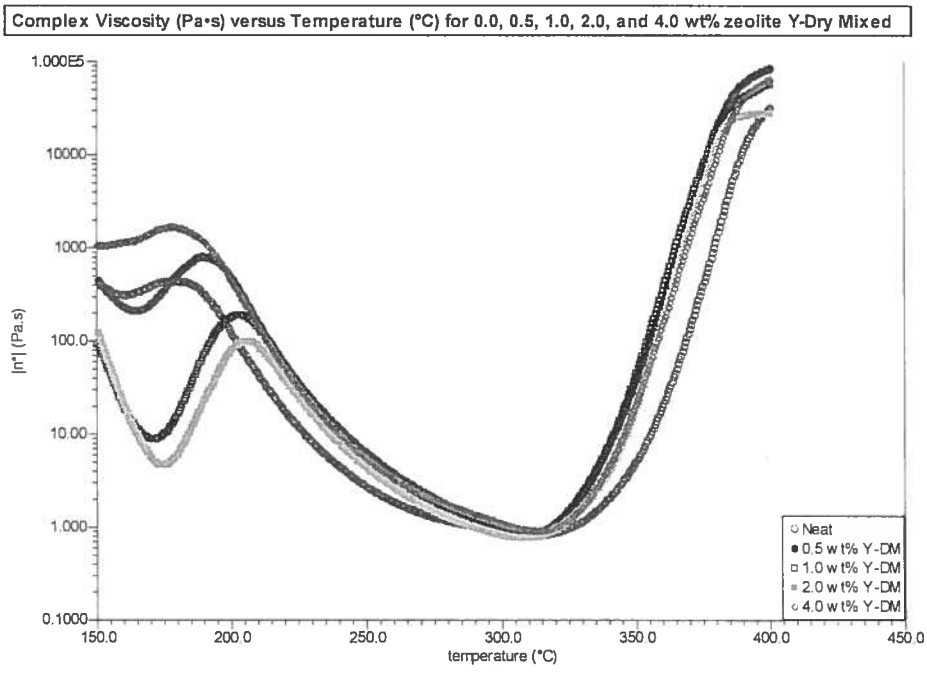

Figure 42. Complex viscosity η* vs. temperature for sample of GRC-A and GRC-A with 0.5, 1.0, 2.0, and 4.0 wt% zeolite Y and dry-mixed for 4 h.

Table 9. Minimum viscosity, temperature at minimum viscosity, and observed gel points of samples of neat GRC-A and GRC-A dry mixed for 4 h.

Samples	minimum viscosity, (η*) Pa·s	T (°C) @ minimum viscosity (η*)	G_c (°C)
Neat DM 4 h	0.59	315	352
0.5 wt% Y DM 4h	0.74	307	341
1.0 wt% Y DM 4h	0.80	308	343
2.0 wt% Y DM 4h	0.87	310	338
4.0 wt% Y DM 4h	0.87	309	340

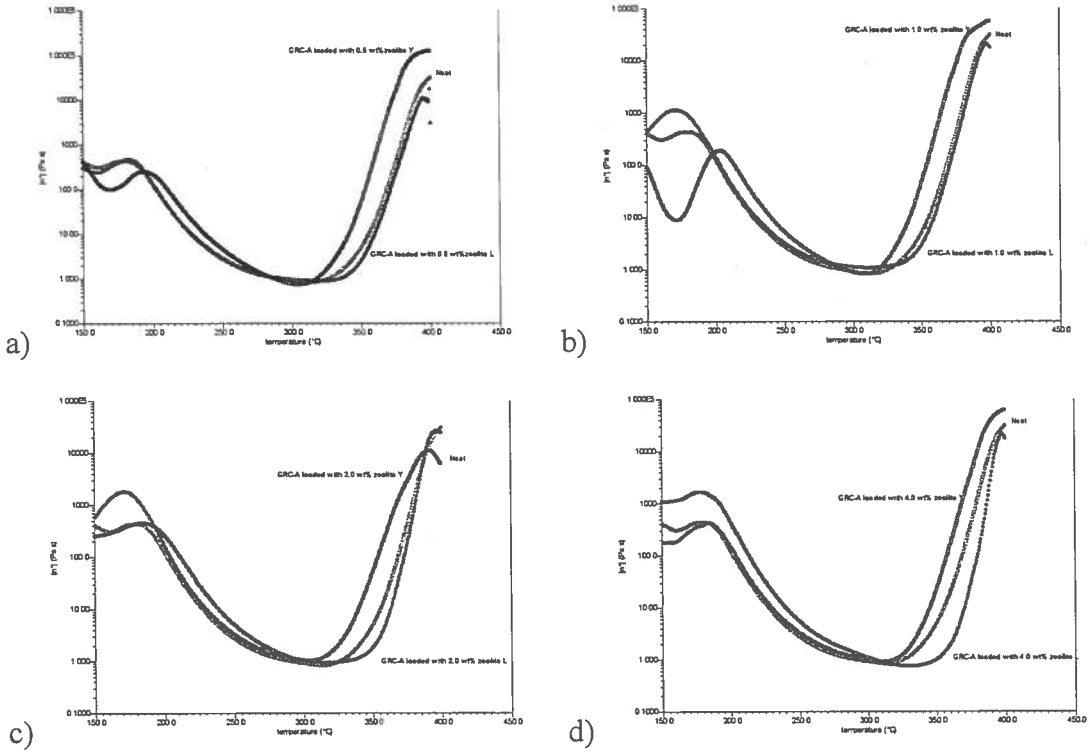

Figure 43. Comparison of the melt rheology curves between the as-received GRC-A, dry-mixed samples of GRC-A loaded with zeolite L and GRC-A loaded with Y with 0.5, 1.0, 2.0 and 4.0 wt% loadings.

As to why zeolite Y is catalyzing the cure chemistry of the phenylethynyl end-groups of GRC-A could be attributed to the accessibility of the Lewis acid on the surface of the zeolites. Zeolite Y has a surface area to volume ratio that is nearly three times that of zeolite L (Please refer to Table 1). Thereby, the presence of zeolite Y in the resin can catalyze the curing of the phenylethyny end-groups by facilitating reactivity between GRC-A and the Lewis acids at the surface of the zeolites. Already discussed in chapter 2, the proposed cure chemistry of the phenylethynyl end-group to include intra- and intermolecular Diels-Alder reactions, and the presence of Lewis acid sites could affect these reactions; ultimately affecting the cure mechanism of phenylethynyl end groups. Earlier studies have observed that the presence of Lewis acids in solutions, similar to those in the zeolite Y, can accelerate Diels-Alder reactions by an order of 10^4 to 10^6.[133-145] In this study, the observation revealed that GRC-A with various loadings of zeolite Y decrease the cure temperature of the phenylethynyl end-groups by 2.5% to 4% and 6% to 11%, relative to neat GRC-A and GRC-A/zeolite L mixtures.

4.10 Comparison Melt Rheology of GRC-A with Zeolite L in the Na^+, K^+, and H^+ Form

Zeolite L was exchanged from the K^+ form to the Na^+ and H^+ form as described in the experimental portion, section 3.6. Figures 44 and 45 give η^* vs. temperature for GRC-A loaded with 4.0 wt% of zeolite L via dry mixing in the K^+ and H^+, and K^+ and Na^+ forms, respectively, with the cation K^+ compared to zeolite L in the H^+ and Na^+ form. Table 10 gives are the minimum viscosity, the temperature at the minimum viscosity, and gel point for these samples.

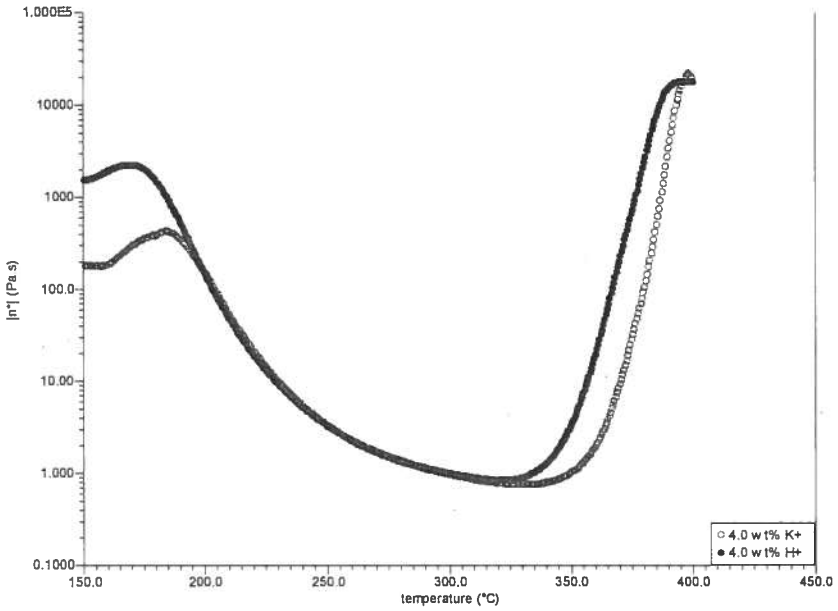

Figure 44. Complex viscosity, η*, vs. temperature for GRC-A loaded with 4.0 wt% zeolite L in the K^+ and H^+ forms.

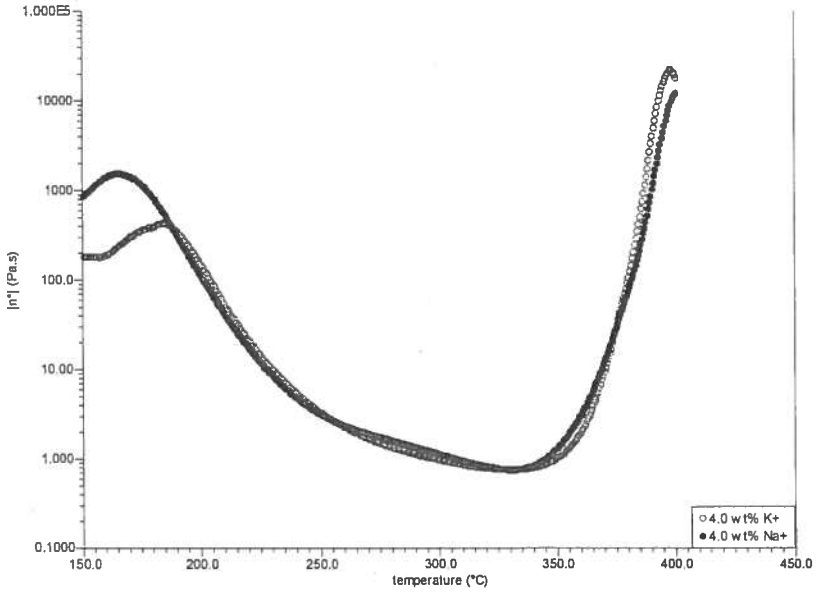

Figure 45. Complex viscosity, η*, vs. temperature for GRC-A loaded with 4.0 wt% zeolite L in the K^+ and Na^+ forms.

Table 10. Minimum η*, temperature at η*, and observed gel points of samples of GRC-A loaded with 4.0 wt% zeolite in the H^+, K^+, and Na^+ forms.

Sample	minimum viscosity, (η*) Pa·s	T (°C) @ minimum η*	G_c (°C)
GRC-A/4.0 wt% zeolite L/K^+	0.79	347	364
GRC-A/4.0 wt% zeolite L/H^+	0.82	322	348
GRC-A/4.0 wt% zeolite L/Na^+	0.73	342	361

The rheology curve for GRC-A with zeolite L in H^+ form demonstrates that onset cure at a much lower temperature than GRC-A with zeolite L in K^+ or the Na^+ form, see Figure 48. In contrast, the cure behavior appears to be similar for GRC-A with zeolite L in either the K^+ or Na^+ form. This suggested that the metal cations do not affect the cure as does the Brønsted acid sites. Besides, the acid strength associated with metal cations has been categorized as weak Lewis acids, when compared to Brønsted acid sites.[20] However, the Brønsted and Lewis acid sites that are housed on the surfaces and within the micropores can interact with one another to enhance the catalytic activity of the zeolite. Lago et al. attributed the increase in catalytic activity for the cracking of n-hexane, and attributed this phenomena to the partially hydrolyzed framework aluminum atoms This aluminum atoms were viewed as strong electron-withdrawing centers in the neighborhood of the Brønsted acid sites.[109] The same assumption could be made for the increase in the cure for GRC-A with zeolite L in H^+ form, in that the addition of the protons made it possible for the aluminum atoms of the Lewis acids sites housed by zeolite L to become partially hydrolyzed by the Brønsted acid sites, thereby, enhancing the catalysis of the cure reaction, and resulting in a lower temperature for the onset of cure.

4.11 Kinetic Studies of PETI GRC-A with zeolite L and Y

There are essentially two forms of kinetic models used to describe thermoset curing reactions: empirical and mechanistic models. Empirical models are more simplistic and assume an overall reaction order, to which the kinetic data is fitted.[146] On the contrary, mechanistic models are derived from an analysis of the individual reactions involved during the curing, which require detailed measurements of the concentration of reactants, intermediates, and products. Essentially mechanistic models are intrinsically more complex than empirical models, and are not restricted by compositional changes. However empirical models do provide important information about the cure kinetics of thermosets.

4.12 Activation Energy for the Onset of Cure of PETI GRC-A with zeolite Land Y

To gain more insight on the cure kinetics of the zeolites loaded systems, we investigated the onset of cure rate by determining its rate constant (k) as a function of temperature. In this study, the empirical model, the Arrhenius equation (Equation 5) was utilized to obtain the activation energy, E_A, of the onset of cure for neat GRC-A and GRC-A loaded with zeolites,

$$\ln k = \ln k_\infty + (-E_k/RT) \qquad \text{Eq 5}$$

where k is the rate constant, A is the pre-exponential constant, E_k is the apparent activation energy for initial increase in viscosity, R is the gas constant, and T is the temperature, K.

Isothermal rheology studies were and have been used to help obtain the cure kinetics of many thermosets. These tests were used to determine the changes in the complex viscosity over time at a fixed frequency at various temperatures. Mussati and

Macosko measured the curing viscosities of a phenolic resin, epoxy resin, and an EPDM rubber as function time at various temperatures.[147] Bullions et al. used isothermal studies to construct a two stage, dual-Arrhenius rheology model to successfully model the complex viscosity of a phenylethynyl terminated poly(etherimide) as a function of time, over the temperature range 325°C to 350°C.[100] In this study, we measured the change in complex viscosity of Neat GRC-A and GRC-A loaded with zeolites as a function of time at of 300, 315, and 330°C. Figure 46 shows the complex viscosity, η* vs. time at these temperatures for neat GRC-A.

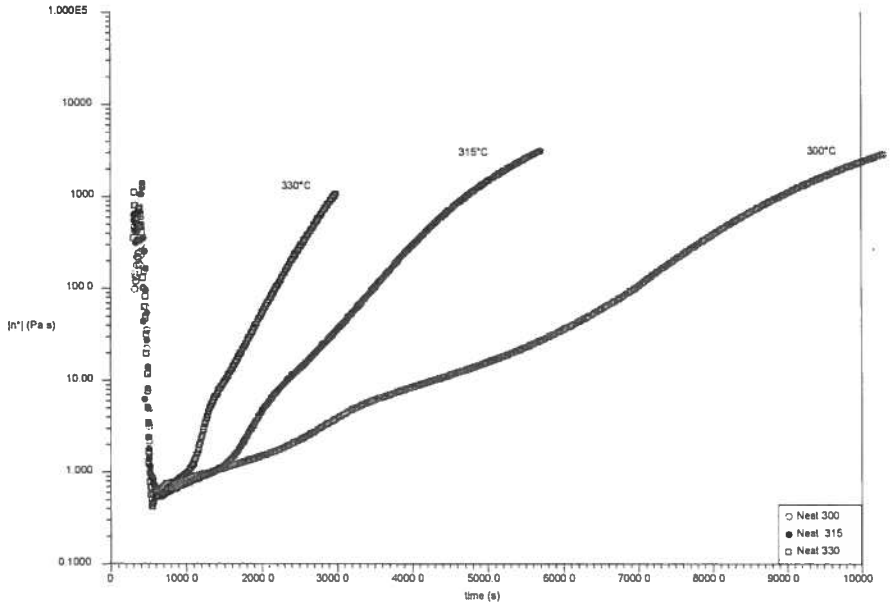

Figure 46. Complex viscosity, η*, vs. time at 300, 315, and 330 °C for neat GRC-A.

Figure 46 shows a clear difference in the cure behavior of GRC-A at these temperatures. For the cure kinetics study, the initial rate of increase in η* for the onset o cure was determined by examining the initial rate of increase in complex viscosity in the linear range just above the point of the minimum viscosity. Table 11 gives the kinetic

values, and Figure 47 shows the Arrhenius plot of the data for neat GRC-A. Tables 12 and 13 gives the activation energies for the Neat GRC-A, and GRC-A loaded with zeolite L and Y prepared via dry mixing.

Table 11. Rate constants, taken at each temperature, for the initial increase in viscosity of neat GRC-A.

T (°C)	1/T (K)	k ($1/s^{-1}$)	ln k ($1/s^{-1}$)
300	0.001745	1.66E-4	-8.70
315	0.001701	3.84E-4	-7.86
330	0.001658	8.16E-4	-7.11

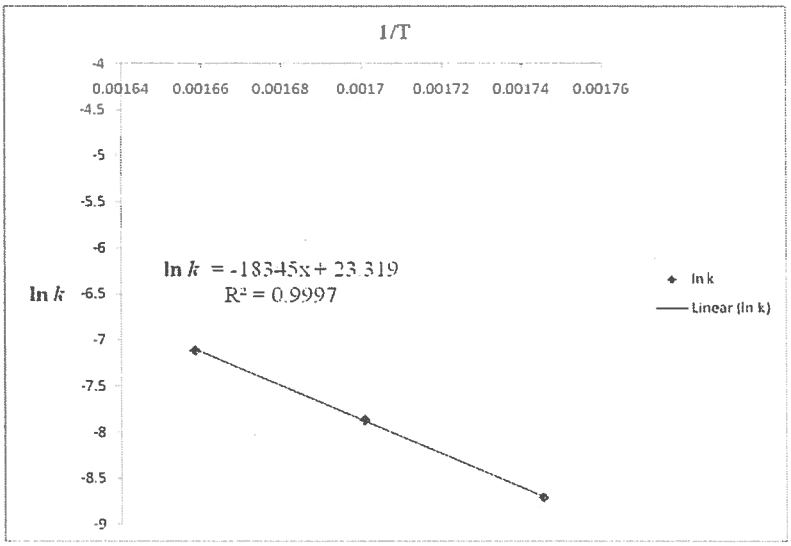

Figure 47. Arrhenius plot for the rate of increase in the initial increase of η* vs. inverse temperature for neat GRC-A.

Table 12. Apparent activation energy for the initial increase in η*, and pre-exponential factor for initial increase in η* for neat GRC-A and GRC-A with zeolite L.

	E_A, kJ/mol	k_∞ (1/s)	Linear Regression
Neat GRC-A	145. ± 2.8	14 ± 1.2	0.998 ± 0.002
GRC-A/0.5 wt% zeolite L	167. ± 5.7	31 ± 1.6	0.997 ± 0.005
GRC-A/1.0 wt% zeolite L	176. ± 5.4	30 ± 1.7	0.998 ± 0.002
GRC-A/2.0 wt% zeolite L	189. ± 5.3	32 ± 1.6	0.997 ± 0.005
GRC-A/4.0 wt% zeolite L	218. ± 5.6	34 ± 1.5	0.999 ± 0.007

Table 13. Apparent activation energy for the initial increase in η*, and preexponential factor for initial increase in η* for neat GRC-A and GRC- A with zeolite Y.

	E_A, kJ/mol	k_∞ (1/s)	Linear Regression
Neat GRC-A	145. ± 3.6	24 ± 1.6	0.997 ± 0.005
GRC-A/0.5 wt% zeolite Y	99. ± 5.7	31 ± 1.6	0.998 ± 0.002
GRC-A/1.0 wt% zeolite Y	127. ± 5.4	30 ± 1.7	0.998 ± 0.002
GRC-A/2.0 wt% zeolite Y	126. ± 5.3	32 ± 1.6	0.998 ± 0.002
GRC-A/4.0 wt% zeolite Y	131. ± 5.6	34 ± 1.5	0.997 ± 0.005

The results of the isothermal tests show that the activation energies for the GRC-A/ zeolite L mixtures increased relative to the neat system, while the activation energies for GRC-A/zeolite Y mixtures decreased. The activation energies for GRC-A/zeolite L mixtures support the temperature sweep experiments, in which zeolite L was retarding the cure, resulting in the onset of the reaction observed at higher temperatures. Likewise, the activation energies of GRC-A/zeolite Y mixtures show that presence zeolite Y also agreed with the temperature sweep experiments, in which the onset of cure was observed at lower temperatures.

4.13 Activation Energy of Gelation of PETI GRC-A with zeolite L and Y

The activation energy of the thermally induced gelation of the filled and neat GRC-A was also examined to determine what effect zeolite L and Y have on the gelation

of GRC-A. Bullions et al. and Dean et al. both demonstrated that the activation energy of gelation for their thermosetting systems, could be obtained by taking the natural logarithm of the gel time (t_{gel}) versus 1/T as demonstrated in the equation below.[148]

$$\ln t_{gel} = \ln t_{gel\infty} + (-E_g/RT) \qquad \text{Eq 6}$$

Where t_{gel} is the gel time, $t_{gel\infty}$ is the preexponential factor for the gel time, and E_g is the apparent activation energy for gelation. The gel time, is defined as the cure time at constant temperature leading up to the infinite three-dimensional network. The gel time was taken from the crossover point, G_c; where G' = G". As expected, the gel time decreased as the cure temperature increased, indicating that the reaction proceeds more rapidly at elevated temperatures Figure 48 gives both G' and G" plotted as a function of time at 300, 315 and 330°C. Table 14 gives the gel times for the respective isothermal temperatures, and Figure 49, shows the Arrhenius plot of the gel times versus temperature for neat GRC-A. Tables 15 and 16 give the activation energy of gelation for GRC-A loaded with L and Y. The data show that for GRC-A loaded with 0.5 wt% and 1.0 wt% of zeolite L, the activation energy of gelation is similar to that of unfilled resin. However, for 2.0 wt% and 4.0 wt% of zeolite L, the activation energy increases relative the neat GRC-A. As for GRC-A loaded with Y, the observation further supports the catalytic behavior of this zeolite, as evidenced by a reduction in the activation energies.

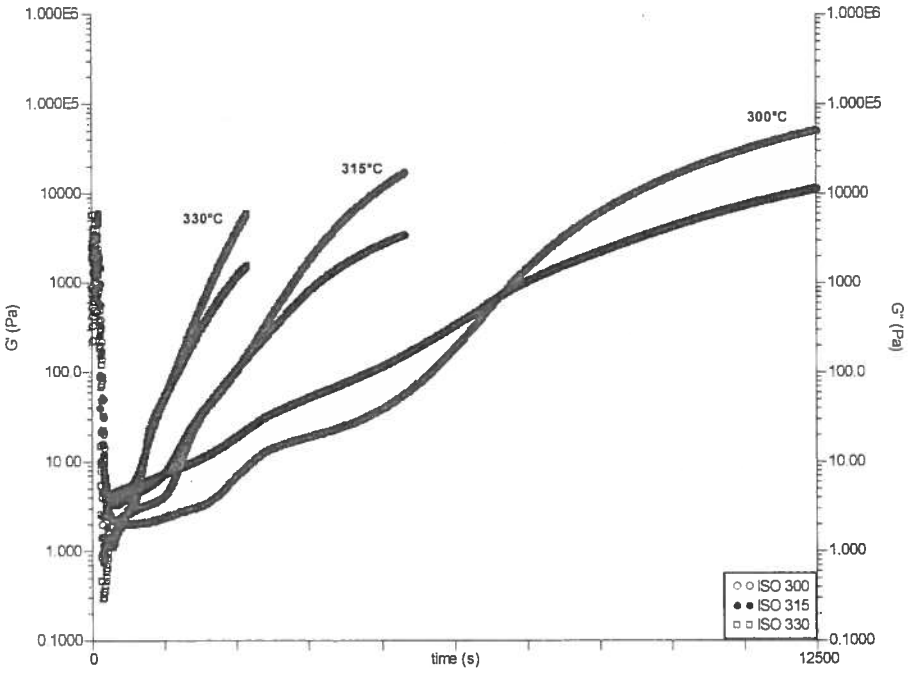

Figure 48. G' and G"vesus time for neat GRC-A at 300, 314, and 330 °C.

Table 14. Gel times for the gelation of neat GRC-A, taken from each temperature.

T (°C)	1/T	t (s)	ln t
300	0.001745	7092.	8.87
315	0.001701	2574.	7.85
330	0.001658	930.	6.83

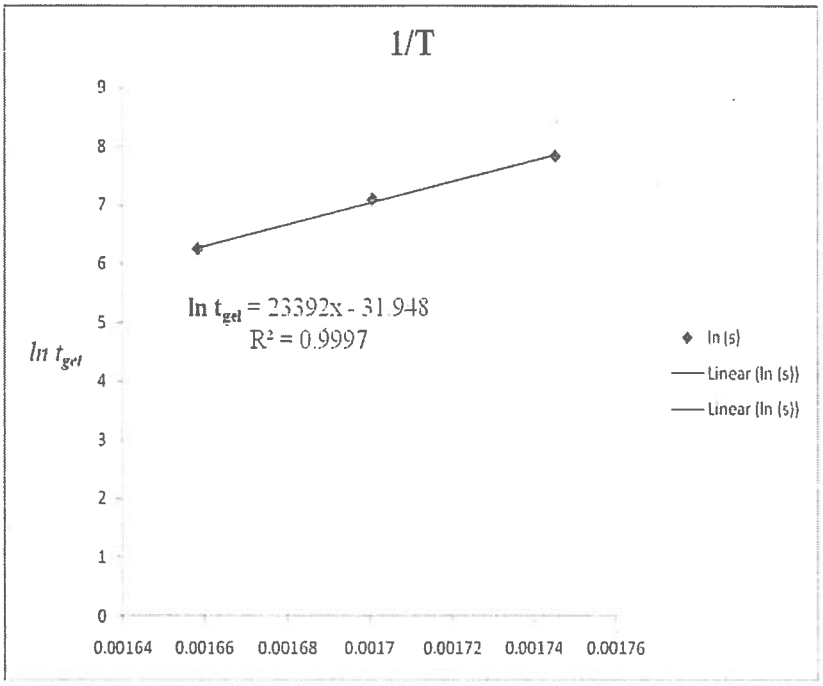

Figure 49. Arrhenius plot of the gel times vs. inverse temperature for neat GRC- A.

Table 15. Apparent activation energy for the gelation, and pre-exponential factor for gelation for neat GRC-A and GRC- A with zeolite L.

	E_A, kJ/mol	**$t_{gel\infty}$ (1/s)**	**Linear Regression**
Neat GRC-A	170. ± 3.6	24 ± 1.6	0.997 ± 0.005
GRC-A/0.5 wt% zeolite L	165.± 5.5	27 ± 1.9	0.997 ± 0.005
GRC-A/1.0 wt% zeolite L	168.± 5.7	26 ± 1.5	0.998 ± 0.002
GRC-A/2.0 wt% zeolite L	180.± 6.1	28 ± 1.7	0.998 ± 0.002
GRC-A/4.0 wt% zeolite L	230.± 6.4	36 ± 1.6	0.998 ± 0.002

Table 16. Apparent activation energy for the gelation, and preexponential factor for gelation for neat GRC-A and GRC-A with zeolite Y.

	E_A, kJ/mol	$t_{gel\infty}$ (1/s)	Linear Regression
Neat GRC-A	170. ± 3.6	24 ± 1.6	0.997 ± 0.005
GRC-A/0.5 wt% zeolite Y	101. ± 5.5	27 ± 1.9	0.997 ± 0.005
GRC-A/1.0 wt% zeolite Y	110.± 5.7	26 ± 1.5	0.998 ± 0.002
GRC-A/2.0 wt% zeolite Y	126.± 6.1	28 ± 1.7	0.998 ± 0.002
GRC-A/4.0 wt% zeolite Y	151.± 6.4	36 ± 1.6	0.998 ± 0.002

4.14 Utilizing Equations and Models to Quantify the Effect of Zeolites on the Melt Rheology and Elasticity of GRC-A: Einstein Equations and Guth-Gold Model

Fillers are commonly used in polymers and rubbers to enhance their properties.[149,150] Fillers are employed as processing aids to improve mechanical properties and thermal stability, enhanced optical properties of polymer films, and gas permeability reduction, or to lower costs.

The immediate effect of fillers is to increase viscosity by interfering with the flow pattern in a given process, produce thixotropy, and give rise to machine wear.[151] The relevant properties of fillers are concentration, size, aspect ratio, stiffness, strength, and specific interaction between filler and the polymer matrix.[150] Einstein established an equation describing the viscosity of a filled Newtonian polymer melt non-deformable, spherical fillers at low concentration.[152] The equation is expressed as:

$$\eta = (1 + 2.5\,\varphi)\,\eta_s \qquad \text{Eq 7}$$

where η is the viscosity of the filled polymer, η_s is the viscosity of unfilled polymer, and φ is the volume fraction of the filler. Unfilled PETI GRC-A flows as a Newtonian fluid from above the melting point up to 315 °C, before it begins to cure, thus the Einstein equation can predict the behavior that zeolites will have on the resin's melt rheology acting purely as a filler. The complex viscosity predicted by the Einstein equation were compared to the temperature sweep (5 °C/min) experimental rheology experiments for GRC-A dry-mixed with zeolites L and Y, and are given in Tables 17 and 18. The values of complex viscosity for the neat resin and resin/zeolite mixtures were recorded at 300 °C. This temperature was below the temperature of minimum viscosity for the neat resin and the resin/zeolite mixtures and all samples had been exposed to the same time temperature history. The density of the PETI GRC-A was found to be. 1.00 g/cm^3 and the densities of zeolite L and Y were reported to be 0.62 g/cm^3 and 0.48 g/cm^3, respectively.[153]

Table 17. Observed and calculated viscosity values for GRC-A and GRC-A/zeolite L mixtures.

Weight Percent, (%)	**Volume Fraction, (φ)**	**η @ 300 °C**	**Calculated η**
0.0	0.00	0.60	-
0.5	0.00805	0.91	0.61
1.0	0.0161	1.12	0.62
2.0	0.0319	1.21	0.64
4.0	0.0631	1.31	0.69

Table 18. Observed and calculated viscosity values for GRC-A and GRC-A/zeolite Y mixtures.

Weight Percent, (%)	**Volume Fraction, (φ)**	**η @300 °C**	**Calculated η**
0.0	0.00	0.60	-
0.5	0.0104	0.78	0.61
1.0	0.0208	0.81	0.63
2.0	0.0411	0.91	0.67
4.0	0.0805	0.87	0.72

The Einstein equation does not fit the observed data well for GRC-A/zeolite L mixtures. The equation is predicting values that are far below the experimental data by as much as 47%. However, the equation does correlate fairly well for GRC-A/zeolite Y mixtures as. Large variations between the experimental data and the equation, as in the case with the GRC-A/zeolite L mixtures, could be attributed to hydrodynamic interactions between the zeolites particles. Thus an extension of the Einstein equation was developed to take into consideration of the hydrodynamic interactions between particles that are in close proximity to one another.[154] Illustrated in Equation 8, the Einstein equation is extended to:

$$\eta_s = (1 + 2.5\,\varphi + 6.2\,\varphi^2)\,\eta_s \qquad \text{Eq 8}$$

This equation has been shown to account for filler interactions up to $\varphi = 1$.[154] Tables 19 and 20 gives the predicted viscosities by the extended Einstein equation, along with the experimental data. Consequently, this equation did not predict any better than the

Einstein equation. However, both equations do support the experimental data, in that the melt viscosity increases with increasing filler concentration.

Table 19. Observed and calculated viscosity values for GRC-A and GRC-A/zeolite L mixtures.

Weight Percent, (%)	Volume Fraction, (φ)	η @ 300 °C	Calculated η
0.0	0.00	0.60	-
0.5	0.00805	0.91	0.61
1.0	0.0161	1.12	0.62
2.0	0.0319	1.21	0.64
4.0	0.0631	1.31	0.70

Table 20. Observed and calculated viscosity values for GRC-A and GRC-A/zeolite Y mixtures.

Weight Percent, (%)	Volume Fraction, (φ)	η @300 °C	Calculated η
0.0	0.00	0.60	-
0.5	0.0104	0.78	0.61
1.0	0.0208	0.81	0.63
2.0	0.0411	0.91	0.66
4.0	0.0805	0.87	0.74

The effect of filler on the modulus is proportional to that of the viscosity, and can also be represented by the Einstein equation, with the viscosity in terms replaced by modulus terms. The Guth-Gold model, relates the effects of fillers on the modulus of polymeric materials, by enabling the ability to obtain the stiffening effect within the polymer.[156] Below, the Guth-Gold model is expressed as:

$$E = (1 + 0.67g\varphi + 1.62\,(g\varphi)^2)E_s \qquad \text{Eq 9}$$

where E is the modulus of the filled polymer, E_s is the modulus of the unfilled polymer, and g is the geometric factor. The geometric factor is applied to account for the fact that

filler aggregate structure could affect the stiffness, and represent initially by the ratio of length to the width of the filler aggregate. Typically, g is used as a fitting parameter, and has values between 4 and 10, but for this study, the aspect ratios for zeolites L and Y were measured to be 2.0 and 1.5, respectively. Using the Guth-Gold equation, the predicted values of the initial modulus of the unfilled polymer and filled polymer was obtained at 300°C as well, and compared to the experimental data for GRC-A dry-mixed with L and Y. The values are given in Tables 21 and 22.

There was not a good correlation between the experimental data and the Guth-Gold model for the GRC-A/zeolite L mixtures. The experimental data demonstrated that zeolite L was having a much lesser stiffening effect on GRC-A than zeolite Y. According to the model, the modulus should increase with increasing loading of zeolite L, but the data showed that zeolite L is retarding the cure. However, the modulus for GRC-A loaded with zeolite Y was greater than the modulus for both the neat resin and for the GRC-A/zeolite L mixtures. This supports already previous data, indicating that the catalytic properties of zeolite Y results in the formation of the network to happen faster, by catalyzing the curing the phenylethyny end-groups.

Table 21. Modulus of unfilled GRC-A normalized against GRC-A filled with zeolite L dry-mixed with zeolite L

Volume Fraction, (φ)	**E @ 300 °C**	**Calculated E**
0.00	2.21	-
0.00805	1.82	2.23
0.0161	1.10	2.26
0.0319	1.07	2.32
0.0631	1.06	2.46

Table 22. Modulus of unfilled GRC-A normalized against GRC-A filled with zeolite Y dry-mixed with zeolite Y

Volume Fraction, (φ)	E @ 300 °C	Calculated E
0.00	2.21	-
0.0104	2.37	2.23
0.0208	2.48	2.26
0.0411	2.77	2.31
0.0805	3.31	2.44

4.15 Differential Calorimetry Studies (DSC) of GRC-A with Zeolite L and Y

DSC studies were conducted on a TA Instruments Q 2000 to measure the cure reaction progress of neat GRC-A and GRC-A resin loaded with zeolites via dry mixing, by detecting the heat given off by the exothermic chain growth and cross-linking reactions. The influence of the zeolites on the cure reaction progress of GRC-A was examined to determine the effect that these additives on the onset of cure, the heat of reaction, ΔH_R, glass transition temperatures, T_g, and cure kinetics.

4.16 Effect of Zeolite L on the Cure Reaction of GRC-A

In this study we determined the onset of cure and glass transition temperature of GRC-A and GRC-A loaded with L and Y. Figure 50 top curve shows heat flow as a function when GRC-A is heated in the DSC at 5 °C/min. The exotherm starting at ~330 °C at a heating rate of 5 °C/min up to 450 °C (upper curve) is due to the curing of GRC-A. The sample was then cooled at 15 °C/min and reheated at 20 °C/min, to obtain the cured T_g of 223 °C (lower curve). Figure 51 exhibits exotherm peaks for the neat resin and the resin filled with zeolite L. Table 23 gives the temperatures for the onset of cure and T_gs for neat GRC-A and GRC-A loaded with zeolites L. The data show that the incorporation of the zeolites increases the temperature for the onset of reaction for the

curing of GRC-A. Figure 52 shows the heating curves for the cured GRC-A and GRCA loaded with zeolite L and exhibit the T_gs. It was found that onset of cure and the cured glass transition temperatures increased with increasingly loadings of zeolites L.

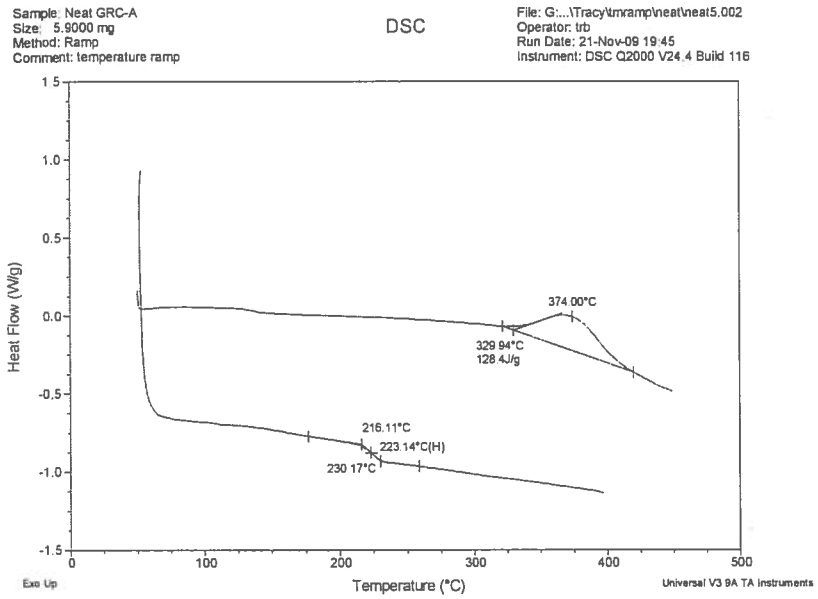

Figure 50. DSC showing heat flow versus temperature for neat GRC-A, heated at 5 °C/min.

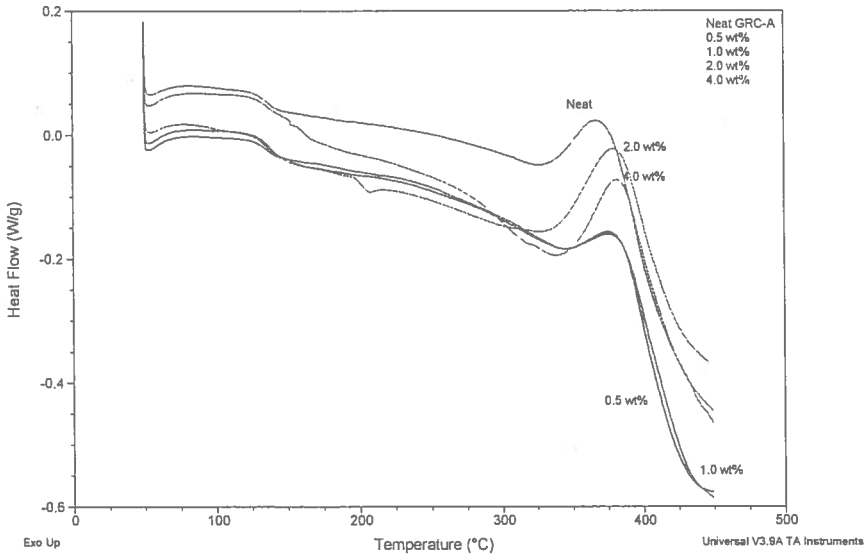

Figure 51. DSC of neat GRC-A and GRC-A loaded with 0.5, 1.0, 2.0, and 4.0 wt% zeolite L via dry-mixing, with a heating rate of 5 °C/min.

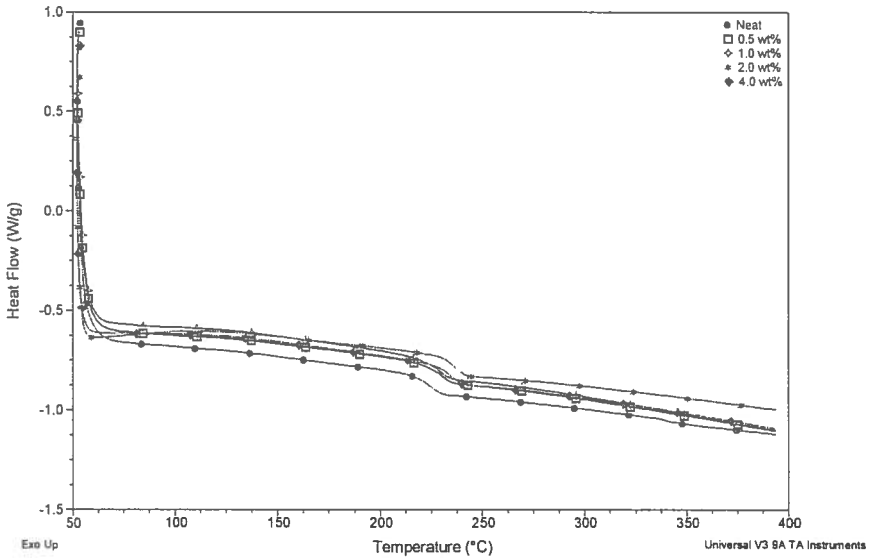

Figure 52. DSC showing the T_g for neat GRC-A and GRC-A loaded with zeolite L, conducted with a hearting rate 20°C/min.

Table 23. The Onset of cure and T_g for unfilled GRC-A and GRC-A filled with zeolite L

	Onset of Cure (^{0}C)	**T_g (^{0}C)**
GRC-A As-Received	331. ± 1.8	223. ± 1.1
GRC-A/0.5 wt% -L	336. ± 2.1	227. ± 1.2
GRC-A/1.0 wt% -L	340. ± 2.3	229. ± 1.5
GRC-A/2.0 wt% -L	344. ± 2.1	234 .± 1.3
GRC-A/4.0 wt% -L	347. ± 2.4	236 ± 1.7

4.17 Effect of Zeolite Y on the Cure Reaction of GRC-A

DSC studies were conducted on the GRC-A loaded with zeolite Y to examine the effect of the zeolite on the cure reaction and the cured T_g (figures 56 and 57, respectively). Table 24 gives the corresponding temperatures for the onset of cure, and cured T_gs. In contrast to zeolite L, zeolite Y lead to a decrease in the temperature for the onset cure and also resulted in increased cured T_gs, with the T_g of GRC-A filled with zeolite Y. The T_g of the cured GRC-A with zeolite Y are greater than 40 degrees higher than GRC-A that was filled with L.

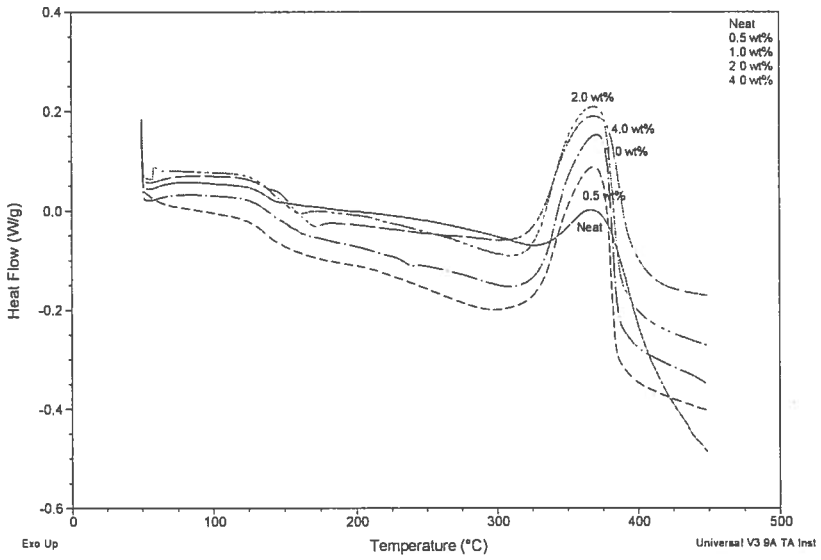

Figure 53. DSC curves for neat GRC-A and GRC-A loaded with 0.5, 1.0, 2.0, and 4.0 wt% zeolite Y via dry-mixing, conducted at 5°C/min.

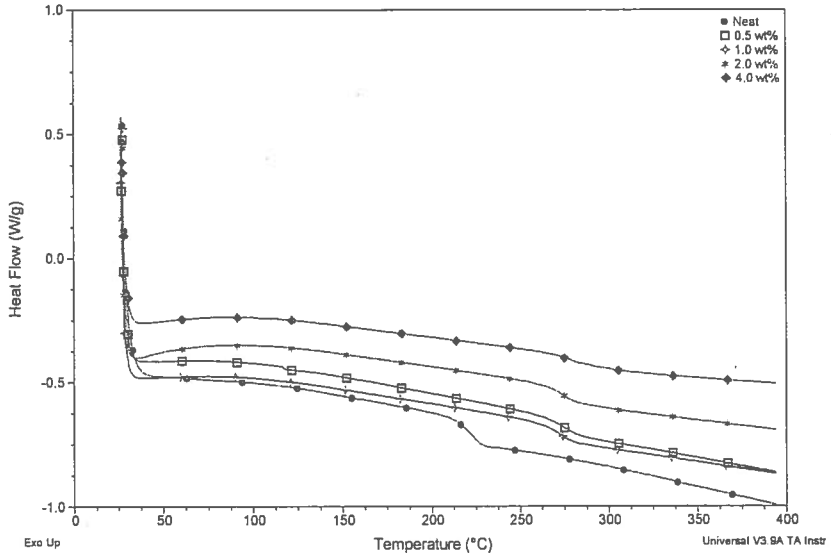

Figure 54. DSC of the cured GRC-A and GRC-A loaded with 0.5 – 4.wt % zeolite Y, conducted at 20°C/min.

Table 24. The Onset of Cure and Cured T_g for unfilled GRC-A and GRC-A filled with zeolite Y

	Onset of Cure (^{0}C)	**T_g (^{0}C)**
Neat GRC-A	331. ± 1.8	223. ± 1.1
GRC-A/0.5 wt% zeolite Y	329. ± 1.9	273. ± 1.4
GRC-A/1.0 wt% zeolite Y	324. ± 2.1	274. ± 1.2
GRC-A/2.0 wt% zeolite Y	325. ± 2.0	275. ± 1.3
GRC-A/4.0 wt% zeolite Y	325. ± 1.9	277. ± 1.4

Figure 55 gives a comparison of the DSC curing curves for GRC-A with 0.5, 1.0, 2.0 and 4.0 wt% percent loadings of zeolite L and Y. The curing curves clearly show that zeolite Y leads to a lower temperature for the onset of cure and a larger exotherm for curing, indicating a higher level of cross linking than occurs with the corresponding

GRC-A/zeolite L mixtures. Table 25 summarizes the integrated heat of reaction for the cure, ΔH_R, for GRC-A loaded with zeolite L and Y. The larger ΔH_R, and higher cured T_g found with zeolite Y loaded samples further supports that zeolite Y is catalyzing the cure of GRC-A.

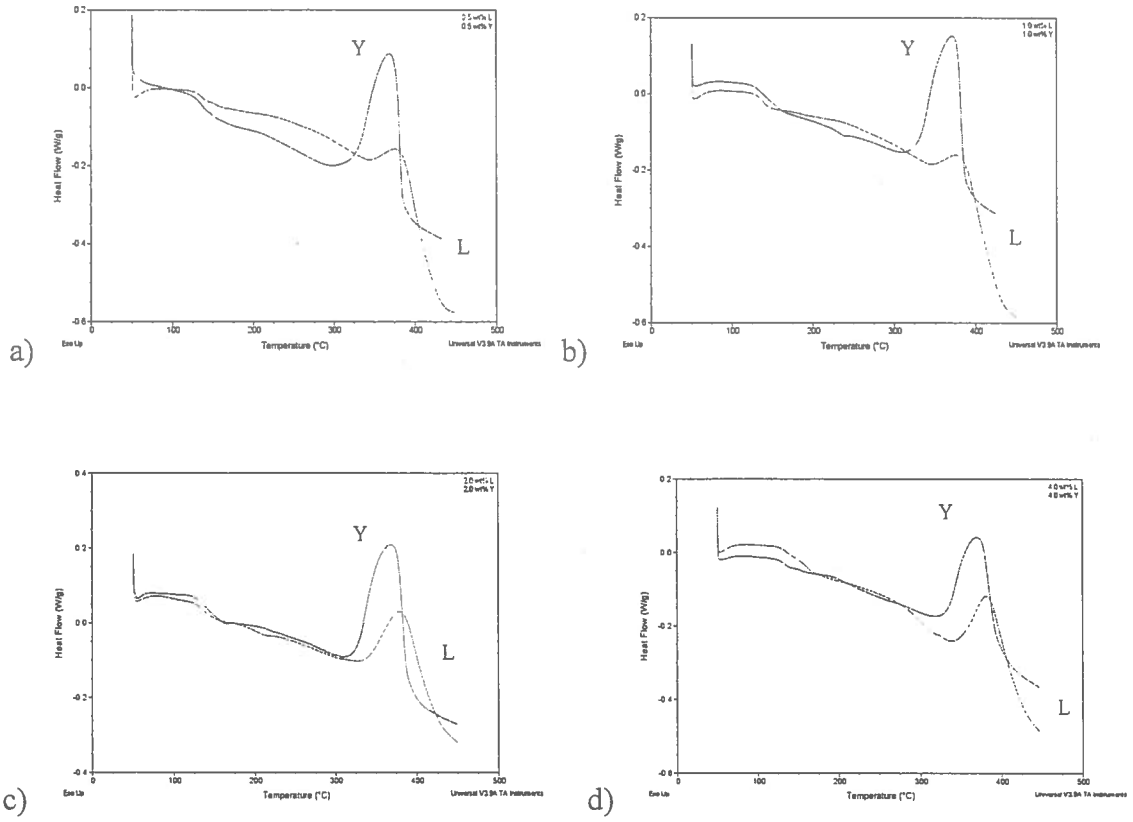

Figure 55. Comparison of ΔH_R with a heating rate of 5 °C/min for GRC-A loaded with zeolites L and Y: a) 0.5 wt%, b) 1.0 wt%, c) 2.0 wt%, d) 4.0 wt%

Table 25. Values of ΔH_R for neat GRC-A and GRC-A loaded with L and Y.

	ΔH_R (J/g)
Neat GRC-A	138. ± 1.6
GRC-A/0.5 wt% zeolite L	99. ± 3.3
GRC-A/1.0 wt% zeolite L	104. ± 3.1
GRC-A/2.0 wt% zeolite L	105. ± 2.7
GRC-A/4.0 wt% zeolite L	117. ± 2.5
GRC-A/0.5 wt% zeolite Y	160. ± 3.5
GRC-A/1.0 wt% zeolite Y	171. ± 3.2
GRC-A/2.0 wt% zeolite Y	185. ± 2.6
GRC-A/4.0 wt% zeolite Y	184. ± 2.8

4.18 Activation Energy for the cure of GRC-A with zeolite L – Isothermal Tests

DSC is extensively used in the determination of kinetic parameters and kinetic equations for the curing of thermosets. In the development of cure kinetic studies, DSC measures the rate of heat generated (dQ/dt) during a chemical reaction. The basic assumption in DSC kinetic measurements is that the change in heat flow is proportional to the change in extent of reaction, or degree of conversion α, as a function of time. That is,

$$dQ/dt \approx d\alpha/dt \qquad \text{Eq 9}$$

There are two experimental techniques of DSC measurements for thermoset reactions; isothermal and variable varying heating rates. In an isothermal test, the rate of

energy released is measured at a constant temperature for a period of time. However, one major assumption with this test is that the total heat of reaction can be determined accurately, and that all the reactions contributing to the overall reaction have the same enthalpy. Isothermal DSC studies have been used to investigate the cure kinetics of several PETI systems, similar to GRC-A. In this study, isothermal tests were conducted at 285, 300, and 315 °C for 4 h on dry mixed samples of neat GRC-A and GRC-A loaded with zeolite L. Figure 56 gives the isothermal DSC curves for neat GRC-A as function of time. The DSC data demonstrates that as the temperature increases, the peak height and peak area increase as the degree of conversion increases. As the peak maximum occurs close to t = 0 and there appears to be no induction time for the reaction and it is assumed that the reaction follows n^{th} order kinetics. Table 19 gives the rate constants for the reaction progress taken for each temperature, and Figure 57 shows the linear fit of rate constant vs. 1/T.

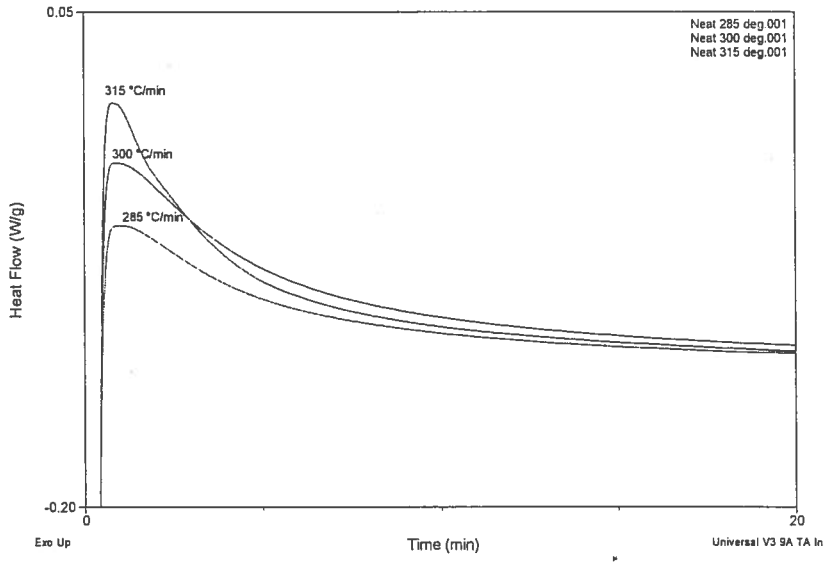

Figure 56. DSC thermograms for neat GRC-A as a function of time at 285, 300 and 315 °C.

Table 26. Kinetic Analysis of the Thermal Cure Reaction Progress of PETI GRC-A by Isothermal DSC

T (°C)	1/T(K)	Rate (1/s)	ln rate
315	0.001701	0.179	-1.72
300	0.001745	0.073	-2.61
285	0.001792	0.044	-3.12

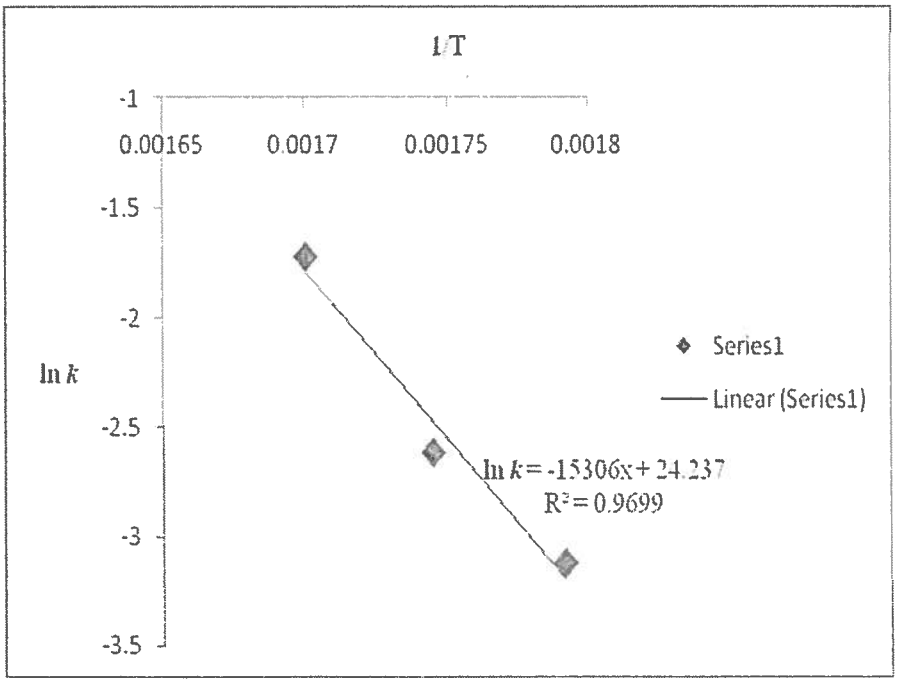

Figure 57. Arrhenius fit of ln k of versus 1/T for Neat GRC-A

Table 27 gives the apparent activation energies and the order of reaction for the cure of neat GRC-A and GRC-A loaded with zeolites L. The data indicates that the activation energy increases with increasing loadings of zeolite L.

Table 27. Apparent activation energies E_A, and reaction order for the cure of neat GRC-A and GRC-A loaded with zeolite L

	E_a, kJ/mol Isothermal	**Reaction Order (n)**	**Linear Regression**
Neat GRC-A	127. ± 1.8	1.51 ± 0.10	0.987 ± 0.010
0.5 wt% - L	130. ± 2.1	1.57 ± 0.12	0.965 ± 0.011
1.0 wt% - L	135. ± 2.2	1.60 ± 0.12	0.986 ± 0.010
2.0 wt% - L	141. ± 2.4	1.58 ± 0.12	0.976 ± 0.011
4.0 wt% - L	147. ± 2.3	1.57 ± 0.11	0.977 ± 0.011

4.19 Determination of the Activation Energy of GRC-A with zeolite L via the Ozawa-Flynn-Wall method

Due to equipment limitations encountered during the isothermal tests, such as, loading of the sample pans into the DSC furnace and long exposure of the sample pans to air before the system reached equilibrium, and initiation of data collection, an alternative method was utilize for obtaining the activation energy of the cure for GRC-A and GRC-A/zeolite. The Ozawa-Flynn-Wall method, ASTM E 698-05, was developed to examine the cure kinetics of thermosetting resins.[122] The ASTM method is based on the change in the exothermic peak size and peak temperature at variable heating rates, usually between 1 and 10°C/min. Two assumptions are made when using this method: 1) the extent of the reaction is equivalent at equivalent peak partials area (e.g. at 10% peak area corresponds to 10% of the reaction regardless of the heating rate), and 2) the extent of reaction is constant at the peak maximum temperature.

The method requires measuring DSC curves at four different heating rates, usually 3, 5, 7, and 9 °C/min. Then temperatures at which the peak maxima (~50% of the reaction) are plotted as a function of their respective heating rates, and then an Arrhenius plot can be constructed and the activation energy obtained. Figure 58 shows the DSC curves for neat GRC-A, and Table 28 gives the temperatures of the peak maxima.

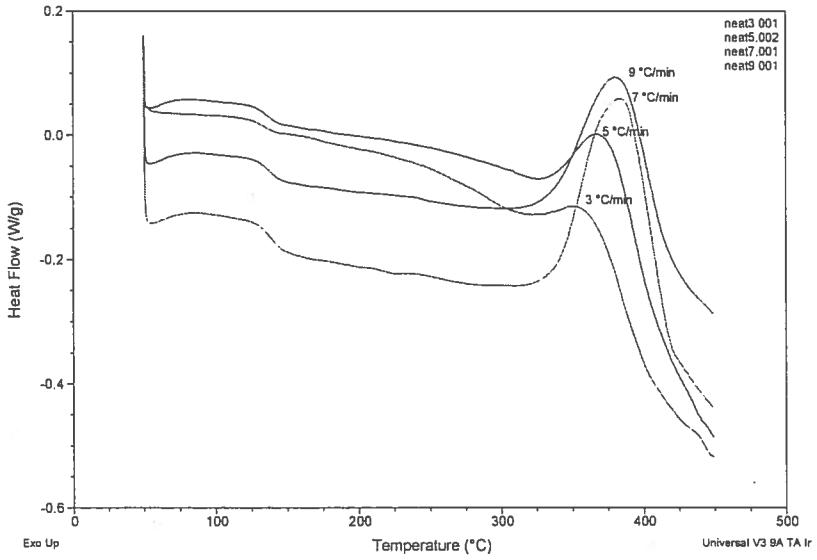

Figure 58. DSC thermograms for neat GRC-A conducted at heating rates of 3, 5, 7, and 9 °C/min.

Table 28. Kinetic Analysis of PETI GRC-A obtained by DSC-ASTM method

Peak Temperature (°C)	**1/T (K)**	**Heating Rate, β (°C/min)**	**ln β**
361.	0.001576	3.0 ± 0.1	1.10
372.	0.001551	5.0 ± 0.1	1.61
378.	0.001535	7.0 ± 0.1	1.94
383.	0.001525	9.0 ± 0.1	2.20

Figure 59 demonstrates a linear fit of the kinetic analysis for neat GRC-A. An analogous linear fit was obtained for the filled systems. From the slope of the plot, E_A was estimated according to the equation below:

$$E_a = -[d(\log_{10}\beta/d(1/T)]R * 2.303 \quad \text{eq 10}$$

where β is the heating rate K/min; T is the peak temperature in K, and R is the gas the constant, 8.3145 J/mol K^{-1}. Using the ASTM method, the observed activation energies for GRC-A loaded zeolite L was found to increase relative to the neat resin, in agreement with the isothermal studies. The activation energies for GRC-A loaded with zeolite Y decreased relative to both neat GRC-A and GRC-A/zeolite L mixture in agreement with the rheology study (see Tables 29 and 30).

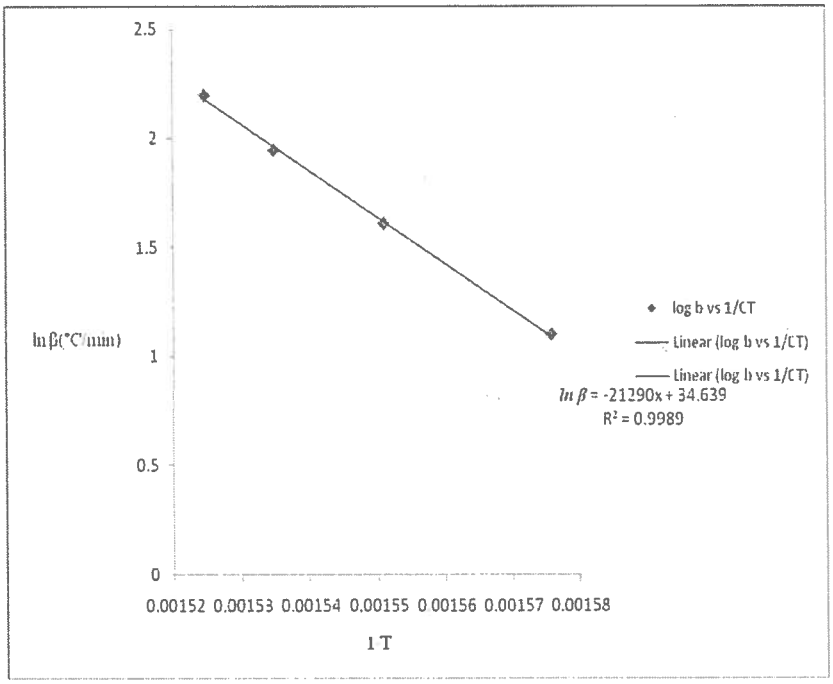

Figure 59. Arrhenius fit of ln β of versus 1/T for Neat GRC-A

Table 29. Apparent activation energy for the cure of neat GRC-A and GRC-A loaded with zeolite L via the ASTM method[a]

	E_a, kJ/mol Ozawa-Flynn-Wall	**Linear Regression**
Neat GRC-A	141. ± 1.5	0.995 ± 0.005
GRC-A/0.5 wt% zeolite L	155. ± 4.6	0.995 ± 0.005
GRC-A/1.0 wt% zeolite L	171. ± 3.7	0.989 ± 0.009
GRC-A/2.0 wt% zeolite L	187. ± 3.2	0.995 ± 0.005
GRC-A/4.0 wt% zeolite L	194. ± 3.3	0.998 ± 0.005

[a] Reaction order of 1 is assumed for this method.

Table 30. Apparent activation energy for the cure of Neat GRC-A and GRC-A loaded with zeolite Y obtained via ASTM method[a]

	E_a, kJ/mol Ozawa-Flynn-Wall	Linear Regression
Neat GRC-A	141. ± 1.5	0.995 ± 0.005
GRC-A/0.5 wt% zeolite Y	123. ± 4.1	0.989 ± 0.006
GRC-A/1.0 wt% zeolite Y	126. ± 3.5	0.998 ± 0.006
GRC-A/2.0 wt% zeolite Y	127. ± 3.2	0.988 ± 0.009
GRC-A/4.0 wt% zeolite Y	128. ± 3.3	0.987 ± 0.009

4.20 The Effect of Cure Temperature and Zeolites on the Glass Transition Temperature after Isothermal Studies

After each of the isothermal DSC experiments described above, the samples were rapidly cooled to room temperature, and then reheated at 20 °C/min to determine the

cured T_g and residual cure if any of the resin. Figures 60 show the result of this reheating on the GRC-A samples, clearly indicting that the resin was not completely cured at the end of the isothermal run, as indicated by the reduction in cure T_g and the observation of a residual cure exotherm.

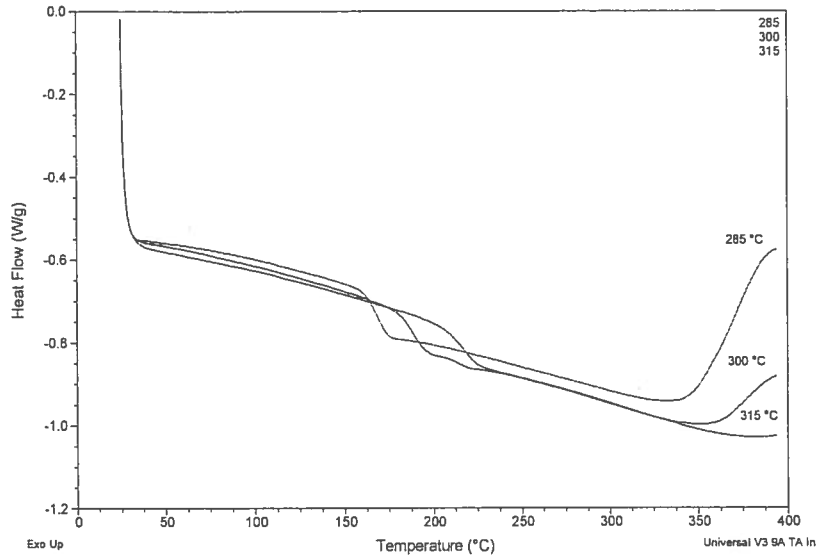

Figure 60. DSC thermograms for neat GRC-A after a 4 h isothermal hold at 285, 300, and 315 °C.

As expected for a thermoset, the residual cure of GRC-A decreases and the cured T_g increased as the temperature of the isothermal hold was increased. Similar results were found for GRC-A loaded with 0.5 and 4 wt% zeolite L and Y as is shown in Figure 61 after isothermally treatment at 285 °C and 315 °C. It was observed that the T_g for the neat resin and GRC-A loaded with 0.5 wt% zeolite L are similar, while the T_g for GRC-A loaded with Y is slightly higher after a 4 h hold 285°C. When the resin loaded with 4.0 wt% zeolite L and held at 285 °C for 4 h the T_g decreased relative to the neat resin as seen in Figure 61. However, the T_g increases for 4 wt% zeolite Y in GRC-A cured at 285

°C for 4 h. In both systems, residual cure was observed, with more residual cure found in the GRC-A zeolite Y mixture. This could be interpreted in two ways; either the zeolite L is retarding the cure relative to neat GRC-A or the zeolite Y catalyzes additional cure steps that are not available to the neat GRC-A at these temperatures. All of our data support the latter explanation.

In a similar study, neat GRC-A and GRC-A with 0.5 and 4.0 wt% loadings of zeolite L and Y was cured at 315 °C for 4h, to determine if there would be any residual cure at this temperature. The data showed that curing GRC-A with similar loadings of zeolite Y for 4 h at 315 °C resulted no residual cure. The results gave cured similar T_gs, ranging from 220 – 223 °C neat GRC-A and GRC-A/zeolite L mixtures. However, the T_g was substantially higher for GRC-A/zeolite Y mixtures, yielding a cured T_gs at 277 °C, see Figure 62. Table 31 summarizes the T_gs after the isothermal hold at 285 °C and 315 °C for 4 h for the neat GRC-A and GRC-A loaded with 0.5 wt% and 4 wt% zeolite L and Y.

Table 31. The onset of cure for GRC-A, and T_g and GRC-A filled with 0.5 and 4.0 wt% zeolite L and Y.

	285 °C 4 h hold T_g (°C)	**315 °C 4 h hold** T_g (°C)
Neat GRC-A	167.	223.
GRC-A/0.5 wt% zeolite L	165.	221.
GRC-A/0.5 wt% zeolite Y	173.	277.
GRC-A/4.0 wt% zeolite L	160.	223.
GRC-A/4.0 wt% zeolite Y	178.	277.

a)

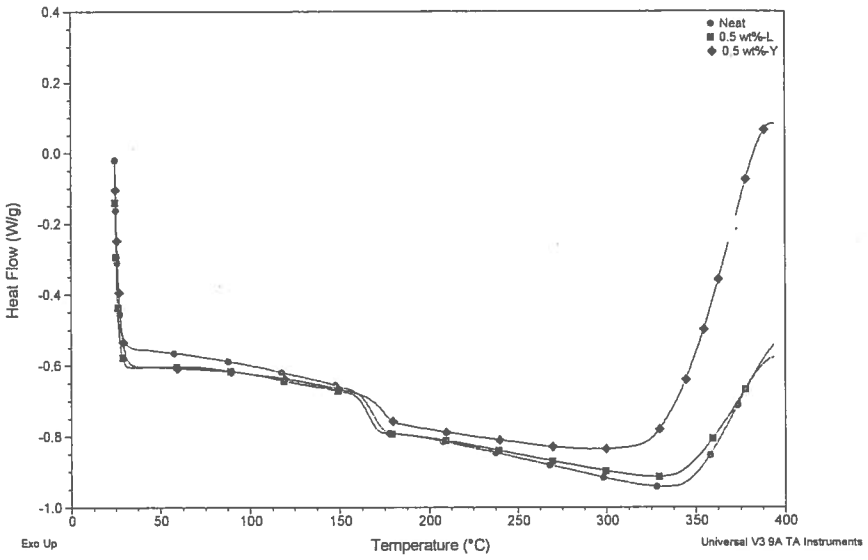

b)

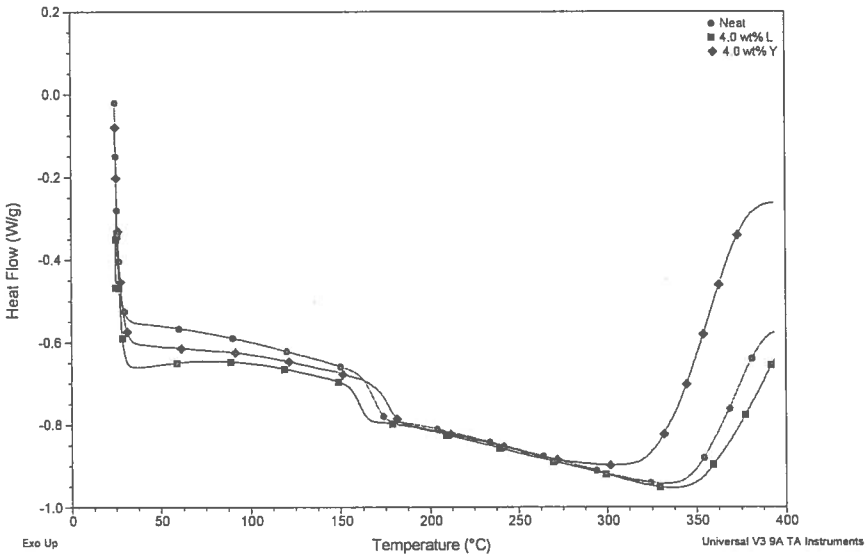

Figure 61. DSC thermograms for neat GRC-A, and GRC-A loaded with a) 0.5 wt% and b) 4.0 wt% L and Y, after a 4 h isothermal hold at 285 °C.

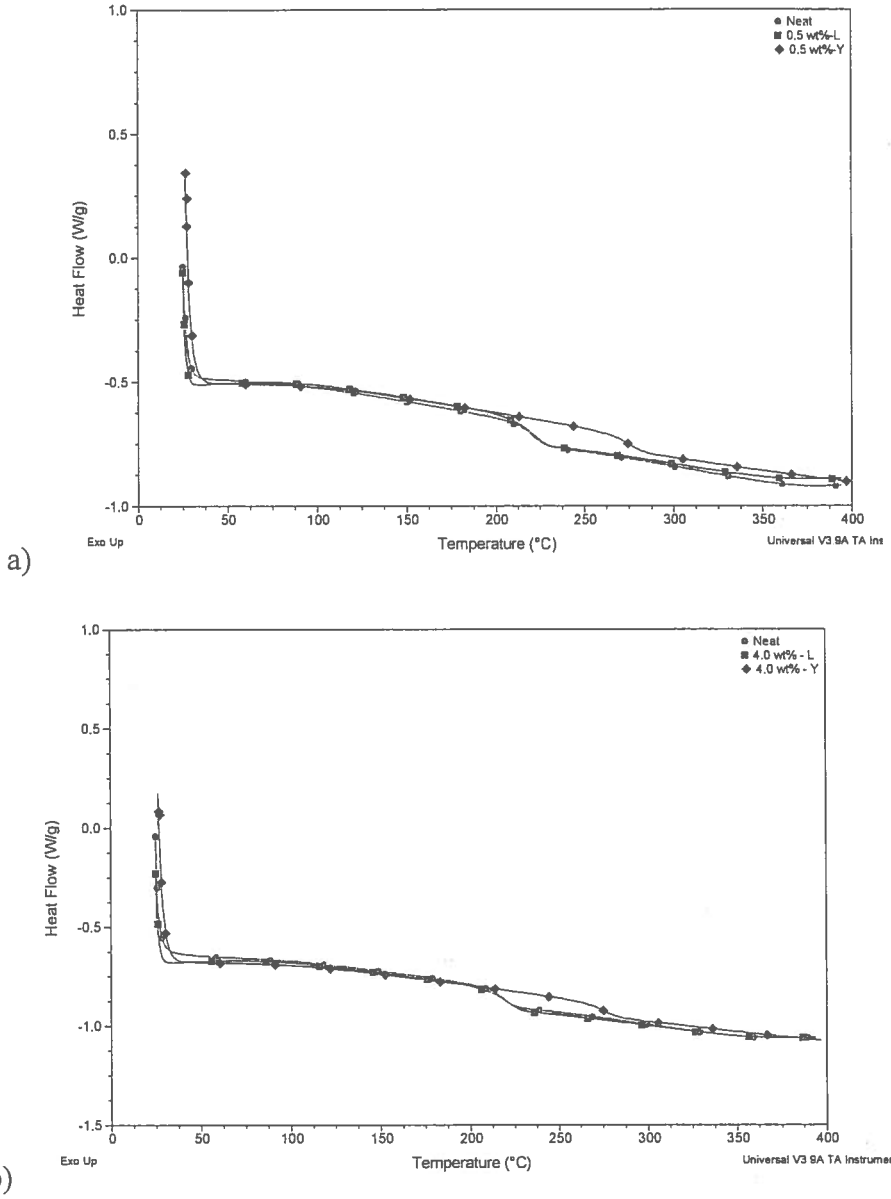

Figure 62. DSC thermograms for neat GRC-A and GRC-A loaded with a) 0.5 and b) 4.0 wt% L and Y, after 4 h isothermal hold at 315 °C.

4.21 Extent of Reaction of PETI GRC-A with Zeolites L and Y

Many equations have been developed to model the relationship between T_g and extent of cure for thermosetting polymers. The original DiBenedetto equation, one of the

most successful models, was modified to calculate the extent of reaction by determining the T_g for a highly cross-linked network as follows:

$$\frac{T_g - T_{g_0}}{T_{g_\infty} - T_{g_0}} = \frac{\lambda x}{1-(1-\lambda)x} \qquad \text{Eq10}$$

where T_{g0} and $T_{g\infty}$ represent the glass transition temperature before cure and after full cure, respectively.[155] T_g is the glass transition temperature after isothermal cure at each temperature for a specified cure time, and λ is equal to the ratio of isobaric heat capacity of fully cured material, $\Delta C_{p\infty}$, to that of uncured material, ΔC_{p0}. The isobaric heat capacities were determined by DSC through the glass transition at a heating rate of 5°C/min under a nitrogen atmosphere. Even if the selected $T_{g\infty}$ does not correspond to the theoretically ideal fully cured state, the extent of cure, x, is still valid for kinetic analysis according to the modified DiBenedetto equation. In this case, $T_{g\infty}$, λ, and x, are substituted by T_{gM}, λ', x' respectively, where T_{gM} represents the T_g of a network, λ' is the ratio of ΔC_{pM} to ΔC_{p0}, and x' refers to x/x_M, the relative extent of reaction . Table 32 gives the values for T_{g0}, $T_{g\infty}$, T_g and λ.

Table 32. Values given for the glass transition temperatures before and after cure, after isothermal cure, and the ratio of the isobaric heat capacity for neat GRC-A and GRC-A with zeolites L.

	285 °C T_g	**300 °C T_g**	**315 °C T_g**	**T_{g0}**	**T_∞**	**λ**
Cured GRC-A	167.	191.	220.	137.	225.	0.61
GRC-A /0.5 wt%-L	165.	184.	221.	136.	231.	0.59
GRC-A/1.0 wt%-L	162.	182.	222.	139.	230.	0.61
GRC-A/2.0 wt%-L	159.	182.	222.	137.	236.	0.58
GRC-A/4.0 wt%-L	160.	174.	223.	138.	237.	0.58

Using the DiBenedetto equation, we found that when GRC-A was loaded with either zeolites L or Y, the extent of cure of GRC-A is affected differently. Table 33 gives the extent of cure of GRC-A loaded with L, and Figure 63 shows the relationship between the extent of cure and isothermal temperatures. The data shows that presence of zeolite L reduces the extent of cure of GRC-A, especially at 285 °C and 300 °C. However, at 315 °C the extent of cure of neat GRC-A and GRC-A with zeolite L are nearly the same with the neat GRC-A is slightly higher.

Table 33. Extent of cure of neat GRC-A and GRC-A loaded with zeolite L obtained via DiBenedetto Equation

Extent of Cure, *x*	**285 °C**	**300 °C**	**315 °C**
Neat GRC-A	46 %	65%	96%
GRC-A/0.5 wt% L	43%	63%	93%
GRC-A/1.0 wt% L	36%	60%	91%
GRC-A/2.0 wt% L	33%	59%	91%
GRC-A/4.0 wt% L	33%	49%	91%

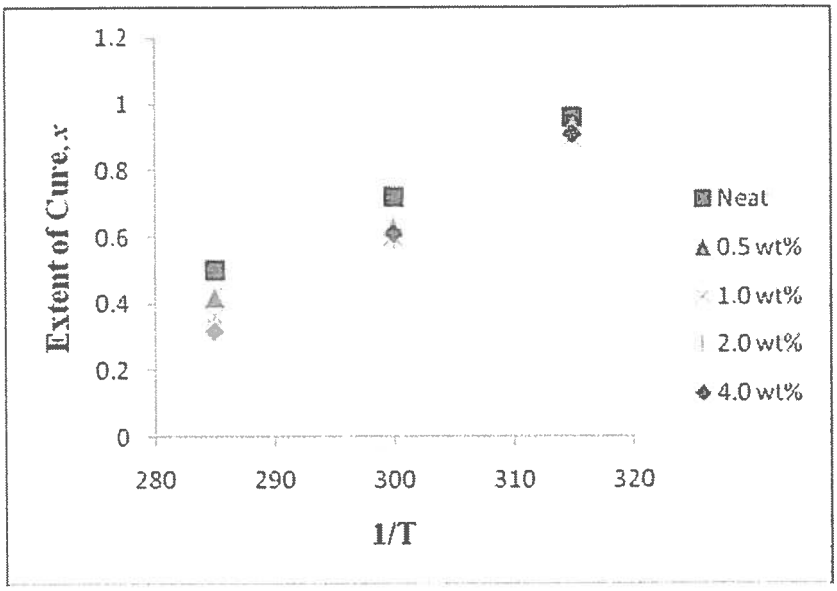

Figure 63. Relationship between extent of cure and the isothermal temperature cure for neat GRC-A and GRC-A loaded with zeolite L

Table 34 gives the values of T_{g0}, $T_{g\infty}$, T_g and λ and Table 35 gives the extent of cure for GRC-A and GRC-A with zeolite Y at 285, 300, and 315 °C. Figure 64 shows the relationship between the extent of cure and isothermal cure temperatures for the resin loaded with zeolite Y. The data show that zeolite Y not only catalyzes the cure of GRC-A, but also increases the extent of cure relative to neat GRC-A and GRC-A with zeolite L.

Table 34. Values given for the glass transition temperatures before and after cure, after isothermal cure, and the ratio of the isobaric heat capacity for neat GRC-A and GRC-A with zeolites Y.

	285 °C T_g	300 °C T_g	315 °C T_g	T_{g0}	T_∞	λ
Cured GRC-A	167.	191.	224.	137.	225.	0.61
GRC-A/0.5 wt%-Y	173.	246.	277.	136.	274.	0.49
GRC-A/1.0 wt%-Y	178.	245.	276.	136.	275.	0.50
GRC-A/2.0 wt%-Y	178.	245.	277.	136.	275.	0.49
GRC-A/4.0 wt%-Y	178.	245.	277.	136.	277.	0.49

Table 35. Extent of cure for neat GRC-A and GRC-A loaded with zeolite Y obtained as determined by the DiBenedetto Equation

Extent of Cure, x	**285 °C**	**300 °C**	**315 °C**
Neat GRC-A	51%	73%	96%
GRC-A/0.5 wt% - Y	47%	87%	100%
GRC-A/1.0 wt% - Y	46%	88%	101%
GRC-A/2.0 wt% - Y	47%	86%	100%
GRC-A/4.0 wt% - Y	46%	87%	100%

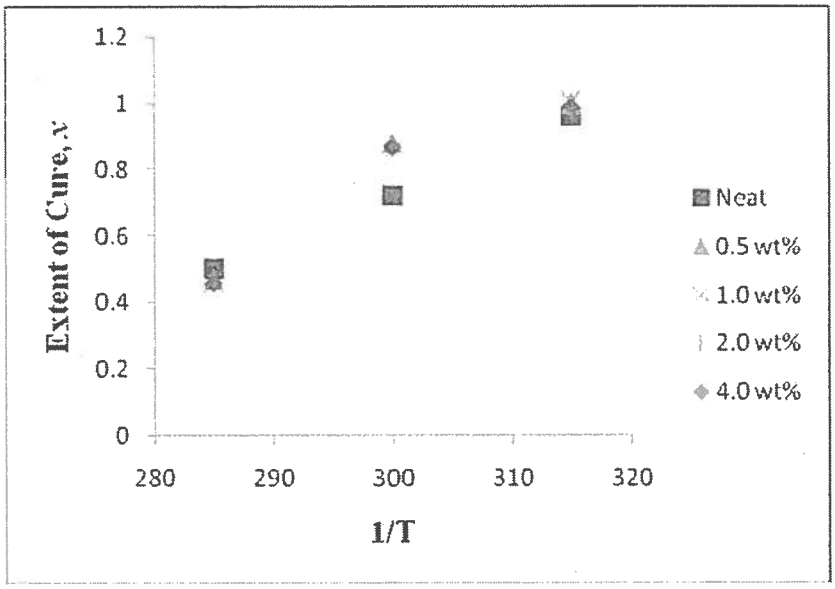

Figure 64. Relationship between extent of cure and isothermal cure temperature for neat GRC-A and GRC-A loaded with zeolite Y

4.22 Glass Transition Temperature of GRC-A loaded with Different and Modified Fillers

As received zeolite L and Y, and cured GRC-A were ground in a Wig-L-Bug for 5 - 7 min to obtain small particles, before incorporating them into the GRC-A resin. These small particles of zeolite L and Y and cured GRC-A were incorporated in to GRC-A by dry mixing as described above and then cured in the DSC with a heating rate of 5 °C/min to determine on the onset of cure, heat of reaction. Subsequent to the cure cycle the samples were reheated in the DSC at 20 °C/min to determine the T_g. The data generated in these experiments are presented Table 36.

Table 36. The glass transition temperatures of GRC-A with ground zeolite L and Y, and ground cured

	Onset of Cure (°C)	ΔH_R (J/g)	T_g (°C)
GRC-A/0.5 wt% ground zeolite L	333.	97.	221.
GRC-A/4.0 wt% ground zeolite L	338.	110.	226.
GRC-A/0.5 wt% ground zeolite Y	335.	147.	255.
GRC-A/4.0 wt% ground zeolite Y	336.	153.	258.
GRC-A/0.5 wt% ground cured GRC-A	329.	135.	278.
GRC-A/4.0 wt% ground cured GRC-A	332.	139.	290.

The data in Table 36 show that glass transition temperatures for GRC-A with ground zeolite L and Y decreased, when compared to GRC-A loaded with as received zeolite L and Y. This could be due to the effect that the grinding has on the structure of the zeolite. Figure 65 gives SEM images of ground zeolite L and shows that the structure of zeolite were crushed and flattened during grinding process.

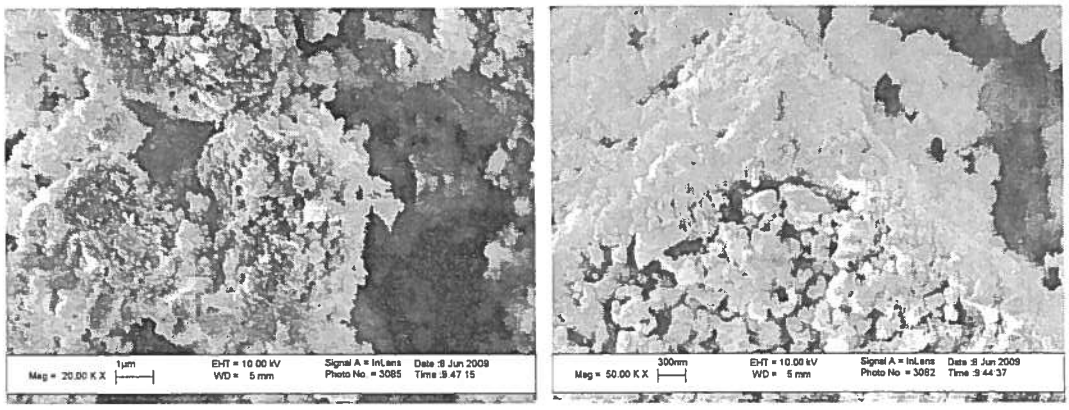

Figure 65. SEMs of zeolite L that had been grounded; magnified 20 and 50 times.

We assumed that the ground cured GRC-A would be inert and only slow the rate of cure based upon the increased viscosity of the resin filler system. The rheology of cure, as shown in Figure 66 and the heat of cure ΔH_R, determined by DSC fit well with this assumption. Interestingly, it was observed that the T_g increases significantly when ground cured GRC-A was incorporated into GRC-A. The assumption is that the ground cured GRC-A is undergoing additional curing that can affect the overall curing of the resin, thereby increasing the total cure T_g of the GRC-A composite.

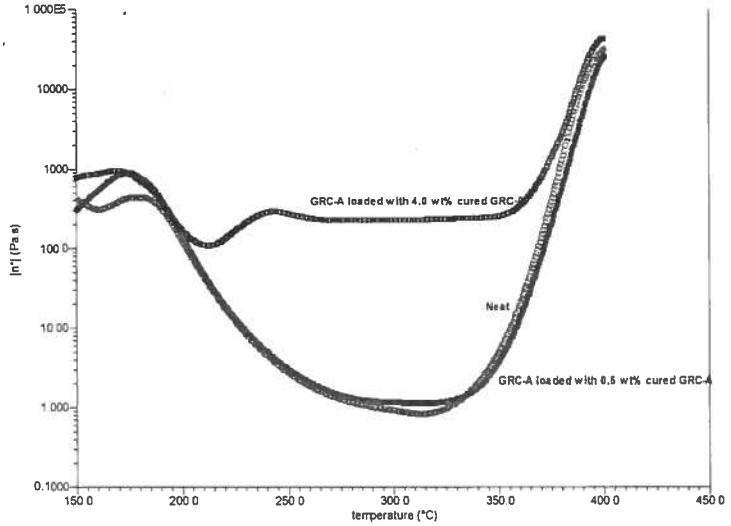

Figure 66. Complex viscosity, η*, as a function of temperature for neat GRC-A, and GRC-A with 0.5 and 4.0 wt% ground cured GRC-A.

4.23 Thermogravimetric Analysis (TGA) of cured GRC-A with Zeolite L

The incorporation of fillers into polymers, can improve their thermooxidative stability, by slowing the thermal oxidation and thermal degradation process, due to lowering the diffusivity of gases into composites.[58] Previous TGA studies have shown that the presence of fillers, including, but not limited to carbon nanotubes (CNTs), polyhedral oligomeric silsesquioxane (POSS), silica, and clay in polymeric materials

improve the thermooxidative properties, including flame retardation, ablation resistance, and enhanced barrier properties.[156-158] Pielichowski et al. observed that the addition of montmorillonite clay to polymeric materials acted as a diffusion barrier to oxygen, resulting in delaying the thermal of decomposition.[159] Alexandre and Dubois demonstrated that intercalated and exfoliated structures of clays increased the thermal stability of the polymer/clay nanocomposites.[160]

4.24 Apparent Activation Energy for the Decomposition of the Cured GRC-A, and Cured GRC-A with of Zeolites L under Air and Nitrogen

The thermooxidative stability of cured GRC-A, and GRC-A loaded with zeolites L was examined up to 900 °C. The weight loss at moderate temperatures may arise from the evaporation of residual moisture or low molecular weight components.[41] However, at higher temperatures, the weight loss results from polymer degradation or oxidation. These types of decomposition can be measured as a function of temperature and time. In this study, the apparent activation energy for thermal oxidative degradation were studied using the ASTM method, E 1641-07 at 3, 5, 7, 9 °C/min in air and nitrogen.[161] An Arrhenius plot was constructed by taking the logarithm of the heating rates versus inverse of temperature at constant conversion to determine the apparent activation energy, E_a, of decomposition using the following equation:

$$E_a = \frac{\frac{d(\log \beta)}{d\left(\frac{1}{T}\right)}}{0.457} * R \qquad \text{Eq 11}$$

where d(log β)/d(1/T) is the slope of the line obtained, β is heating rate in K/min, T is the temperature (K) at the constant conversion, and R is the gas constant, 8.314 J/mol·K. Figure 67 gives thermograms for cured GRC-A measured at 3, 5, 7, 9 °C/min in air. Table 37 gives the temperatures at 5% conversions for each of the respective heating rates, and Figure 68 shows the corresponding Arrhenius plot. In table 38, the apparent activation energy of thermal oxidation was calculuated for 5% and 10% conversion for cured GRC-A and GRC-A loaded zeolites.

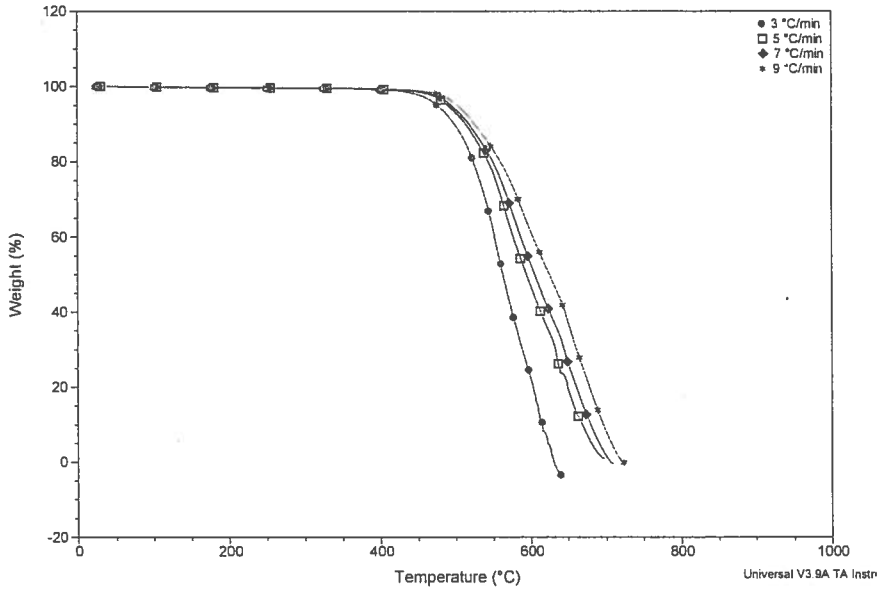

Figure 67. Thermograms for GRC-A, at heating rates of 3, 5, 7, and 9 °C/min under air

Table 37. Temperatures of 5% conversion of cured GRC-A under air, and the corresponding heating rates.

T (K)	1/T(K)	β(K/min)	log β(K/min)
749	0.001335	3.0 ± 0.1	0.477
763	0.001310	5.0 ± 0.1	0.699
768	0.001301	7.0 ± 0.1	0.845
777	0.001287	9.0 ± 0.1	0.954

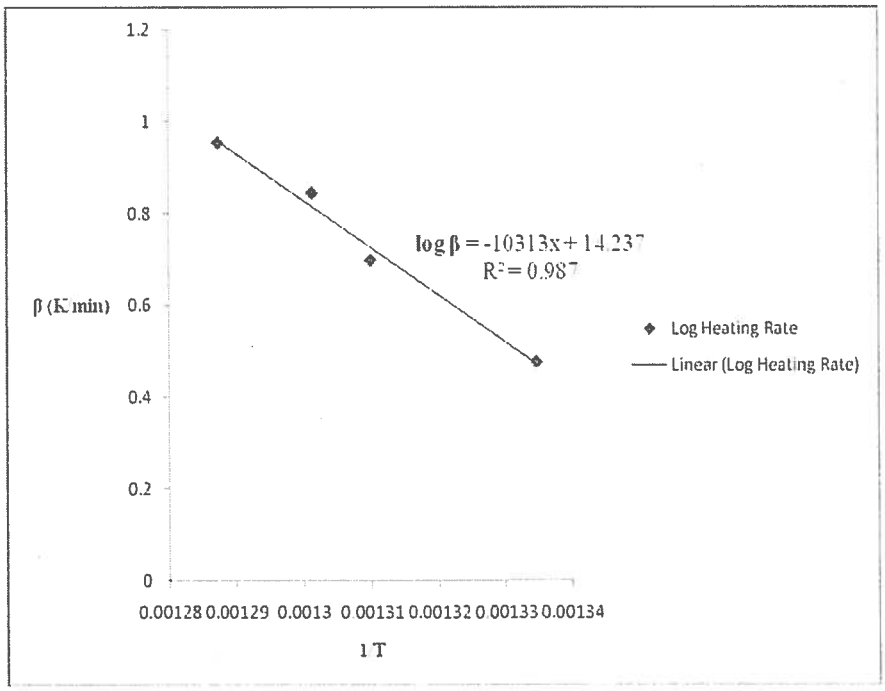

Figure 68. Arrehenius plot for the thermal oxidation of cured GRC-A vs. inverse temperature, at the 5 % weight loss in air.

Table 38. The apparent activation energy, E_a, for the thermal oxidation of cured GRC-A and GRC-A loaded with zeolites L and 5% and 10 % weight loss in air.

Sample/conversion	**5% (kJ/mol)**	**10% (kJ/mol)**
Neat GRC-A	189. ± 5.7	181. ± 5.1
GRC-A with 0.5 wt% zeolite L	242. ± 10.3	227. ± 9.7
GRC-A with 1.0 wt% zeolite L	256. ± 8.1	236. ± 8.8
GRC-A with 2.0 wt% zeolite L	312. ± 7.8	278. ± 8.1
GRC-A with 4.0 wt% zeolite L	375. ± 6.2	322. ± 7.3

The apparent activation energy for the decomposition for cured GRC-A loaded with zeolite L in air increased with increasing loading of the zeolite. This increase in the apparent activation energy demonstrates how the zeolites can retard the thermal oxidation by decreasing air permeability. Figure 69 gives the corresponding thermograms the for cured GRC-A under nitrogen, Table 39 gives the temperatures at 5% weight loss, and Figure 70 gives the corresponding Arrhenius plot. Table 40 gives the apparent activation energies for thermal degradation for both cured GRC-A and GRC-A loaded with zeolite L.

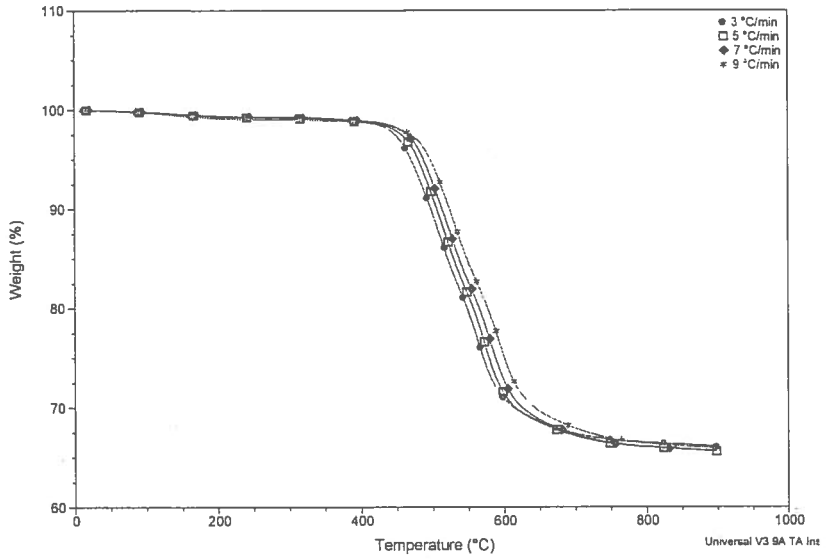

Figure 69. Themograms of cured GRC-A at 3, 5, 7, and 9 °C/min under nitrogen.

Table 39. Temperatures for 5% conversion of cured GRC-A and the corresponding heating rates

T (°C)	1/T(K)	β(K/min)	log β(K/min)
744	0.001344	3	0.477
779	0.001284	5	0.699
787	0.001271	7	0.845
797	0.001255	9	0.954

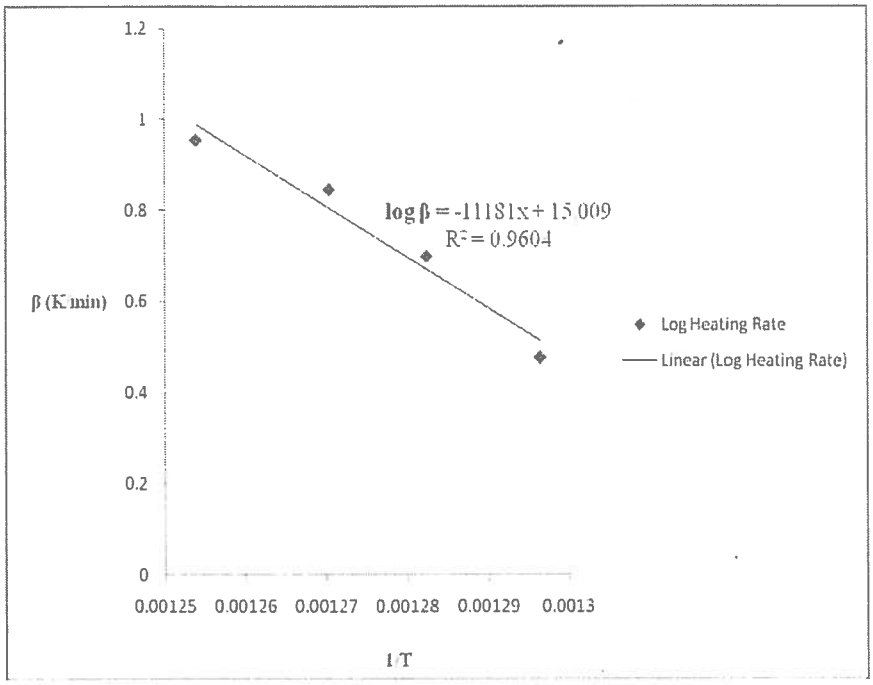

Figure 70. Arrehenius plot for the thermal degradation of cured GRC-A vs. inverse temperature, at the 5 % weight loss in nitrogen.

Table 40. The apparent activation energy, E_a for thermal degradation of cured GRC-A and cured GRC-A loaded with zeolites L at 5% and 10 % weight loss under nitrogen.

Nitrogen	5%	10%
Cured GRC-A	203. ± 4.8	194. ± 5.6
0.5 wt%	213. ± 7.1	262. ± 7.7
1.0 wt%	216. ± 6.3	265. ± 7.1
2.0 wt%	225. ± 6.1	277. ± 5.9
4.0 wt%	228. ± 5.8	292. ± 6.5

4.25 Dynamic Mechanical Thermal Analysis (DMTA) Studies of GRC-A and GRC-A loaded with Zeolite L and Y

Dynamic Mechanical Thermal Analysis (DMTA) was used to measure the storage modulus, G', and loss modulus, G" for cured plaques of GRC-A and GRC-A loaded with zeolite L and Y. The storage modulus measures the stored energy, representing the elastic portion, and the loss modulus measures the energy dissipated as heat, representing the viscous portion when a material is subjected to deformation in response to an applied strain. Together, they make up the complex modulus G*, which was discussed earlier in section 4.4. Tan delta (δ) is the ratio of the loss modulus to the storage modulus, and can be used to measure the glass transition of composites. Fillers have been extensively used in polymers to enhance stiffness, strength, toughness, and energy dampening.[151] These particular properties of the filled polymers are determined by the properties of the components, by the shape of the filler phase, by the morphology of the system, and the polymer-filler interfacial interactions. The overall value of fillers is a complex function of its intrinsic material characteristics, such as average particle size, particle shape, intrinsic strength, and chemical composition. Process dependent factors, such as distribution, surface chemistry, particle agglomeration, and bulk density also make important contributions to the filled polymer properties.

The incorporation of nanoscale fillers (on the order of 10^{-9} m) into polymers, including PETI resins, has been shown to enhance the properties of the resulting composite. Nanoscale fillers can yield dramatic changes in material properties because of their large surface area for a given volume. For example, carbon nanotubes have excellent good mechanical properties that are often translated into the overall

performance of the resulting composites, and nanoclay filled polymeric systems have been reported to exhibit a 30% increase in modulus and strength.[162-164] We have carried out DMTA studies on neat resin plaques of GRC-A and GRC-A loaded with zeolites L and Y.

DMTA measurements were carried out as per ASTM method D 5279[156] using TA Instruments AR G2 with a sinusoidal deformation. Rectangular composite specimens with dimensions of 30 x 6.5 x 3.5 mm were gripped longitudinally between two clamps. Then the specimen was subjected to a mechanical torsional displacement at a fixed frequency of 1 Hz and a controlled strain of 0.5 %, with a linear increase in temperature. Measurement were made of G' and G" as function temperature, see Figures 71 and 73.

4.26 The Effect of Zeolite loading on Storage Modulus

Figure 71 shows the elastic modulus of the GRC-A/zeolite L composites plotted as a function of temperature. Table 41 gives the values for G' taken at temperatures below and above the T_g from 50 °C to 325 °C and Figure 72 shows the plot of those values of G' versus the temperatures form 50 °C to 325 °C. The data obtained from the DMTA studies showed that zeolite L improved the storage modulus of the final composite at the temperatures below the T_g, however, as the temperatures increased the presence of the zeolites did not afford any additional advantages. Basically at temperatures above the T_g, the GRC-A filled composites were behaving similar to that of unfilled cured GRC-A composite. The conjecture could be made that at temperatures below the T_g, the zeolites are trapped within the composite structure, possibly filling any voids or cracks, thereby improving upon mechanical properties of the composite.

However, as the temperature increase beyond the T_g, the composite becomes flexible enough for the zeolites move around and no longer are able to maintain its ability to fill the voids or cracks.

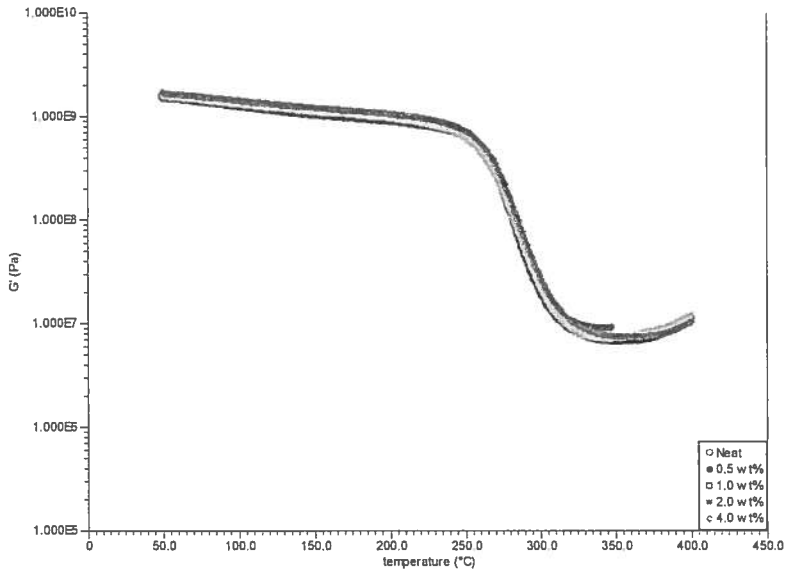

Figure 71. Storage modulus, G' of cured GRC-A and cured GRC-A with 0.5. 1.0, 2.0 and 4.0 wt% L as a function of temperature with a heating rate of 5 °C/min.

Table 41. G' at temperatures before and after the T_g for GRC-A/zeolite L composites.

Temperature (°C)	**Neat** x10^9	**0.5 wt%** x10^9	**1.0 wt%** x10^9	**2.0 wt%** x10^9	**3.0 wt%** x10^9
50	1.47	1.58	1.57	1.61	1.75
75	1.36	1.50	1.46	1.44	1.57
100	1.22	1.36	1.33	1.30	1.44
125	1.11	1.25	1.22	1.20	1.32
150	1.01	1.16	1.13	1.11	1.23
175	9.47	1.08	1.06	1.04	1.16
200	8.78	1.00	9.81	9.60	1.07
225	7.92	8.96	8.84	8.44	9.49
250	6.26	6.74	6.87	6.19	7.33
275	2.14	1.73	2.31	1.92	2.40
300	2.26	1.80	2.53	2.30	2.86
325	9.70	7.89	8.34	8.30	9.71

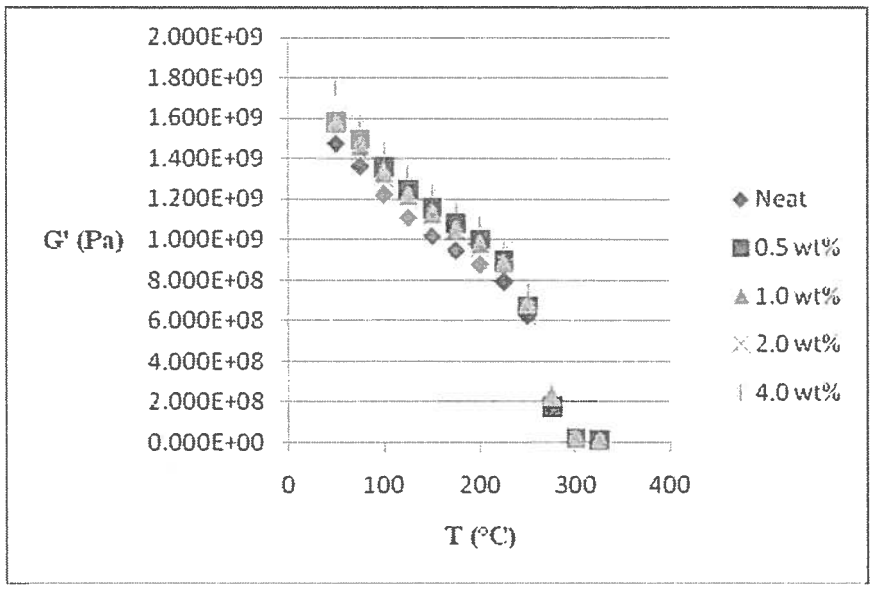

Figure 72. Storage modulus, G', of the plaque composites versus temperature for GRC-A and GRC-A/zeolite L composites.

4.27 The Effect of Zeolite loading on the Loss Modulus

The loss modulus, G", which measures the amount of energy dissipated, demonstrates the liquid-like behavior of the complex modulus. Figure 73 shows the plot of the loss modulus of the filled and unfilled GRC-A composites. Table 42 gives the values for G" taken at temperatures below and above the T_g, from 50 °C to 300 °C. Figure 74 shows the plot for the values of G" versus temperature from 50 °C to 300 °C. The plot indicates that the presence of the zeolite L slightly increases the loss modulus. Also, results between GRC-A/zeolite mixtures with 4wt% L and Y, showed that the results were nearly similar.

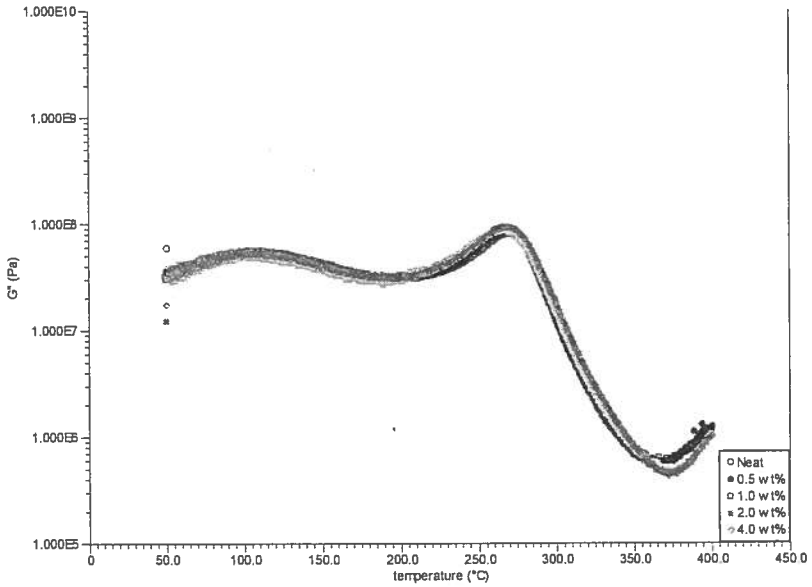

Figure 73. The loss modulus, G", of cured GRC-A and cured GRC-A loaded with 0.5. 1.0, 2.0 and 4.0 wt% zeolite L as a function of temperature with a heating rate of 5 °C/min

Table 42. G" at temperatures before and after the T_g. for GRC-A/zeolite L composites.

Temperature (°C)	**Neat** x 10^9	**0.5 wt%** x 10^9	**1.0 wt%** x 10^9	**2.0 wt%** x 10^9	**3.0 wt%** x 10^9
50	2.41	2.32	2.42	2.43	2.44
75	4.41	4.54	4.26	4.03	4.85
100	5.30	5.22	5.13	5.10	5.68
125	5.04	4.82	4.87	4.93	4.85
150	4.23	3.91	3.99	3.92	4.18
175	3.33	3.40	3.25	3.46	3.42
200	3.04	3.19	3.02	3.31	3.18
225	3.45	3.85	3.61	3.88	4.02
250	5.44	6.61	5.98	6.76	6.64
275	7.57	7.55	8.18	7.54	8.59
300	1.32	1.15	1.58	1.46	1.80

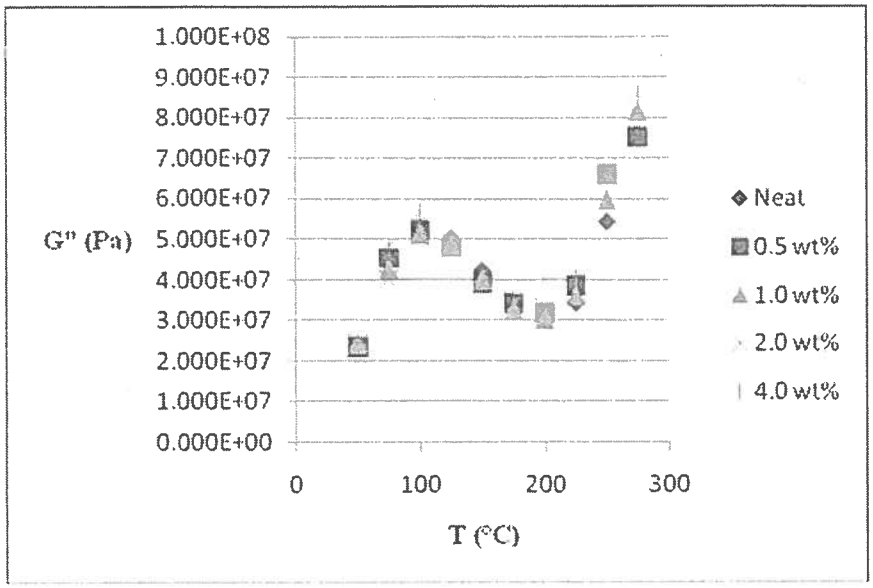

Figure 74. Loss modulus, G''of the placque composites versus temperature for GRC- A and GRC-A/zeolite L composites

A comparison between the resin loaded with 4 wt% zeolite L and the resin loaded with 4 wt% zeolite Y, showed that zeolite Y did not increase the storage modulus relative zeolite L; see Table 43 and Figure 75. Moreover, the data showed that the storage modulus for the composite with zeolite Y was lower than the storage modulus for the composite with zeolite L at 4wt% loading. Despite the fact that zeolite Y catalyzes the cure reaction of the phenylethynyl end groups, which led to higher cure T_gs of the resin powder; this however, did not translate into additional improvement in the storage modulus relative to the resin loaded with zeolite L.

Table 43. Values of the G' recorded at temperatures below and above the T_g for GRC-A/zeolite 4.0 wt% L and Y mixtures.

Temperature (°C)	**4.0 wt% x 10^9 L**	**4.0 wt% x 10^9 Y**
50	1.75	1.66
75	1.57	1.43
100	1.44	1.28
125	1.32	1.18
150	1.23	1.11
175	1.15	1.04
200	1.07	9.75
225	9.49	8.62
250	7.33	6.33
275	2.40	2.09
300	2.86	2.62
325	9.71	9.75

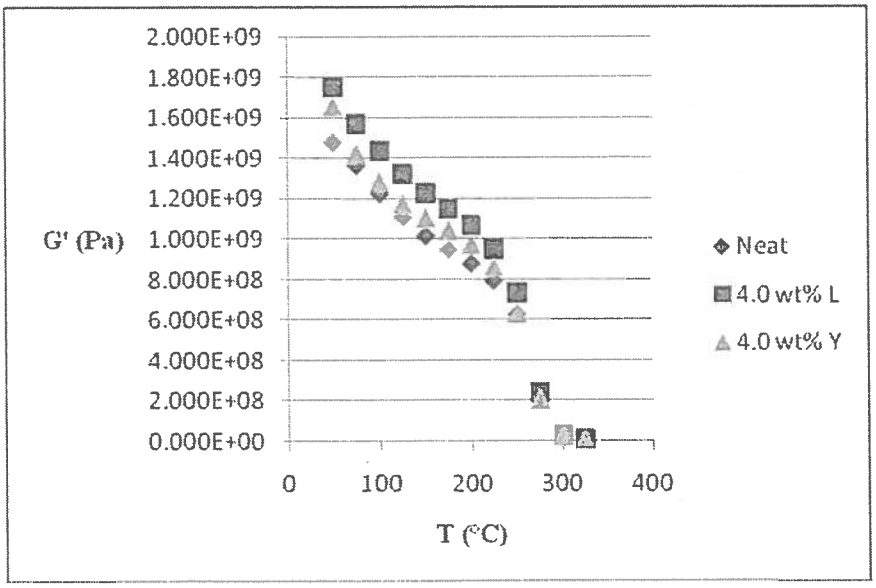

Figure 75. Storage modulus of the composites versus temperature for GRC- A/4.0 wt% L and GRC-A/4.0 wt% Y

4.28 Measuring the Glass Transition Temperature of GRC-A/Zeolite mixtures using Tan Delta

DMTA was also used to measure the glass transition temperature for the cured GRC-A composites based on changes in tan delta (δ) as a function of temperature. Tan δ is expressed as:

$$\tan \delta = G''/G' \quad \text{Eq 12}$$

where δ is the angle between the in-phase and out-of-phase components during an oscillatory test. Figure 76, illustrates tan delta as a function of temperature for the both the neat GRC-A and GRC-A/zeolite L cured composites,and giving Table 44 is the T_g of the composite obtained from the peak of the tan delta curves. Little differnece was observed in the T_g of the neat and zeolite loded cured compoistes by this method. This supports the DSC and thermomechanical analysis (TMA) results which showed that the T_g of the cured composites were also similar, although lower than the T_g obtained from DMTA, see Table 44. Deviations in the vlaues of T_gs of composites measured in differint ways are expected[85] For comparison, the T_gs the of neat GRC-A and GRC-A losded with zeolites L and Y were examined, and are shonw in Table 44. The deviations found by the different metods are in line with what has been reported in the literature.[83]

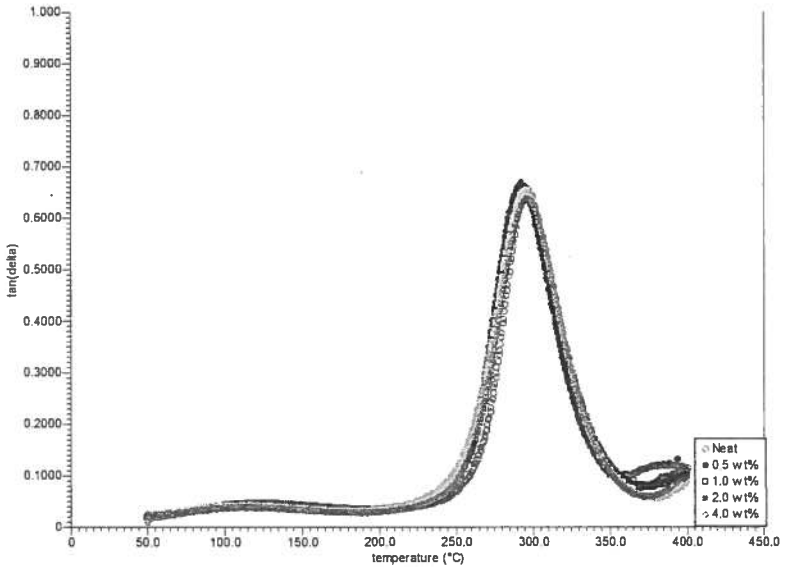

Figure 76. Tan δ of cured GRC-A and cured GRC-A loaded with 0.5. 1.0, 2.0 and 4.0 wt% L.

Table 44. Glass Transition Temperatures for GRC-A and GRC-A loaded with zeolite L plaque composites obtained by DMTA, DSC, and TMA

	DMTA[1]	**DSC**[2]	**TMA**[3]
Sample	**T_g(°C)**	**T_g(°C)**	**T_g(°C)**
Cured GRC-A	296.	278.	280.
GRC-A/0.5 wt% zeolite L	295.	279.	279.
GRC-A/1.0 wt% zeolite L	296.	280.	279.
GRC-A/2.0 wt% zeolite L	296.	278.	279.
GRC-A/4.0 wt% zeolite L	297.	279.	279.
GRC-A/4.0 wt% zeolite Y	298.	278.	277.

[1]DMTA heating rate 10 °C/min, 0.05% strain, frequency 1.0 hertz
[2]DSC heating rate 20 °C/min
[3]TMA heating rate 3 °C/min, force 0.020 N; via penetration probe

4.29 Thermomechanical (TMA) Studies and Coefficient of Thermal Expansion (CTE) of GRC-A and GRC-A with Zeolites

The coefficient of thermal expansion (CTE) is a material property indicative of the extent to which materials (metals, alloys, polymers, etc.) expands upon heating. Different substances expand by different amounts, depending on the chemical make-up. Table 45 gives a list of different materials and their corresponding CTEs.[165]

Table 45. CTE of various materials

	CTE (μm/m °C)
Structural Steel	12
Polyamide – Nylon 6	95
Polyamide – Nylon 6,6	90
Polyamide – Nylon 6,6 – 30% Carbon Fiber Reinforced	30
Polyimide	30-60
Polyimide – 30% Glass Fiber Filled	17-53
Polyimide – 30% Carbon Fiber Reinforced	6-47

TMA measurements were carried out on composites of GRC-A and GRC-A loaded with zeolites L on a TA Instruments Q 400. In this study, the thermal expansion for composites of GRC-A and GRC-A with zeolite L were studied using an expansion probe The area which the probe covers, detects a change in the material's dimensions (μm), as the material expands with increasing temperature. Figure 77 illustrates the change in dimensions for the unfilled GRC-A composite as a function of time, at a

heating rate of 3 °C/min. The CTE values were obtained for GRC-A and GRC-A/zeolite L e composites and are given along with the T_gs in Table 46.

Table 46. The CTE and T_g values for neat GRC-A and GRC-A with zeolites

Expansion Probe	CTE (µm/ m°C)	T_g (°C)
Neat As-Received	64. ± 1.5	276. ± 1.7
0.5 wt%	50. ± 2.3	278. ± 2.2
1.0 wt%	54. ± 2.2	277. ± 2.1
2.0 wt%	54. ± 1.9	275. ± 2.1
4.0 wt%	59. ± 2.1	275. ± 1.9

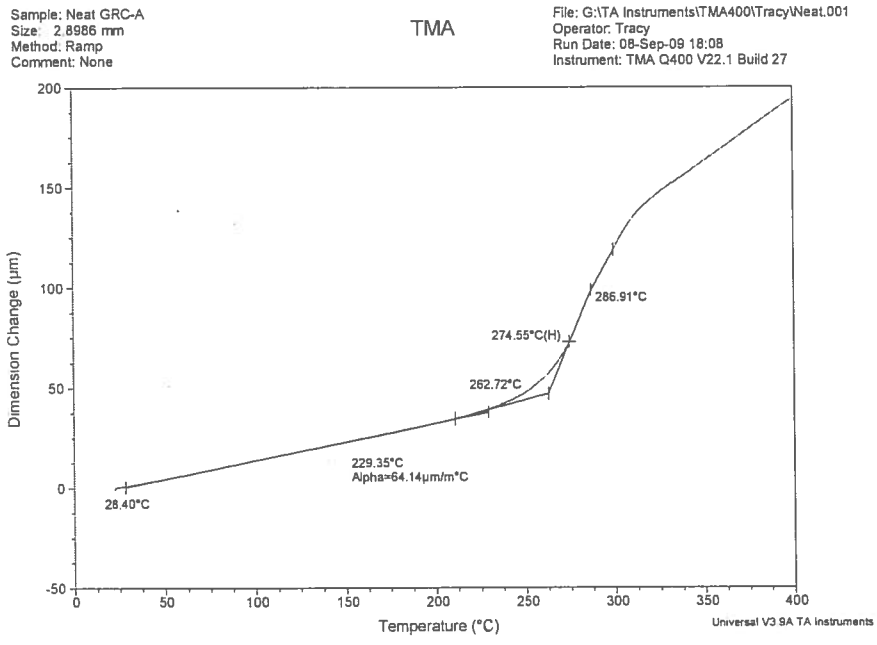

Figure 77. Change in dimensions (µm) of neat GRC-A versus temperature (at a heating rate 3 °C/min).

The CTEs obtained from the expansion probe shows an initial decrease in the thermal expansion, in particularly for GRC-A loaded with 0.5 wt%, but begins to increase in its thermal expansion as the loadings increase. However the thermal expansion for the composites loaded with zeolites was still lower than for the cured GRC-A composite.. The data shows that the incorporation of zeolites decreases the amount that the composites expand upon heating. However, the expansions probe measurements did reveal that the glass transition temperatures did not increase for GRC-A/zeolites composites relative to the cured GRC-A composite, but instead remained similar. These observations agree with T_gs obtained via penetration probe, which was discussed in section 4.28, and further supports that the presence of zeolites does not afford additional advantages over the unfilled composite at temperatures beyond the cured T_g.

CHAPTER 5

CONCLUSION

We have found that the addition of nanoporous zeolites to PETI GRC-A, a phenylethynyl terminated imide resin, alters its melt rheology, cure kinetics, and thermo-mechanical properties. Rheological and DSC studies demonstrated that zeolite L acts as a filler and retards the cure of the phenylethynyl end-groups, shifting the onset of cure to higher temperatures. Just the opposite, zeolite Y catalyzes the cure, reducing the activation energy and shifting the onset of cure to lower temperatures. In this study we found that the activation energies for the onset of cure and gelation of GRC-A/zeolite L mixtures are higher than for neat GRC-A. In contrast to this, we found that zeolite L catalyzes the cure of GRC-A, giving a 10 to 12 % lowering of the activation energy of cure.

DSC studies also showed that GRC-A filled with zeolite Y had a larger heat of reaction, ΔH_R, than neat GRC-A, indicating the formation of additional chemical bonds that do not occur in the uncatalyzed system. The additional cross-linking in the GRC-A/zeolite Y mixtures gave higher postcured T_gs by DSC, but not by DMTA and TMA. The addition of either zeolites led to improvement in the storage, G′, and loss modulus, G″, below T_g, increased the thermooxidative stability of cured composites, and decreased the coefficient of thermal expansion (CTE) compared to the cured neat composites.

The reduction in the activation energy of the onset of cure and gelation, the increase in T_g, as determined via DSC, increase in thermooxidative stability, decrease in CTE, increase in G′ and G″ below T_g by the incorporation of zeolite Y into GRC-A warrants further study. These further studies could also include other Lewis acid catalysts, both solid and liquid, and further elucidation of the mode of action. Optimization of a catalyst for the cure of PETI resins could lead to composites with improved properties and reduced production costs.

REFERENCES

1. Hergenrother, P. M.; *High Perfom. Polym.* **2003**, 15, 3.

2. Scroog, C. E. *Polym. Sci.* 1991, *16*.

3. Takekoshi, T. In Polyimide; Ghosh, M. K.; Mittal, K. L., Eds.; Marcel Dekker: New York, 1996.

4. Mazumder, S. K. C. M., Materials, Product and Process Engineering; CRC Taylor & Francis, 2002.

5. Wang, L.; Harris, F. W.; Chuang, K. C. *Polym. Prepr.* **2004**, 45, 92.

6. Harris, F. W.; Sridhar, K.; Das, S. *Polym. Prepr.* **1984**, 25, 110.

7. Harris, F. W.; Pamidimukkala, A.; Gupta, R.; Das, S.; Wu, T.; Mock, G. *J. Macromol. Sci., Chem.* **1984**, A21 (8 & 9), 1117.

8. Paul, C. W. S., R. A.; Fenelli, S. P. US Patent 5 138.028, 1992.

9. Hergenrother, P. M.; Bryant, R. G.; Jensen, B. J.; Havens, S. J. J. *Polym. Sci., Part A: Polym. Chem.* **1994**, 32, 3061.

10. Hergenrother, P. M.; Smith, J. W., Jr. *Polymer*, **1994**, 35, 4857.

11. Fenelli, S. P. S., R. A.; Paul, C. W. Polyimide Science & Technology, Ferger, C.; Khojasteh, M. M.; Htoo, M. S., Eds., Technomic Publishers, Lancaster, PA, 1991, p. 220.

12. Bryant, R. G.; Jensen, B. J.; Hergenrother, P. M. ACS *Polym. Prepr.* **1992**, 33, 910.

13. Jensen, B. J.; Hergenrother, P. M.; Nwokogu, G. *Polymer*, **1993**, 34, 630.

14. Meyer, G. W.; Jayaraman, S.; McGrath, J. E. ACS *Polym. Prepr.* **1993**, 34, 540.

15. Jayaraman, S.; McGrath, J. E.; Srinivasan, R. J. *Polym. Sci., Part A*, **1995**, 33, 1551.

16. Connell J. W.; Smith Jr. J. G.; Hergenrother P. M.; Rommel M. L. Int. *SAMPE Tech. Conf. Ser.* **1998**, 545.

17. Criss J. M.; Arendt C. P.; Connell J.W.; Smith Jr J.G.; Hergenrother P.M. *SAMPE J.* **2000**, 32.

18. Smith Jr. J. G.; Connell J. W., Hergenrother P. M.; Criss J. M. *J. Comp. Mat.* **2002**, 36, 2255.

19. Smith Jr. J.G.; Connell J. W.; Hergenrother P. M.; Ford L. A.; Criss J.M. *Macromol. Symp.* **2003**, 401.

20. Cejka, J. Corma, A.; Schuth, F.; Bekkum, H. *Introduction to Zeolite Science and Practice*; 3rd ed.; Elsevier, 2007; Vol. 168.

21. Lauriente, D. H. Inoguchi, Y. *The Chemical Economics Handbook*, SRI Consulting, 2005, p 599.1000 A.

22. Sherman, J. D. *Proc. Nat. Acad. Sci.* **1999**, *96*.

23. Tanabe, K.; Holderich, W. F. *Appl. Catal., A* **1999,** *181*.

24. Hsu, C. S.; Robinson, P. R. *Practical Advances in Petroleum Processing, Vols 1 and 2*; Springer: New York City, 2006.

25. Weller, M. T. *J. Chem. Soc.* **2000**.

26. Larsen, S. C. *Environ. Catalysis* **2005**.

27. Glaeser, R.; Weitkamp, J. *in Basic Principles in Applied Catalysis*; Springer: New York City, 2004; Vol. 161

28. Pavelic, K.; Subotic, B.; Colic, M. *Surf. Sci. Catal.* **2001**, *135*.

29. Clerici, M. G. *Oil, Gas (Hamburg, Germany)* **2006,** *32*.

30. Lercher, J. A.; Jentys, A. *in Handbook of Porous Solids*; Wiley-VCH: Weinheim, 2002; Vol. 2.

31. Gorte, R. J. *in Handbook of Porous Solids*; Wiley-VCH: Weinheim, 2002; Vol. 1.

32. Elanany, M.; Koyama, M.; Kubo, Broclawik, M.; Miyamoto, A. *Appl.Surf. Sci.* **2005**, *246*.

33. Szostak, R. *Stud. Surf. Sci. Catal.* **1991**, *58*.

34. Kuhl, G. H. *in Catalysis and Zeolites*; Springer: Berlin, 1999.

35. Men, A., Chen, T.; Sun, P.; Zhou, J.; Yuan, Z.; Guo, A.; Wang, J.; Ding, D.; Li, H. *Catal. Today* **1996**, *30*.

36. Kuhl, G. H. *J. Phys. Chem. Solids* **1977**, *38*.

37. Amer, I.; Bernstein, T.; Eisen, M.; Blum, J. Volhardt, K. P. C. *J. Mol. Catal* **1990**, 60, 313

38. Musso, F. S., E.; Floriana, C. *Organometallics* **1997**, *16*

39. Reppe, W. S., W. *Liebigs Ann. Chem.* **1948**, *560*

40. Schetter, M. C. R. *Hebd. Seances Acad. Sci.* **1866**, *6*

41. Stevens, M. P. *Polymer Chemistry: An Introduction*; 3rd ed.; Oxford University Press: New York, 1934.

42. Simionescu, C. I. P., V.; Dumitrescu, S. *J. Polym. Sci. : Polym. Chem. Ed.* **1977**, *15*.

43. Natta, G. M., G.; Corradini, P. *Rend. Accad. Nazl. Lincei Rend., Classe Sci. Fis., Mat. Nat.* **1958**, *25*.

44. Watson, W. H., Jr., McMordie, Jr.; Lands, L. G. *J. Polym. Sci.* **1961**, *55*.

45. Snider, B. B. *Acc. Chem. Res.* **1980**, *13*

46. Snider, B. B.; Ron, E. *J. Amer. Chem. Soc.* **1985**, *107*.

47. Yates, P.; Eaton, P. *J. Amer. Chem. Soc.* **1960**, *82*.

48. Sbai, A.; Branchadell, V.; Ortuno, R. M.; Olivia, A. *J. Org. Chem.* **1997**, *62*.

49. Bonnesen, P. V. P., C. L.; Honey-chuck, R. V.; Hersh, W. H. *J. Amer. Chem. Soc.* **1989**, 111.

50. Konovalov, A. I. *Russ. Chem. Rev.* **1989**, *58*.

51. Fleming, I. *Molecular Orbitals and Organic Chemical Reactions; Reference Ed.*; Wileys & Sons, 2010.

52. Bordiga, S.; Ricchiardi, G.; Spoto, D.; Scarano, D.; Carnelli, L.; Zecchina, A. *J. Chem. Soc., Faraday Trans.* **1993**, *89*.

53. Paze, C.; Bordiga, C.; Lamberti, M.; Salvalaggio, M.; Zecchina, A. *J. Phys. Chem.: B* **1997**, *101*

54. Shchukin, A. O.; Vasilyev, A. V. *Appl. Catal., A* **2008**, *336*.

55. Jin, T.; Himuro, M.; Yamamoto, Y. *J. Amer. Chem. Soc.* **2010**, *132*.

56. Sun, J.; Kozmin, S. *J. Amer. Chem. Soc.* **2005**, *127*.

57. Yamamto, H.; Kurihara, H. Ishihara, K *J. Am. Chem. Soc.* **1996**, *118*

58. Husaain, F.; Hojjati, M.; Okamoto, M.; Gorga, E. R. *J. Comp. Mater.* **2006**, *40*.

59. Yuen, S.; Ma, C. M.; Chiang, C.; Teng, C.; Yu, Y. *J. Polym. Sci., Part A: Polym. Chem.* **2008**, *46*.

60. Du, F.; Scogna, R. C.; Zhou, W.; Brand, S.; Fisher, J. E.; Winey, K. I. *Macromolecules* **2004**, *37*.

61. Ghose, S.; Watson, K. A.; Delozier, D. D.; Working, D. C.; Siochi, E. J.; Connell, J. W. *Composites: Part A* **2006**, *37*, 465.

62. McGrath, J. E.; Grubbs, H. J.; Glass, T. E.; Meyer, G. W. *J. Polym. Sci., Part A: Polym. Chem.* **1995**, *33*.

63. Li Y. "Synthesis and Cure Characterization of High Temperature Polymers for Aerospace." Ph.D. Dissertation, Texas A&M, 2004

64. Delvigs, P.; Hsu, C.; Serafini, T. T. *J. Polym. Sci.* **1970**, *29*.

65. Serafini, T. T. NASA SP-227, 1970, p 207

66. Burns, E. A.; Lubowitz, H. R.; Jones, J. F. In *TRW-05937-6019-RO-00* NASA CR-72460, 1968

67. Lubowitz, H. R. U.S. Patent 3, 528, 950 1970.

68. Ghosh, M. K.; Mittal, K. L. *Polyimide: Fundamentals and Applications.*; Marcel Dekker, Inc.: New York, 1996.

69. Ghosh, M. K.; Mittal, K. L. *"Comparison of Graphite-Fabric-Reinforced PMR-15 and Avimid N Composites After Long-Term Isothermal Aging at Various Temperatures" NASA/TM-107529*, Lewis Research Center and Gilcrest Corp., 1998

70. Gibbs, H. H. *J. Appl. Polym. Sci.* **1979**, *5*.

71. DuPont. NR-150 Polyimide Solutions. DuPont Product Information Pamplet, 1976.

72. Serafini, T. T.; Delvigs, P.; Lightsey, G. R. *J. Appl. Polym. Sci.* **1972**, *16*.

73. Jensen, B. J.; Chang, A. C. *High Perform. Polym.* **1998**, *10*.

74. Chang, A. C.; Jensen, B. J. *Adhesion J.* **2000**, *72*

75. Scola, D. A.; Simone, C. D. *Macromolecules* **2003**, *36*.

76. Thompson, C. M. Connell, J. W.; Hergenrother, P. M.; Yokota, R. *Int. SAMPE Symp. Exhibition* **2002**, *47*.

77. Inoue, H. O., H.; Hiraoka, Y. *Radiat. Phys. Chem.* **1987**, *29*

78. Yamaguchi, H. in: Yokota, Hasegawa, M. editors *"Recent Advances in Polyimides"*, 1997.

79. Hasegawa, M.; Sensui, N.; Shindo, Y.; Yokoto, R. *J. Photopolym. Sci.* **1996**, *9*.

80. Takahashi, T.; Takabayashi, S.; Inoue, H. *High Perform. Polym.* **1998**, *10*.

81. Hasegawa, M. Shi, Z.; Yokoto, R.; He, F.; Ozawa, H. *High Perform. Polym.* **2001**, *13*.

82. Criss J. M.; Meador, M. A.; Chuang, K. C.; Connell J.W.; Smith Jr J.G.; Hergenrother P.M.; Mintz, E. A. *Soc. Adv. Mater. Proc. Eng. Ser.* **2003**, *48*.

83. Connell J. W.; Smith Jr. J. G.; Hergenrother P. M.; Criss, J. M. *Int. SAMPE Tech. Conf. Ser.* **2003**, *35*.

84. Connell J. W.; Smith Jr. J. G.; Hergenrother P. M.; Criss, J. M. *Soc. Adv. Mater. Proc. Eng. Ser.* **2003,** *48*.

85. Smith Jr. J. G.; Connell J. W.; Li, C-J.; Criss J. M.; Wu, W. *International SAMPE Technical Conference* **2004**, *36*.

86. Fang, X. X., X.-Q.; Simone, C. D.; Stevens, M. P.; Scola, D.A. *Macromolecules* **2000**, 33, 1671.

87. Holland, T. V. G., T. E.; McGrath, J. E. *Polymer* **2000**, 41, 4965

88. Roberts, C. C.; Apple, J. M.; Wnek, G. E. J. *J. Polym. Sci., Part A: Polym. Chem.* **2000**, 36, 3486.

89. Andur, S.; Cheng, A. J. Y.; Wong, A.; Ehrlich, P. E. *J .Polym. Sci., Polym. Chem. Ed.* **1978**, 16, 407

90. Preston, C. M. L.; Hill, D. J. T.; Pomery, P. J.; Whittaker, A. K.; Jensen, B. J. *High Perform. Polym.* **1999**, 11, 453

91. Swanson, S. A.; Fleming, W. W.; Hofer, D. C. *Macromolecules* **1992**, 25, 582

92. Harrington, K. A.; Orwoll, R. A.; Young, P. R.; Jensen, B. J.; Young, P. R. *Int. SAMPE Symp. Exhibition* **1996**, *27*.

93. Wood, K. H.; Orwoll, R. A.; Young, P. R.; Jensen, B. J.; Mcnair, H. M. *Int. SAMPE Symp. Exhibition* **1997**, *42*.

94. Meyer, G. W.; Glass, T. E.; Grubbs, H. J.; McGrath, J. E. *J. Polym. Sci. Part A: Polym. Chem.* **1995**, *33*.

95. Takekoshi, T. T., J. M. *Polymer* 1994, *35*.

96. Meyer, G. W. Ph.D thesis, Virginia Polytechnic Institute and State University, 1995.

97. Pickard, J. M. J., E. G.; Goldfarb, I. *Macromolecules* 1979, *12*.

98. Fang, X.; Xie, X.-Q.; Simone, C. D.; Stevens, M. P.; Scola, D.A. *J. Polym. Sci.* **1998**, *36*.

99. Wright, M. E.; Schorzman, D. A. *Macromolecules* **2000**, *33*.

100. Bullions, T. A.; McGrath, J. E.; Loos, A.C. *Polym. Eng. Sci.* 2002, *42*.

101. Bullions, T. A., Ph.D Thesis Virginia Polytechnic Institute and State University, Sept. 2000.

102. Barrer, R. M. *Zeolites and Clay Minerals as Sorbents and Molecular Sieves*; Academic Press: London, 1979.

103. Wan, Y. Y., Yang, H. F.; Zhao, D. Y. *Acc. Chem. Res.* **2006,** *39*.

104. Schuth, F. Schmidt, W. *Adv. Mater.* **2002**, *14*.

105. Ying, J. Y.; Mehnert, C. P.; Wong, M. S. *Angew Chem., Int. Ed.* **1999**, *38*.

106. Yang, H. F.; Zhao, D. Y. *J. Mater. Chem.* **2006**, *15*.

107. Corma, A. *Chem. Rev.* **1995**, *95*.

108. Mirodatos, C. Barthomeuf, D. J. *Chem. Commun., Chem. Soc.* **1981**, *39*.

109. Lago, R. M. H., W. O.; Mikovski, R. J.; Olson, D. H.; Hellring, S. D.; Schmitt, K. D.; Kerr, G. T. *in New Development in Zeolites Science and Technology*; Elsevier: Amsterdam, 1986; Vol. 28.

110. Corma, A.; Garcia, H. *Chem. Rev.* **2002**, *102*.

111. Shigeishi, R. A.; Chiche, B. H.; Fajule, F. *Microporous Mesoporous Mater.* **2001**, *43*.

112. Sartori, G.; Maggi, R. *Chem. Rev.* **2006**, *106*.

113. Ruck, R. T.; Jacobson, E. N. *J. Amer. Chem. Soc.* **2002**, *124*.

114. Endo, K.; Koike, T.; Sawaki, T.; Hayashida, O.; Masuda, H.; Aoyama, Y. *J. Amer. Chem. Soc.* **1997**, *119*.

115. Eklund, L.; Axelsson, A.-K.; Nordahl, A.; Carlson, R. *Acta Chem. Scand.* 1993, *47*.

116. Isaev, Y.; Fripiat, J. J. *J. Catal.* **1999**, *182*

117. Pindur, V.; Haber, M. *Heterocycles* **1991**, *32*.

118. Ipaktschi, J. *Z. Naturforsch, B* **1986**, *41*.

119. Narayana Murthy, Y. V. S.; Pillai, C. N. *Synth. Commun.* **1991**, *21*.

120. Karge, H. G. *Z. phys. Chem., Neue Folge* **1971**, *76*.

121. Nguyen, M. L.; Tanner, C. C. *New Zealand J. Agr. Res.* **1998**, *41*.

122. Frullano, L.; Wang, C.; Miller, R. H.; Wang, Y. *J. Amer. Chem. Soc.* **2011**, null.

123. Connell J. W.; Smith Jr. J. G.; Li, C.-J. W., W.; Criss, J.M. *High Perform. Polym.* **2006**, *18*.

124. Baerlocher, C. M., W. M.; Olson, D. H. *Atlas of Zeolite Framework Types*; 5th ed.; Elsevier, 2001.

125. Dealy, J. M.; Wissbrun, K. F. *Melt Rheology And Its Role In Plastics Processing*; Chapman & Hall, 1995.

126. Halley, P. J.; Mackay, M. E. *Polym. Eng. Sci.* **1996**, *36*.

127. Gonzalez-Romero, V. M.; Macosko, C. W. *J. Rheol.* **1985**, *29*.

128. Harran, D.; Laudoudard, A. *J. Appl. Polym. Sci.* **1986**, *32*.

129. Tung, C. Y. M; Dynes, P. J. *J. Appl. Polym. Sci.* **1982**, *27*.

130. Frank, A. J. *Rheological Testing of Thermosetting Polymers*; www.tainstruments.com/pdf/literature/AAN015_V1c_U_Thermoset.pdf (Viewed October 5, 2010)

131. Ghose, S. W., K. A.; Delozier, D. D.; Working, D. C.; Siochi, E. J.; Connell, J. W. *Composite: Part A* **2006**, *37*.

132. Konya, Z.; Zhu, J.; Niesz K.; Mehn, D.; Kirsci, I. *Carbon* **2004**, *42*

133. Hirst, S. C.; Hamilton, A. D. *J. Am. Chem. Soc.* **1991**, *113, 382*

134. Walter, C. J.; Anderson, H. L.; Sanders, J. K. M. *J. Chem. Soc., Chem. Commun.* **1993**, *458*.

135. Kang, J.; Rebek Jr, J. Nature 1997, 385, 50 *Nature* **1997**, *385*.

136. Kang, J.; Hilmersson, G.; Santamaria, J.; Rebek Jr, J. *J. Am. Chem. Soc.* **1998**, *120*.

137. Laszlo, P.; Lucchetti, J. *Tetrahedron Lett.* **1984**, *25*.

138. Cativiela, C.; Fraile, J. M.;García, J. I.; Mayoral, J. A. *J. Mol. Catal. 1993, 79, 3052*.

139. Collet, C.; Laszlo, P. *J. Phys.Org. Chem.* **1995**, *8*.

140. Pagni, R. M.; Kabalka, G. W.; Hondrogiannis, G.; Bains, S.; Kurt, R. *Tetrahedron Lett.* **1993**, *49*.

141. Proust, S. M.; Ridley, D. D. *J. Chem. Soc.* **1984**, *3*

142. Conrads, M. *J.Chem. Ber.* **1991**, *124*.

143. Cativiela, C.; García, J. I.; Mayoral, J. A.; Pires, E.; Royo, A. J.*Tetrahedron Lett.* **1995**, 51

144. Bischoff, S.; Kasper, F. *J. Prakt. Chem.* **1986**, *328*.

145. Riant, O.; Kagan, H.; Ricard, L. *Tetrahedron Lett.* **1994**, *50*.

146. Halley, P. J.; Mackay, M. E. *Polym. Eng. Sci.* **1996**, *36*.

147. Mussati, F. G.; Macosko, C. W. *Polym. Eng. Sci.* **1973**, 13.

148. Ganguli, S.; Derrick, D.; Jordan, K.; Price, G.; Vaia, R. *Polymer* **2003**, 44.

149. Hoffmann, W. *Rubber Technology Handbook*; Hanser: Munich, 1989.

150. *Fillers. Encyclopedia of Polymer Science Technology, 3rd ed.*; Wiley & Sons: New York, 2004; Vol. 10.

151. Larson, R. G., *The Structure and Rheology of Complex Fluids*, Oxford University Press, New York, 1999, p. 279

152. Einstein, A. *Ann. Phys.* **1911**, *34*

153 Database of Zeolite Structures. http://www.iza-structure.org/databases/ (accessed Dec 1, 2010).

154. Batchelor, G. K. *J. Fluid Mech.* **1971**, *48*.

155. Pascault, J. P. W., R. J. J. *J. Polym. Sci. Part B: Polym. Phys.* **1990**, *28*.

156. Kopesky, E. T.; Haddad, T. S.; Cohen, R. E.; McKinley, G. H. *Macromolecules* **2004**, *37*, 8992.

157. Utracki, L. A. *Clay-Containing Polymeric Nanocomposites*; Rapra: Shawbury 2004

158. Njuguna, J. P., K. *Adv. Eng. Mater.* **2004**, *6*.

159. Leszczyńskaa, A., Njugunab, J. Pielichowskia, K. Banerjeec, J. R. *Thermochim. Acta* **2007**, *453*.

160. Alexandre, M. D., P. *Mater. Sci. Eng.* **2000**, *28*.

161. Hatakeyama, T. L., Z. *Handbook of Thermal Analysis*; Wiley & Sons: New York 2000.

162. Vaia, R., Ganguli, S.; Dean, D.; Jordan, K.; Price, G. *Polymer* **2003**, *44*.

163. Park, C. O., Z.; Watson, K. A.; Crook, R. E.; Smith, Hr., J.; Lowther, S. E.; Connell, J. W.; Siochi, E. J.; Hasrrison, J. S.; Clair, T. L. S. *Chem. Phys. Lett.* **2002**, *364*.

164. Gelves, G. A. L., B.; Sundararaj, U.; Haber, J. A. *Nanotechnology* **2008**, *19*.

165. Professional Plastics. www.professionalplastics.com/professionalplastics/ThermalPropertiesofPlasticMaterials.pdf (accessed Nov 25, 2010).